Stony Brook University

Multinuclear Solid-state NMR Studies of Brønsted Acid Sites in Zeolites HY, HZSM-5 and HMOR

A Dissertation Presented

by

Hua Huo

to

The Graduate School

in Partial Fulfillment of the Requirements

for the Degree of

Doctor of Philosophy

in

Chemistry

Stony Brook University

December 2009

Stony Brook University

Hua Huo

We, the dissertation committee for the above candidate for the **Doctor of Philosophy** degree, hereby recommend acceptance of this dissertation.

Clare P. Grey, D. Phil., Advisor
Professor, Department of Chemistry, SUNY at Stony Brook

Stanislaus S. Wong, Ph. D., Chairperson
Professor, Department of Chemistry, SUNY at Stony Brook

Brian L. Philips, Ph. D., Third Member
Professor, Department of Geosciences, SUNY at Stony Brook

Philip J. Grandinetti, Ph. D., Outside Member
Professor, Department of Chemistry, Ohio State University

This dissertation is accepted by the Graduate School.

Lawrence Martin
Dean of the Graduate School

Abstract of the Dissertation

Multinuclear Solid-State NMR Studies of Brønsted Acid Sites in Zeolites HY, HZSM-5 and H-MOR

by

Hua Huo

Doctor of Philosophy

in

Chemistry

Stony Brook University

2009

The research presented in this dissertation involves the use of variable temperature solid-state NMR techniques to investigate the local structure and dynamic properties of the Brønsted acid sites in a variety of zeolites, including HY, HZSM-5 and H-MOR.

Brønsted acid sites play a key role in controlling the catalytic performances in acidic catalysts. A determination of the structure of the acid site, in particular, the O-H bond length, is fundamental to the understanding of its acid strength. The O-H distances in zeolite HY and HZSM-5 extracted from ^{17}O-^{1}H CP rotational-echo double resonance (CP-REDOR) NMR data acquired at room temperature are noticeably longer than the results from *ab-initio* calculations due to the presence of some restricted motions at room temperature, such as zeolite framework vibrations and O-H librational motion. We present here our ^{17}O-^{1}H CP-REDOR NMR results of zeolite HY and HZSM-5 at the lower temperature of 183 K, where some of these motions are frozen out. By comparing the line shapes of simulation results from the SIMPSON package with the experimental data, an O-H distance of about 0.97 ~ 0.98 Å was obtained for zeolite HY, which is consistent with the previous *ab-initio* calculation results. The results demonstrate that low temperature REDOR NMR spectroscopy can provide more accurate estimates of the O-H distance, which should prove useful in understanding zeolite structure and acidity.

In order to further illustrate the dynamics of protons in zeolite HZSM-5, low temperature ^{1}H MAS NMR spectroscopy has been carried out on both samples that have been dried using procedures that are standard in the literature, and samples that have been more carefully dehydrated. A significant enhancement of proton mobility is seen for the "standard" dehydrated HZSM-5 sample, in comparison to that seen for the much drier sample. This is ascribed to a vehicle-hopping mechanism involving the residual water

that is present in these zeolites. A gradual change of the framework structure is observed on cooling to approx. 213 K, as monitored via the change in ^{1}H chemical shift values of the Brønsted acid resonances and by X-ray diffraction. A more sudden change in structure is seen by differential scanning calorimetry (DSC) and NMR, at approx. 220 - 230 K, which is associated with changes in both the mobility and the modes of binding of the residual water to the Brønsted acid sites and the zeolite framework.

$^{17}O/^{1}H$ double resonance NMR spectroscopy was used to study the local structure of zeolite H-Mordenite. Different contact times were used in cross polarization magic angle spinning (CPMAS) NMR, CP-REDOR NMR and heteronuclear correlation (HETCOR) NMR spectroscopy to selectively investigate Brønsted acid sites with different O-H distances. Efforts were made to distinguish the locations of different Brønsted acid sites in H-Mordenite (H-MOR) and develop correlations between the NMR parameters and the local/long range structure and Brønsted acidity. ^{17}O multiple-quantum (MQ) MAS NMR was applied to monitor both the normal framework and Brønsted acid oxygen sites in zeolite HMOR. The results demonstrate that $^{17}O/^{1}H$ double resonance NMR provides a powerful and sensitive method to investigate the local structure of different Brønsted acid sites and to probe their changes upon adsorption.

Table of Contents

Table of Contents vi

List of Abbreviations xiii

List of Symbols xiv

List of Figures xvii

List of Tables xxvi

Acknowledgments xxix

List of Publications xxx

Chapter 1

Introduction

1.1 Introduction to Zeolites 2

1.1.1 The Brønsted Acidity of Zeolites 3

1.1.2 The Structure of Faujasite Type Zeolites 5

1.1.3 The Structure of MFI Type Zeolites 6

1.1.4 The Structure of Mordenite Type Zeolites 8

1.2 Interactions in Solid State NMR Spectroscopy 10

1.2.1 Zeeman Interaction 11

1.2.2 Radiofrequency Interaction 14

1.2.3 Chemical Shielding Anisotropy 16

1.2.4 Dipole-Dipole Interaction 19

1.2.5 Quadrupolar interaction 23

1.2.6 Scalar Coupling 28

1.3 Introduction to Solid-State NMR Techniques 29

1.3.1 Magic Angle Spinning (MAS) 29

1.3.2 Cross Polarization (CP) 30

1.3.3 Multiple Quantum Magic Angle Spinning (MQMAS) 32

1.3.4 Transfer of Population Double-Resonance (TRAPDOR) NMR 35

1.3.5 Rotaional Echo Double Resonance (REDOR) NMR 37

1.3.6 Heternuclear Correlation (HETCOR) NMR 38

1.4 Multinuclear Solid-State NMR Studies of Zeolites 40

1.4.1 ^{29}Si MAS NMR Studies on Zeolites 40

1.4.1.1 ^{29}Si MAS NMR 40

1.4.1.2 ^{1}H to ^{29}Si cross-polarization experiments 42

1.4.2 ^{27}Al MAS NMR Studies on Zeolites 42

1.4.3 ^{1}H MAS NMR Studies on Zeolites 43

1.4.4 ^{17}O MAS NMR Studies on Zeolites 44

1.5 Reference 45

Chapter 2

Probing Brønsted acid sites in zeolite HY and HZSM-5 with low temperature ^{17}O - ^{1}H Double Resonance MAS NMR spectroscopy

2.1 Introduction 53

2.2 Experimental Section 56

2.2.1 Materials Preparation 56

2.2.2 Solid-state NMR Spectroscopy 57

2.2.3 NMR Simulation Details 58

2.3 Results and Discussion 59

2.3.1 Low temperature $^{1}H \rightarrow {}^{17}O$-$^{1}H$ CP-REDOR NMR of zeolite HY 59

2.3.2 Low temperature $^{1}H \rightarrow {}^{17}O$-$^{1}H$ CP-REDOR NMR of zeolite HZSM-5 67

2.4 Conclusions 70

2.5 References 71

Chapter 3

Low Temperature ^{1}H MAS NMR Spectroscopy Studies of Proton Motion in Zeolite HZSM-5

3.1 Introduction 74

3.2 Experimental Section 78

3.2.1 Materials Preparation 78

3.2.2 Solid-state NMR Spectroscopy 79

3.2.3 X-ray powder diffraction 79

3.2.4 Differential scanning calorimetry (DSC) 80

3.2.5 Elemental analysis 80

3.3 Results and Discussion 81

3.3.1 Variable temperature ^{1}H MAS NMR of HZSM-5-He 81

3.3.2 Variable temperature ^{1}H MAS and low temperature ^{1}H/^{27}Al TRAPDOR NMR of HZSM-5-V 84

3.3.3 2D-Magnetization Exchange NMR 95

3.3.4 DSC 98

3.3.5 XRD 100

3.3.6 Discussion 107

3.4 Conclusions 113

3.5 References 115

Chapter 4

Probing Brønsted Acid Sites in Zeolite H-MOR with Trimethylphosphine Molecules and Solid State NMR Spectroscopy

4.1 Introduction 119

4.2 Experimental Section 121

4.2.1 Materials Preparation 121

4.2.2 Solid-state NMR Spectroscopy 122

4.3 Results and Discussion 123

4.3.1 Preliminary Assignments of ^{1}H MAS NMR Spectra 123

4.3.2 Variable Temperature ^{1}H MAS NMR and ^{1}H/^{27}Al TRAPDOR NMR 123

4.3.3 Properties of the Probe Molecules 129

4.3.4 ^{1}H MAS NMR of TMP/ zeolite H-MOR complexes 131

4.3.5 The ^{31}P→^{1}H / ^{1}H→^{31}P CP-MAS NMR and Deconvolution Details 133

4.3.6 Stabilization effect of the framework on the probe molecules 134

4.3.7 Correlation of the ^{1}H Chemical Shift Values and the Motion of Probe Molecules. 138

4.3.8 The Locations of Brønsted Acid Sites in Zeolite H-MOR 139

4.4 Conclusions 140

4.5 References 140

Chapter 5

Use of ^{1}H→^{17}O and ^{1}H→^{29}Si Double Resonance Experiments to Measure Connectivity and Internuclear Distances in Zeolite H-MOR

5.1 Introduction 144

5.2 Experimental Section 146

5.2.1 Materials Preparation 146

5.2.2 Solid-state NMR Spectroscopy 147

5.3 Results and Discussion 148

5.3.1 $^{1}H \rightarrow {}^{17}O$ CP MAS NMR 148

5.3.2 2D ^{1}H-^{17}O HETCOR NMR 150

5.3.3 $^{1}H \rightarrow {}^{17}O$-$^{1}H$ CP-REDOR 156

5.3.4 2D ^{1}H-^{29}Si HETCOR NMR 165

5.3.5 The Nature of the Brønsted Acid Site at $\delta_{CS}{}^{1}H$ = 4.8 ppm 170

5.4 Conclusions 171

5.5 References 173

Chapter 6

^{17}O MQMAS NMR Studies of Zeolites H-MOR

6.1 Introduction 176

6.2 Experimental Section 177

6.2.1 Materials Preparation 177

6.2.2 Solid-state NMR Spectroscopy 177

6.3 Results and Discussion 179

6.3.1 ^{17}O single pulse MAS NMR 179

6.3.2 2-D MQMAS Spectrum Obtained at A 14.1 T Magnet 181

6.3.3 2-D MQMAS Spectrum Obtained at a 19.4 T Magnet 187

6.4 Conclusions 196

6.5 References 197

Chapter 7 Conclusions 199

References 202

List of Abbreviations

2-D	two-dimensional
CP	cross polarization
CSA	chemical shielding (shift) anisotropy
DAS	double-angle spinning
DOR	double-rotation
DSC	differential scanning calorimetry
EFG	electric field gradient
HETCOR	heteronuclear correlation
IZA	International Zeolite Association
MAS	magic angle spinning
MQMAS	multiple quantum magic angle spinning
PAS	principal axis system
QCC	quadrupole coupling constant
REDOR	rotational echo double resonance
rf	radio frequency
TRAPDOR	transfer of population in double resonance

List of Symbols

α'	adiabaticity parameter
α, β, γ	Euler angles: relative orientation between two tensors
γ	magnetogyric ratio
δ_{11}, δ_{22}, δ_{33}	principal components of the chemical shift tensor
δ_{CS}	isotropic chemical shift
δ_{iso}	isotropic chemical shift
δ_{cg}^{iso}	shift of the center of gravity at the isotropic dimension of MQMAS data
η	quadrupolar asymmetry parameter
μ	value of magnetic moment of a nuclei
ω_0	Larmor frequency, $rad \cdot s^{-1}$
ω_r	rotor (sample) spinning frequency, $rad \cdot s^{-1}$
$\boldsymbol{\sigma}$	chemical shielding tensor
σ_{11}, σ_{22}, σ_{33}	principal components of the chemical shielding tensor
σ_{iso}	isotropic chemical shielding
σ_{ref}	chemical shielding of a reference standard
σ_{sample}	chemical shielding of a sample
σ_{xx}, ..., σ_{zz}	nine components of the chemical shielding tensor
τ_p	pulse width (rf duration)
$\mathbf{B_0}$	external applied magnetic field

B_0	external applied magnetic field strength
$\mathbf{B_1}$	applied rf field
B_1	applied rf field strength
$\mathbf{B}_{loc}$	local field about a nucleus
$\mathbf{D}$	dipolar tensor
e	electron charge
E_m	energy level
eq	largest component of EFG tensor, V_{zz}
eQ	nuclear quadrupole moment
$\mathcal{H}$	Hamiltonian operator
$\mathbf{I}$	nuclear spin angular momentum operator
I	nuclear spin number
I_+, I_-	raising, lowering operators, spin I
I_z	z-component angular momentum operator, spin I
p	coherence order
Q	nuclear quadrupole moment
ω_Q,	first-order qaudrupole splitting
r_{ij}	rate constant for magnetization exchange between sites i and j
$\mathbf{r_{IS}}$	internuclear vector, or dipolar vector between spin I and S
r_{IS}	internuclear distance between spin I and S
$\mathbf{S}$	nuclear spin angular momentum operator

S	nuclear spin number
$\mathbf{r_{IS}}$	internuclear vector, or dipolar vector between spin I and S
t_1, t_2	first, second dimension FID in a two-dimensional spectrum
$\mathbf{V}$	EFG tensor
V_{XX}, V_{YY}, V_{ZZ}	principal components of the EFG tensor
V_{ZZ}	the largest components of the EFG tensor

List of Figures

Chapter 1

Figure 1.1. Structure of the faujasite type zeolite and the 4 crystallographically distinct oxygen sites. 6

Figure 1.2 Structure of MFI type zeolites, showing the straight channel along b axis and sinusoidal channel along *a* axis both circumscribed by 10-rings. 7

Figure 1.3 The structure of mordenite type zeolites, showing the main channel along the c axis circumscribed by 12-rings. 9

Figure 1.4 Energy level diagram of a spin-1/2 nucleus with positive γ showing the Zeeman interaction. 12

Figure 1.5 The Larmor precession of a magnetic moment $\boldsymbol{\mu}$ in an applied magnetic field $\mathbf{B_0}$. 14

Figure 1.6 (a) An ellipsoid represents the chemical shielding tensor oriented in the laboratory frame. (b) The orientation of the chemical shielding tensor with respect to the external magnetic field, where θ and ϕ represent polar and azimuthal angles, respectively. 17

Figure 1.7 Spherical coordinates of a coupled spin pair (**I** and **S**) in a magnetic field $\mathbf{B_0}$, in which r_{IS} represents distance and θ and ϕ are the polar angles describing the orientation of the dipolar vector $\mathbf{r_{IS}}$ with respect to the laboratory frame. 21

Figure 1.8 (a) Effects of the first- and second-order quadrupolar interactions on a spin-5/2 nucleus with negative γ. The shifts caused by the second-order quadrupolar interaction are exaggerated here. (b) Schematic NMR spectra of a spin-5/2 nucleus in a single crystal showing effect of the first-order quadrupolar interaction. 26

Figure 1.9 Schematic representation of a sample spinning at magic angle $\theta = 54.74°$ with respect to the external magnetic field. 30

Figure 1.10 (a) Pulse sequences and coherence pathway for 2-D, z-filtered MQMAS NMR; (b) schematic 2D-MQMAS NMR spectrum. CS and QIS show the directions of chemical shift and quadrupolar induced shift, respectively. 34

Figure 1.11 Schematic illustration for the pulse sequence of TRAPDOR NMR. 37

Figure 1.12 Schematic illustration for the pulse sequence of REDOR NMR: (a) control and (b) double resonance experiments. 38

Figure 1.13 (a) Schematic illustration of the pulse sequence of HETCOR NMR. (b) Schematic 2-D NMR spectrum of HETCOR NMR, the signals due to the close proximities of the spin pairs I_1-S_2 and I_2-S_1 can be observed. 39

Chapter 2

Figure 2.1 NMR pulse sequence: $^1H \rightarrow {}^{17}O$-^1H CP-REDOR with shifted π pulses..... 57

Figure 2.2 (a) $^1H \rightarrow {}^{17}O$-^1H CP-REDOR NMR fraction ($1 - S/S_0$) measured as a function of the shift of the first dephasing pulse (time, t) without ^1H decoupling during the acquisition period at two different conditions. (b) comparison of the REDOR

fractions obtained from experimental data with the SIMPSON simulation results. The dipolar coupling constants used in these simulations are 13.0, 15.0, 17.5 and 19.5 kHz, corresponding to O-H distances of 1.078, 1.028, 0.976 and 0.942 Å. Spinning speed, 13 kHz; recycle delay, 1 s; ^{1}H π pulse, 6.2 μs (17.6 T) or 6.0 μs (14.1 T)..... 60

Figure 2.3 (b) Experimental ^{1}H → ^{17}O-^{1}H CP-REDOR NMR spectra, acquired without ^{1}H decoupling, as a function of the shift of the first dephasing pulse (time, *t*) at 17.6 T at 298 K and (a, c, d) simulations performed with dipolar coupling constants of 19000, 17308 and 15811 Hz, corresponding to O-H distances of 0.95, 0.98 and 1.01 Å, respectively, and no ^{1}H decoupling [7]. NMR parameters used are δ_{CS} = 21, QCC = 6.175 MHz, and η = 1. (f) ^{1}H → ^{17}O-^{1}H CP-REDOR NMR spectra at 14.1 T at 183 K and (e, g, h) simulations performed with dipolar coupling constants of 19000, 17576 and 16291 Hz, corresponding to O-H distances of 0.95, 0.975 and 1.00 Å, respectively, and no ^{1}H decoupling. NMR parameters used are δ_{CS} = 21, QCC = 6.175 MHz, and η = 1..... 64

Figure 2.4 (b) Experimental ^{1}H → ^{17}O-^{1}H CP-REDOR NMR spectra, acquired without ^{1}H decoupling, as a function of the shift of the first dephasing pulse (time, *t*) at 17.6 T at 298 K and (a, c, d) simulations performed with dipolar coupling constants of 19000, 17308 and 15811 Hz, corresponding to O-H distances of 0.95, 0.98 and 1.01 Å, respectively, and no ^{1}H decoupling [7]. NMR parameters used in all simulations are δ_{CS} = 21, QCC = 6.0 MHz, and η = 1. (f) Experimental ^{1}H → ^{17}O-^{1}H CP-REDOR NMR spectra at 14.1 T at 183 K and (e, g, h) simulations performed with dipolar coupling constants of 19000, 17576 and 16291 Hz, corresponding to O-H distances of 0.95, 0.975

and 1.00 Å, respectively, and no ^{1}H decoupling. NMR parameters used in all simulations are δ_{CS} = 21, QCC = 6.0 MHz, and η = 1. (e', g', h) simulations performed with dipolar coupling constants of 19000, 17576 and 16291 Hz, corresponding to O-H distances of 0.95, 0.975 and 1.00 Å, respectively, and no ^{1}H decoupling. NMR parameters used in all simulations are δ_{CS} = 21, QCC = 6.2 MHz, and η = 1. 65

Figure 2.5 (a) ^{1}H→ ^{17}O-^{1}H CP-REDOR NMR spectra of HZSM-5 acquired with ^{1}H decoupling, as a function of the shift of the first dephasing pulse (time, t), at 183K, 14.1 T, spinning speed, 8 kHz; recycle delay, 2 s; ^{1}H π pulse, 6.2 μs. (b) ^{1}H→ ^{17}O-^{1}H CP-REDOR NMR fraction (1 - S/S_0) measured as a function of the shift of the dephasing time (4 times of the first dephasing pulse time, t). Spinning speed, 13 kHz; recycle delay, 1 s; ^{1}H π pulse, 6.2 μs (293K, 17.6 T). Comparison of the REDOR fractions obtained from the experimental data with the simulated universal REDOR fraction curves. The dipolar coupling constants used in the simulations are 12.5kHz, 17.5kHz and 19.5kHz, corresponding to the O-H distance of 1.092Å, 0.976 Å and 0.942 Å, respectively. 69

Chapter 3

Figure 3.1 Variable temperature ^{1}H MAS NMR spectra of HZSM-5-He at 14.1 T; single pulse spectra; spinning speed =8 kHz. 83

Figure 3.2 Variable temperature ^{1}H MAS NMR spectra of HZSM-5-V at 14.1 T, single pulse, spinning speed =8 kHz. 86

Figure 3.3 $^{1}H/^{27}Al$ TRAPDOR NMR of HZSM-5-V. Low temperature data were acquired at 203K, at 14.1 T, spinning speed = 8 kHz, with ^{27}Al irradiation times of (a) 2 (250μs) and (b) 8 rotor periods (1000μs). Room temperature data were acquired at 298K, at 8.45 T, spinning speed=5 kHz, with irradiation times of (c) 1 (200 μs) and (d) 5 rotor periods (1000μs). A loss of intensity on applying ^{27}Al irradiation (the double resonance experiment) indicates that the ^{1}H species is near Al. 87

Figure 3.4 Schematic illustrations for the proton motion processes in sample HZSM-5-V upon heating from (a) 183K to (b) 213-223K and finally to (c) 293K. 92

Figure 3.5 2D ^{1}H MAS magnetization exchange spectra of HZSM-5-V at 14.1 T with mixing times of (a) 1ms, (b) 5ms and (c) 500ms at 223K, spinning speed = 9kHz; (d) mixing time 500ms at 303K, spinning speed = 8kHz. 97

Figure 3.6 DSC curve for sample HZSM-5-V, acquired with a temperature ramp rate of 2K/min 99

Figure 3.7 The Rietveld refinement (with the GSAS program) of the HZSM-5 structure with the XRD patterns obtained at two different temperatures (a) 200 and (b) 290 K, performed with the room temperature monoclinic zeolite HZSM-5 structure as a staring model..... 103

Figure 3.8 The channel structure of HZSM-5, (a) double 10-ring sinusoidal channel along the *a* direction, (b) 10-ring straight channel viewed along the *b* direction. The center oxygen atoms of those T-O-T angles increase and decrease upon cooling are labeled in red and green, respectively. 106

Chapter 4

Figure 4.1 ^{1}H MAS NMR of (a) dry zeolite H-MOR and (b) a zeolite H-MOR that contains a trace amount of water, at 17.6 T, spinning speed = 13kHz. Spinning sidebands are denoted by *. Both these samples are samples that were previously ^{17}O-enriched as described. 126

Figure 4.2 Variable temperature ^{1}H MAS NMR spectra of H-MOR at 14.1 T, single pulse, spinning speed =8 kHz. 127

Figure 4.3 Low temperature ^{1}H/ ^{27}Al TRAPDOR NMR of H-MOR acquired at 183K, at 14.1 T, spinning speed = 8 kHz, with ^{27}Al irradiation for 8 rotor periods (1000μs). A loss of intensity on applying ^{27}Al irradiation (the double resonance experiment) indicates that the ^{1}H species is nearby Al. Spinning speed = 8 kHz. 128

Figure 4.4 Measurements of (a) side pocket 8-ring of zeolite H-MOR and (b) the TMP molecule 130

Figure 4.5 ^{1}H MAS NMR of TMP/ zeolite H-MOR complexes with a loading level of 2 TMP/ u.c., sample equilibrium temperature: (a) 293 and (b) 323K. Room temperature ^{1}H MAS csecho NMR spectra of deuterated d_9-TMP/H-MOR complexes with loading levels of (c) 3.5 and (d) 10 d_9-TMP/u.c., sample equilibrium temperature: 323K. The dashed lines show the deconvoluted components. All spectra were acquired at 8.47T, with a recycle delay 2 s, at room temperature. 132

Figure 4.6 (a) $^{31}P \rightarrow {}^{1}H$ and (b) $^{1}H \rightarrow {}^{31}P$ CP MAS NMR of d_9-TMP loaded H-MOR samples with loading levels of 3.5 and 10 TMP/u. c. at 8.47T, spinning rate 9kHz, spinning sidebands are denoted with *. 136

Chapter 5

Figure 5.1 NMR pulse sequence: $^{1}H \rightarrow {}^{17}O$-$^{1}H$ CP-REDOR with shifted-pulses. 147

Figure 5.2 (a) $^{1}H \rightarrow {}^{17}O$ CP MAS NMR spectra and (b) signal intensities of zeolite H-MOR acquired at 17.6 T as a function of contact time..... 149

Figure 5.3 ^{1}H-^{17}O HETCOR NMR at 17.6T of (a) dry H-MOR, contact time: 70μs; (b) dry H-MOR, contact time: 100μs and (c) H-MOR containing trace amount of H_2O, contact time: 120μs. 154

Figure 5.4 $^{1}H \rightarrow {}^{17}O$-$^{1}H$ CP-REDOR fraction ($1-S/S_0$) measured as function of the shift of the first dephasing pulse at 17.6 T. Spinning speed: 13 kHz, recycle delay: 1s..... 157

Figure 5.5 The plot of $^{1}H \rightarrow {}^{17}O$-$^{1}H$ CP-REDOR NMR spectra as a function of the shift of the dephasing pulse with contact time of (a) 80 and (b) 120μs, at 17.6 T. Spinning speed: 13 kHz, recycle delay: 1s..... 161

Figure 5.6 Scheme for the lineshape analysis. (a) The experimental spectrum of the control experiment obtained with the contact time of 80 μs and simulations of the (b) small η and (c) large η sites resolved from the 2D ^{17}O-^{1}H HETCOR spectra. 162

Figure 5.7 NMR line shape simulations performed with the SIMPSON package[12] (a-f) show the center bands, while (a'- f') show the corresponding spectra in larger chemical

shift scale to include the spinning sidebands. (a-c) simulations performed with dipolar coupling constants of 22346, 19000 and 16290 Hz, respectively. NMR parameters used in the simulations are δ_{CS} = 27.5, QCC = 6.25 MHz, and η = 0.75 (the average values taken from the simulation results of the "large η" sites resolved in the ^{17}O-^{1}H HETCOR spectra). (d-f) simulations performed with dipolar coupling constants of 22346, 19000 and 16290 Hz, respectively. NMR parameters used in all simulations are δ_{CS} = 31, QCC = 6.4 MHz, and η = 0.45 (the values taken from the simulation results of the "small η" sites resolved in the ^{17}O-^{1}H HETCOR spectra). 164

Figure 5.8 ^{1}H-^{29}Si HETCOR NMR of zeolite H-MOR at 8.45T with contact times of (a) 500μs and (b) 10 ms. 168

Chapter 6

Figure 6.1 ^{17}O single pulse MAS NMR of zeolite H-MOR obtained at 17.6 T, spinning speed 13kHz. Spinning sidebands are denoted by " * "..... 180

Figure 6.2 (a) 2-D-^{17}O MQMAS NMR spectrum of ^{17}O-enriched H-MOR acquired at 14.1 T, with a spinning speed of 13 kHz and recycle delay of 1 s. The projections (sum) of F_2 and F_1 dimension are shown on the above and right side of the 2D-spectrum, respectively. (b), (c) and (d): slices of anisotropic dimension at 31.5, 47.0 and 54.5 ppm, respectively, in isotropic dimension (top), in comparison with simulations performed with WSolids NMR package (bottom). Simulation parameters are shown in Table 6.1a. The dotted lines in the 2-D spectrum show where the slices are taken. Note: (d) left and right

figures show one Si-O-Si site and Si-O-Si + Si-(OH)-Al two sites simulations of the slice taken at 54.5 ppm in isotropic dimension. 184

Figure 6.3 (a) 2-D-^{17}O MQMAS NMR spectrum of ^{17}O-enriched H-MOR acquired at 19.4 T, with a spinning speed of 10 kHz and recycle delay of 0.5 s. The projections (sum) of F_2 and F_1 dimension are shown on the above and right side of the 2D-spectrum, respectively. (b), (c), (d), (e), (f) and (g): slices of anisotropic dimension at 18.5, 24.0, 28.0, 34.5, 41.0 and 44.5 ppm in the isotropic dimension (top), in comparison with simulations performed with WSolids NMR package (bottom). Simulation parameters are shown in Table 6.1b. The dotted lines in 2-D spectra show where the slices are taken. Note: (f) left and right figures show one Si-O-Si site and Si-O-Si + Si-O(H)-Al two sites simulations of the slice taken at 41.0 ppm in the isotropic dimension. 190

List of Tables

Chapter 3

Table 3.1 Unit cell parameters of HZSM-5-V. 101

Table 3.2 Comparison of T-O-T angles at 200K and 290K. 104

Chapter 4

Table 4.1 Parameters extracted from the deconvolution of ^{1}H MAS and $^{31}P \rightarrow {}^{1}H$ CP-MAS NMR lineshape. 137

Chapter 5

Table 5.1 NMR parameters of ^{17}O atoms directly bound to Brønsted acid sites obtained from simulations of the HETCOR NMR slices 155

Table 5.2 ^{29}Si chemical shift values of Si atoms with different nearest neighbor atoms in typical aluminosilicates..... 169

Chapter 6

Table 6.1 δ_2s and δ_1s are the observed center of gravities of the resonances in the anisotropic (F_2) and isotropic (F_1) dimension for oxygen atoms at 14.1 T in zeolite H-MOR, respectively. The predicted values of P_Q and δ_{iso} were calculated from the observed shifts of center of gravity of the resonances, using Eq. 6.1 and 6.2. The simulation data values of QCC, η and δ_{iso} were obtained from the Wsolid simulation result of each slice. The value of P_Q can also be calculated with Eq. 6.3 using the simulation data. The predicted δ_{iso} and P_Q have been used to examine the results of lineshape simulation. 185

Table 6.2 Predicted centers of gravities of the Brønsted acid sites in the ^{17}O MQMAS spectrum obtained at 14.1T. ^{17}O NMR parameters (QCC, η and δ_{iso}) and corresponding coupled nearby ^{1}H sites were obtained in ^{1}H-^{17}O HETCOR NMR studies. The predicted centers of gravities (δ_1, δ_2) were calculated with Equation 6.1, 6.2 and 6.3.. 186

Table 6.3 δ_2s and δ_1s are the observed center of gravities of the resonances in the anisotropic (F_2) and isotropic (F_1) dimension for oxygen atoms at 19.4 T in zeolite H-MOR, respectively. The predicted values of P_Q and δ_{iso} were calculated from the observed shifts of center of gravity of the resonances, using Eq. 6.1 and 6.2. The simulation data values of QCC, η and δ_{iso} were obtained from the Wsolid simulation result of each slice. The values of P_Q calculated with Eq. 6.3 using the simulation data in comparison to the predicted values of P_Q from the observed center of gravities can be taken as an examination of the reliability of the simulation. 191

Table 6.4 Predicted centers of gravities of the Brønsted acid sites in the ^{17}O MQMAS spectrum obtained at 14.1T. ^{17}O NMR parameters (QCC, η and δ_{iso}) were obtained in ^{1}H-^{17}O HETCOR NMR studies. The predicted centers of gravities (δ_1, δ_2) were calculated with Eq. 6.1, 6.2 and 6.3. 192

Table 6.5 Structural parameters for the Brønsted acid sites of zeolites D(H)-MOR, H-Y and H-ZSM-5 reported in literatures**.**..... 193

Acknowledgments

I would like to sincerely thank my advisor, Professor Clare P. Grey, for her patience, kindness, encouragement, guidance and support during my PhD. study. I learned a lot from her, both in life and science. Having her as my advisor endows me the memory which I will cherish all my life.

I would also like to thank my committee members, Professors Stanislaus S. Wong, Brian L. Phillips, Peter Khalifah, for their guidance and help in the past five years. Professor Philip J. Grandinetti is thanked for serving as outside member.

I want to thank Dr. Boris Itin at New York Structural Biology Center (NYSBC) for his help in running the experiments at NYSBC. I am grateful to Dr. Martine Ziliox at Center for Structural Biology, SUNY at Stony Brook for helping me with high magnetic field Bruker NMR spectrometers. Dr. Zhehong Gan is acknowledged for his help during my visit to National High Magnetic Field Lab at Tallahassee.

I would like to extend my sincere gratitude to all the past and present members of our research group for their kindness and help. I have been so lucky to share science and friendship with them. I would also like to thank all my friends their support.

Finally I thank all my family, for the understanding, encouragement and help; I could never have accomplished this without their endless love.

List of Publications

1. "Low Temperature ^{1}H MAS NMR Spectroscopy Studies of Proton Motion in Zeolite HZSM-5", **Huo, Hua**; Peng, Luming; Grey, Clare P., *J Phys. Chem. C,* **2009**, 113(19), 8211-8219.

2. "Probing Brønsted acid sites in zeolite HY with low temperature ^{17}O MAS NMR spectroscopy", **Huo, Hua**; Peng, Luming; Grey, Clare P., *Studies in Surface Science and Catalysis*, 2007, 170A (From Zeolites to Porous MOF Materials), 783-789.

3. "^{17}O Magic Angle Spinning NMR Studies of Brønsted Acid Sites in Zeolites HY and HZSM-5", Peng, Luming; **Huo, Hua**; Liu, Yun; Grey, Clare P., *J. Am. Chem. Soc.*, 2007, 129(2), 335-346.

4. "^{17}O MQMAS NMR studies of zeolite HY", Peng, Luming; **Huo, Hua**; Gan, Zhehong; Grey, Clare P., *Micropor. Mesopor. Mater.*, **2008**, 109(1-3), 156-162

5. "The Search for Microporous, Strongly Basic Catalysts: Experimental and Calculated ^{29}Si NMR Spectra of Heavily Nitrogen-Doped Y Zeolites", Dogan, Fulya; Hammond,

Karl D.; Tompsett, Geoffrey A.; **Huo, Hua**; Conner, William C.; Auerbach, Scott M.; Grey, Clare P., *J. Am.. Chem. Soc.*, **2009***, 131(31),* 11062-11079.

6. "Probing Brønsted acid sites in zeolite HY and HZSM-5 with low temperature ^{17}O and ^{1}H MAS NMR spectroscopy", **Huo, Hua**; Peng, Luming; Grey, Clare P. (to be submitted)

7. "Multinuclear Solid state NMR Studies of Brønsted Acid Sites in Zeolite H-Mordenite", **Huo, Hua**; Peng, Luming; Grey, Clare P. (to be submitted)

Chapter 1

Introduction

The motivations of this dissertation are to seek explanations for some fundamental questions concerning the measurements of the O-H bond lengths of the Brønsted acidic hydroxyl groups in a model system, zeolite HY, using ^{17}O-^{1}H CP-REDOR NMR spectroscopy[1]; and to establish a systematic methodology with which to investigate the local structure and acidity of Brønsted acid sites with multinuclear NMR techniques, which can be widely applied to zeolites with more complex structures.

In Chapter 1, a brief introduction is given of the structures of the three types of zeolites (HY, HZSM-5 and H-MOR) and the NMR techniques related to the research work described in this thesis. The O-H distances in zeolite HY and HZSM-5 extracted from ^{17}O-^{1}H CP-REDOR NMR data acquired at room temperature are noticeably longer than the results from *ab-initio* calculations due to the presence of some restricted motions at room temperature.[1] Chapter 2 describes the measurement of "real" O-H bond lengths of zeolites HY and HZSM-5 at low temperature, where the motional processes can be frozen out to a large degree. In order to further illustrate the dynamics of protons in zeolite HZSM-5, low temperature ^{1}H MAS NMR spectroscopy has been performed and discussed in detail in Chapter 3. In Chapter 4-6, a combination of multinuclear NMR

techniques has been employed to determine the locations and local structures of the Brønsted acid sites in a more complex zeolite, H-MOR.

1.1 Introduction to Zeolites

Zeolites are a class of crystalline microporous aluminosilicates containing regular pore structures (i.e. cavities and channels) of molecular dimensions. The term *zeolite* originates from the Greek, meaning "boiling stone". By April 2009, 191 unique zeolite frameworks had been identified and collected in the International Zeolite Association (IZA) database of zeolite structures. The primary building units of zeolites are SiO_4 and AlO_4 tetrahedra, which link together to form the three dimensional framework by corner sharing oxygen atoms. The general formula of the zeolites is:

$$M_{x/n}(AlO_2)_x(SiO_2)_y \cdot mH_2O$$

where M^{n+} stands for a cation with the valence of +n which can balance the negative charge caused by the substitution of Si (IV) by Al(III) in the framework. The M^{n+} cations are loosely bound to framework oxygen and water molecules and can be easily exchanged for other cations in a contact solution. In most cases, water molecules can be absorbed and removed reversely without bringing an obvious change to the framework structure.[2] Zeolites are well known as “molecular sieves”, which refers to another important property of zeolites based on the pores which have molecular dimensions, that they can selectively sort molecules with suitable sizes and provide space for reactions.

Based on the properties mentioned above, exchangeable cations and selectivity controlled by the size of apertures, zeolites possess wide applications in water/gas purification, separation, detergent and reprocessing of nuclear waste. However, the most important property of zeolites is their catalytic activity. Zeolites are widely used as catalysts in the petrochemical industry, for instance in fluid catalytic cracking and hydro-cracking. Especially, the protonic forms of zeolites (prepared by ion-exchange) are powerful solid-state acids. The resultant Brønsted acid site can facilitate a host of acid-catalyzed reactions, such as isomerisation, alkylation, and cracking [3].

1.1.1 The Brønsted Acidity of Zeolites

The cation M^{n+} for the framework charge balance can be replaced by H^+. The preparation of protonic form of a zeolite involves heating a NH_4-zeolite under vacuum, which is commonly referred to as a deammoniation process. The Brønsted acidity, along with the unique porous structure of zeolites, plays an important role in controlling the performances of the many zeolite-based industrial catalysts.

Several techniques have been applied to characterize zeolite Brønsted acidity.[4] Since there is no scale of solid acidity comparable to the pK_a scale for solution, the general idea of most of these methods is to detect a measurable parameter, and then correlate this parameter with acidity. One of the most widely used methods is IR spectroscopy. Evaluation of the acid strength using IR spectroscopy is based on the theory that within force field approximation, there is a relation between electric field

gradient at the protonic site and the vibrational frequency of the OH group[4,5]. Unfortunately, the vibrational frequencies of the Brønsted groups of most zeolites are distributed over a very narrow range of frequencies (3650-3610 cm^{-1}). To make the method more sensitive, basic molecules have been added to the system to probe the electric fields[6]. IR spectroscopy can be considered as a quick semi-quantitative method for zeolite acidity detection.

Solid state NMR is also a powerful technique for investigating zeolite structure and acidity. Many ^{1}H NMR experiments have been carried out to characterize Brønsted acid sites in zeolites.[7]. Recently, ^{27}Al multiple quantum magic angle spinning (MQMAS) NMR has been successfully applied to detect the signal due to Al atoms near Brønsted acid sites.[8] Our group has developed a method to probe the oxygen atoms directly bound to acid sites by using ^{17}O NMR.[9] Efforts were made to quantify the O-H bond length in the model system of zeolite HY[10]. In this presented dissertation, in addition to the model material zeolite HY, more zeolites with equal importance in petrochemical industry and more complex structures, HZSM-5 and H-Mordenite (H-MOR), are chosen to explore the structure and the nature of Brønsted acidity of acidic catalysts by solid-state NMR techniques. According to the results of *ab-initio* calculations, the acidity of H-MOR is in between HY and H-ZSM-5[11-13], while the exact relative acidity sequence is undetermined. Our study on the acidity of these three chosen zeolites is helpful in constructing a measurement system of the strength of Brønsted acidity.

1.1.2 The Structure of Faujasite Type Zeolites

Based on different types of connections, zeolites are classified into many structural types. Zeolites with faujasite (FAU) topology attract much interest among the 191 known zeolite framework strcutures.[14] The characteristic framework of faujasite type zeolites (Figure 1.1) is composed of sodalite cages (β-cages) and hexagonal prisms (double 6-rings or D6R). Each sodalite cage connects four hexagonal prisms with their 6-rings in a tetrahedral arrangement.[15] This connection creates double 12-ring large cavities with diameters of about 7.4 Å which are so called "supercages". The supercages can allow relatively large absorbed molecules to be bound inside the pores.[15]

According to the different framework silicon/aluminum ratios, or the n(Si)/n(Al) ratio, which is equal to y/x in the general formula describing the composition of a zeolite, faujasite type zeolites can be divided into two subtypes, zeolite X with the n(Si)/n(Al) ratio from 1.0 to 1.5 and zeolite Y with the n(Si)/n(Al) ratio between 1.5 and 3.

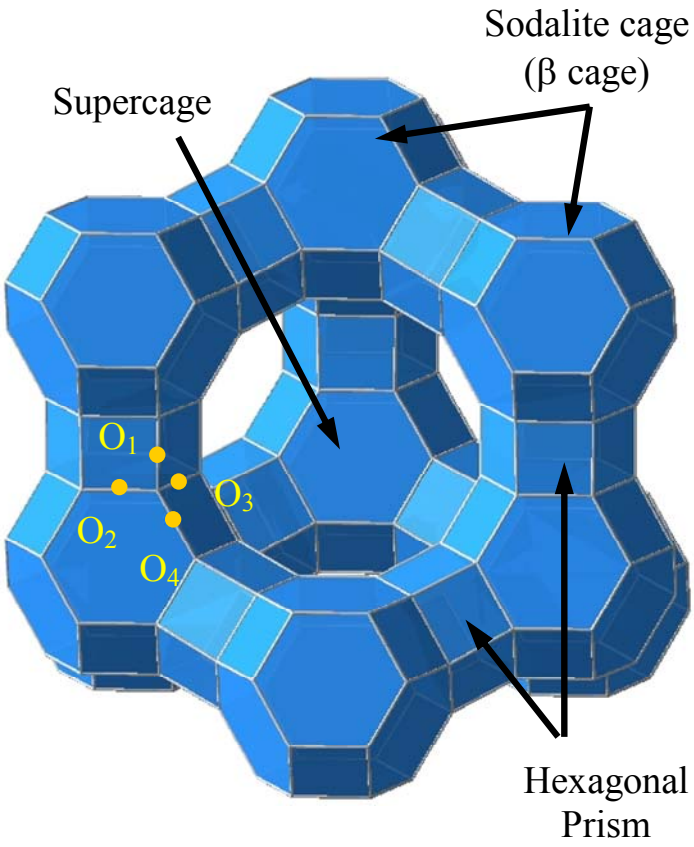

Figure 1.1. Structure of the faujasite type zeolite and the 4 crystallographically distinct oxygen sites.

1.1.3 The Structure of MFI Type Zeolites

MFI zeolites are also known as ZSM-5. The 3-dimensional structure of zeolite ZSM-5 is built up from pentasil chains running along the *c* direction. These pentasil chains form (010) pentasil layers containing the 10-rings of the straight channels oriented along the *b* direction, and (100) pentasil layers containing the sinusoidal double 10-ring channels oriented along the *a* direction[16] (Figure 1.2). HZSM-5 undergoes a transition from monoclinic ($P2_1/n.1.1$) to orthorhombic (Pnma) symmetry just above room

temperature, involving shifts of alternate (010) layers, along the c direction.[17,18] This results in a distortion of the shapes of the 10-ring straight channels. Similar monoclinic-to-orthorhombic phase transitions are frequently observed on loading NH_3, *p*-xylene, *p*-nitroamiline and various organic molecules at room temperature. [19-24]

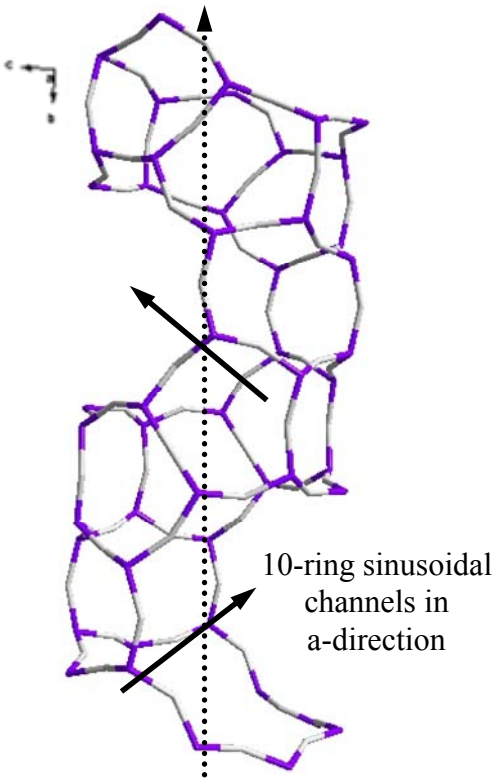

Figure 1.2 Structure of MFI type zeolites, showing the straight channel along b axis and sinusoidal channel along *a* axis both circumscribed by 10-rings.

1.1.4 The Structure of Mordenite Type Zeolites

The structure of mordenite type zeolites is shown in Figure 1.3. There are four symmetrically independent tetrahedral cation sites (T_1-T_4) and ten framework oxygen sites (O_1-O_{10}). The main channels circumscribed by 12-rings are along the *c* axis, measuring 6.5 Å * 7.0 Å. The smaller 8-ring channels are parallel to the main channels, measuring 2.6 Å * 5.7 Å. The third type of cavity in mordenite is along the *b* direction, circumscribed by 8-rings, measuring 3.4Å * 4.8 Å. This cavity which connects the 12-ring channel with the 8-ring channel through 8-rings is often referred to as the "side pocket".

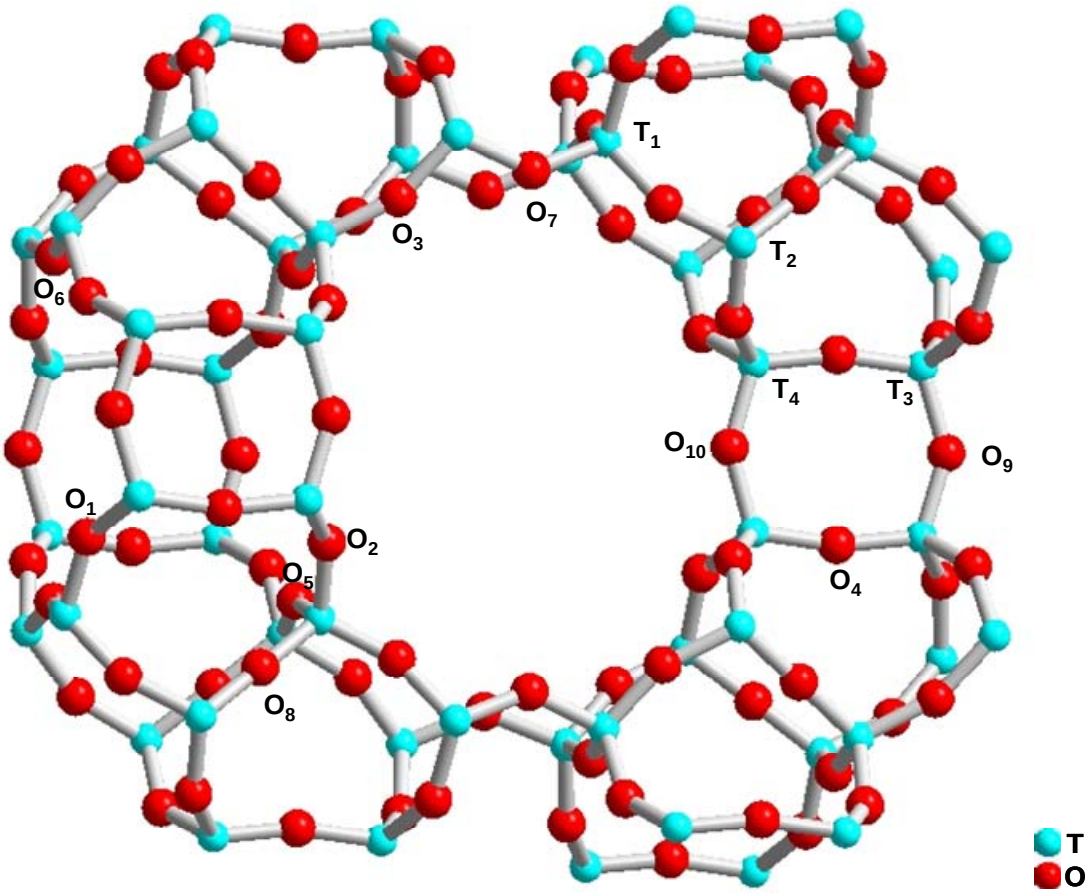

Figure 1.3 The structure of mordenite type zeolites, showing the main channel along the c axis circumscribed by 12-rings.

1.2 Interactions in Solid State NMR Spectroscopy

The interactions in solid state NMR spectroscopy can be divided into two categories: external spin interactions and internal spin interactions. The solid state NMR Hamiltonian can be described as the sum of all the interactions (summarized in Equation 1.1).

$$\mathcal{H}_{\mathbf{NMR}} = \mathcal{H}_{\mathbf{Z}} + \mathcal{H}_{\mathbf{rf}} + \mathcal{H}_{\mathbf{D}} + \mathcal{H}_{\mathbf{CS}} + \mathcal{H}_{\mathbf{K}} + \mathcal{H}_{\mathbf{J}} + \mathcal{H}_{\mathbf{P}} + \mathcal{H}_{\mathbf{Q}}^{(1)} + \mathcal{H}_{\mathbf{Q}}^{(1)} + \ldots \quad (1.1)$$

External spin interactions are the interactions between nuclear spins and a magnetic field generated by external apparatus, such as static field (Zeeman interaction) and radiofrequency transverse field. The internal spin interactions are between nuclear spin and magnetic or electric fields arising from the sample itself, including, dipole-dipole interactions (through space with nearby magnetic moments), J-coupling interactions (through surrounding electrons or indirect spin-spin coupling), shielding interactions (chemical shift, Knight shift and paramagnetic shift) and the quadrupolar interaction.

Generally, the Hamiltonian of each interaction can be described by the following equation:

$$\mathcal{H}_{\lambda} = C_{\lambda} \mathbf{I}_{\mathbf{i}} \cdot \mathbf{T}_{\mathbf{ij}}^{\lambda} \cdot \mathbf{A}_{\mathbf{j}}^{\lambda} \quad (1.2)$$

where C_{λ} is the constant for a specific interaction λ, I_i is the nuclear spin, $\mathbf{T}_{\mathbf{ij}}^{\lambda}$ is the 3×3 second-rank space tensor describing the anisotropy of the interaction and $\mathbf{A}_{\mathbf{j}}^{\lambda}$ is the coupling partner of spin I (i.e., spin I or S, or external magnetic field). Line broadening

often occurs in solid state NMR spectra due to the presence of angular dependent anisotropic interactions and once was thought as a hindrance. Actually, these spin interactions in NMR spectroscopy can provide valuable information on chemistry, structure or dynamics in the solid state. In the past two decades, solid state NMR spectroscopy has become an extremely important tool for structure determination.

In the following sections, a brief introduction on selected important interactions in solid-state NMR will be given based on selected books and dissertations.[25-33]

1.2.1 Zeeman Interaction

The classical Zeeman interaction is the interaction between a magnetic moment and an externally applied magnetic field. The Hamiltonian can be described as

$$\mathcal{H}_Z = -\gamma\hbar\mathbf{I}\cdot\mathbf{B_0} \tag{1.3}$$

where γ and $\mathbf{B_0}$ are the gyromagnetic ratio of spin **I** and the external static magnetic field, respectively. In the usual convention of NMR, $\mathbf{B_0}$ is defined along the z-axis of the lab frame, i.e., $\mathbf{B_0} = (0, 0, B_0)$. Thus Equation 1.3 can be re-written as:

$$\mathcal{H}_Z = -\gamma\hbar\left(I_x, I_y, I_z\right)\cdot\begin{pmatrix}0\\0\\B_0\end{pmatrix} = -\gamma\hbar B_0 I_z \tag{1.4}$$

If no external field is applied, the energy of a single spin **I** is independent on the magnetic quantum number, m, where $m = -I, (-I+1),\ldots, (I-1), I$. Upon the application of an

externally magnetic field, the degenerate energy levels of nuclear spin **I** is split into (2*I*+1) non-degenerate levels according to the values of *m*. The energy levels, E_m, are determined by the eigenvalues of the Hamiltonian operator. Thus,

$$E_m = -\gamma\hbar m B_0 . \qquad (1.5)$$

In the simplest case of a spin ½ nucleus, where *I*=1/2 and *m*=±1/2, there are only two possible eigenstates with energies $E_{\mp 1/2} = \pm \tfrac{1}{2}\gamma\hbar B_0$. The energy levels are shown in Figure 1.4.

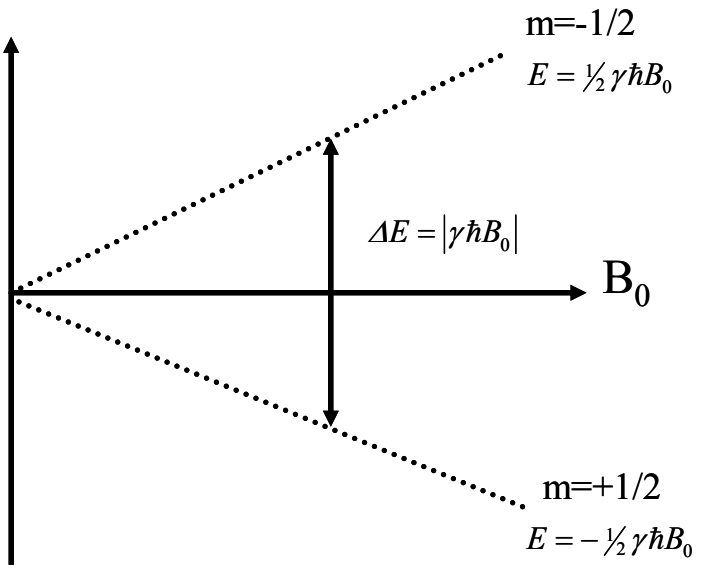

Figure 1.4 Energy level diagram of a spin-1/2 nucleus with positive γ showing the Zeeman interaction.

These states are known as the Zeeman states. At equilibrium, the populations of these states follow the Boltzmann distribution, which is given by (with the high temperature approximation)

$$\frac{N_{\pm 1/2}}{N} = \frac{\exp(^{-E_{\pm 1/2}}/_{k_B T})}{\exp(^{-E_{+1/2}}/_{k_B T}) + \exp(^{-E_{-1/2}}/_{k_B T})} \approx \frac{1}{2} \pm \frac{\gamma \hbar B_0}{k_B T} \qquad (1.6)$$

where k_B and T stand for the Boltzmann constant and the absolute temperature, respectively. For a spin-1/2 nucleus with a positive γ value, the +1/2 state is lower in energy thus is more populated. This indicates a net longitudinal polarization, or a magnetization in the same direction as the external magnetic field.

Transitions between neighboring states (Δm=±1), can be introduced by applying electromagnetic radiation with appropriate frequency ν_0. The energy of this transition is expressed as

$$\Delta E = h\nu_0 = \left|\gamma \hbar B_0\right| \qquad (1.7)$$

where $\nu_0 = |\gamma/2\pi|B_0$ is known as the Larmor frequency with the unit of Hz or written as $\omega_0 = \gamma B_0$ in term of rad·s^{-1}. The rotation of a magnetic moment about the direction of external field B_0 is named as the Larmor precession (Figure 1.5).

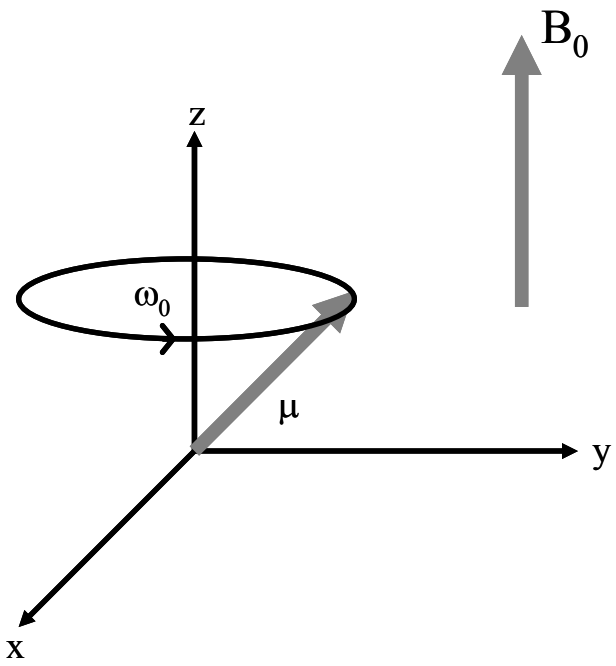

Figure 1.5 The Larmor precession of a magnetic moment $\boldsymbol{\mu}$ in an applied magnetic field $\mathbf{B_0}$.

1.2.2 Radiofrequency Interaction

In a Fourier transformation NMR experiment, a pulsed radiofrequency (rf) field with a frequency ω_{rf}, so-called carrier frequency, is applied to excite the nuclear spin system under study. This frequency ω_{rf} is usually close to the Larmor frequency ω_0. The Hamiltonian of this spin-rf field interaction is written as,

$$\mathcal{H}_{rf} = -\gamma\hbar\mathbf{I}\cdot\mathbf{B_1} \tag{1.8}$$

where $\mathbf{B_1}$ is the rf field. This field is set to be along the x-direction, perpendicular to the external field B_0, and can be expressed by

$$\mathbf{B_1} = (2B_1 \cos(\omega_{rf} t + \varphi), 0, 0) \tag{1.9}$$

where B_1 and φ represent the amplitude and the phase of the rf field, respectively. Now Equation 1.8 can be expressed as

$$\mathcal{H}_{rf} = -2\gamma\hbar B_1 \cos(\omega_{rf} t + \varphi) I_x \tag{1.10}$$

The total external spin Hamiltonian H_{ext} during a pulse is

$$\mathcal{H}_{ext} = \mathcal{H}_Z + \mathcal{H}_{rf} = \hbar\omega_0 I_z + 2\hbar\omega_1 \cos(\omega_{rf} t + \varphi) I_x \tag{1.11}$$

where $\omega_1 = -\gamma B_1$ is the frequency of the rf field. It will be easier to treat the Hamiltonian if the time-dependent term can be converted to time-independent. The concept of the "rotating frame", which rotates around the z-axis with a frequency ω_{rf}, is introduced to deal with this problem. The rf field in the rotating frame becomes stationary and can be described as

$$\mathbf{B_1} = (B_1 \cos\varphi, B_1 \sin\varphi, 0) \tag{1.12}$$

The new time-independent external spin Hamiltonian H'_{ext} in this frame can be written as

$$\mathcal{H}'_{ext} = \hbar(\omega_{rf} - \omega_0) I_z + \hbar\omega_1 (I_x \cos\varphi + I_y \sin\varphi) \tag{1.13}$$

where $(\omega_{rf} - \omega_0)$ is the resonance offset. When the 'on resonance' condition is met, $(\omega_{rf} - \omega_0) \ll \omega_1$, thus the effective field B_{eff} in the rotating frame is approximately B_1. Therefore, during an rf pulse, the bulk magnetic moment associated with the nuclear

spins, or magnetization, can be considered as rotating around the direction of the B_1 field in the rotating frame. The tipping angle of the magnetization, θ_P, is determined by the duration of the rf pulse, τ_P:

$$\theta_P = \gamma B_1 \tau_P \tag{1.14}$$

1.2.3 Chemical Shielding Anisotropy

The chemical shielding arises from the change in the actual magnetic field at the nucleus since the applied magnetic field induces changes in electrons about the nucleus with generate local fields. This effect can either add to or subtract from the main applied field (termed paramagnetic or diamagnetic, respectively). Hence, this interaction between the nuclear spin and the field induced by the electrons is called the 'chemical shielding interaction', as it reflects the local electronic environments. The corresponding Hamiltonian is

$$\mathcal{H}_{CS} = -\gamma h \mathbf{I} \cdot (-\boldsymbol{\sigma}) \cdot \mathbf{B_0} = \gamma h \mathbf{I} \cdot \boldsymbol{\sigma} \cdot \mathbf{B_0} = \gamma h \mathbf{I} \cdot \mathbf{B_{loc}} \tag{1.15}$$

where σ is a second-rank Cartesian tensor called the chemical shielding tensor, which is a 3×3 matrix with 9 components used to define the relative orientation of chemical shielding tensor with respect to the lab frame (Equation 1.16), while B_{loc} is the induced local magnetic field.

The tensor $\boldsymbol{\sigma}$ can be diagonalized to yield a tensor with only three principal components σ_{11}, σ_{22}, σ_{33}, which describe the interaction in its own principal axis system (PAS (Equation 1.16).

$$\boldsymbol{\sigma} = \begin{pmatrix} \sigma_{xx} & \sigma_{xy} & \sigma_{xz} \\ \sigma_{yx} & \sigma_{yy} & \sigma_{yz} \\ \sigma_{zx} & \sigma_{zy} & \sigma_{zz} \end{pmatrix}_{sym} \xrightarrow{L \to P} \begin{pmatrix} \sigma_{11} & 0 & 0 \\ 0 & \sigma_{22} & 0 \\ 0 & 0 & \sigma_{33} \end{pmatrix} \tag{1.16}$$

The relative orientation of the NMR tensor, e.g., chemical shielding tensor, in its PAS, with respect to the laboratory frame, is shown in Figure 1.6.

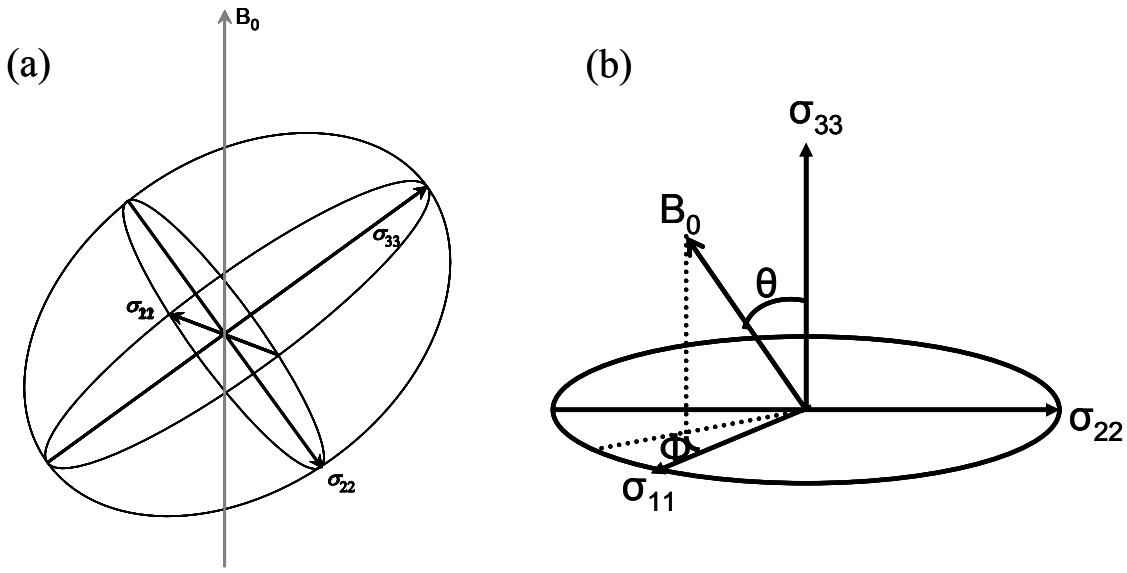

Figure 1.6 (a) An ellipsoid represents the chemical shielding tensor oriented in the laboratory frame. (b) The orientation of the chemical shielding tensor with respect to the external magnetic field, where θ and ϕ represent polar and azimuthal angles, respectively.

The principal components of the chemical shift tensor can be defined as $\sigma_{11} \leq \sigma_{22} \leq \sigma_{33}$ where σ_{33} is the most shielded. However, the variation of different components of the shielding tensor is characterized by three parameters (σ_{iso}, Ω and κ) rather than these three principal components. The isotropic chemical shielding, σ_{iso}, can be written as

$$\sigma_{iso} = \frac{1}{3}\left(\sigma_{11} + \sigma_{22} + \sigma_{33}\right). \tag{1.17}$$

It reflects the local electric structure and has been used to identify chemical distinct species. The breadth of the powder pattern arising from the presence of the chemical shift anisotropy (CSA) is described by the *span* (Ω).

$$\Omega = \sigma_{33} - \sigma_{11} \tag{1.18}$$

And the shape of the powder pattern is described by the skew (κ),

$$\kappa = 3(\sigma_{iso} - \sigma_{22}) / \Omega = 3(\sigma_{iso} - \sigma_{22}) /(\sigma_{33} - \sigma_{11}) \tag{1.19}$$

where $-1 \leq \kappa \leq 1$.

Instead of chemical shielding, the practical parameter measured in NMR experiments is chemical shift, which is the nuclear magnetic shielding with respect to some reference compound. The two parameters are related to each other by

$$\delta = \frac{\sigma_{ref} - \sigma_{sample}}{1 - \sigma_{ref}} \tag{1.20}$$

which to a good approximation for $|\sigma_{ref}| \ll 1$ gives

$$\delta_{sample} = \sigma_{ref} - \sigma_{sample} \tag{1.21}$$

The principal components of the chemical shift tensor are defined as $\delta_{11} \geq \delta_{22} \geq \delta_{33}$, where δ_{33} is the most shielded component. Equation 1.17, 1.18 and 1.19 can be rewritten as $\delta_{iso} = \frac{1}{3}(\delta_{11} + \delta_{22} + \delta_{33})$, $\Omega = \delta_{11} - \delta_{33}$ and $\kappa = 3(\delta_{22} - \delta_{iso})/\Omega$.

In solution NMR, the anisotropy of the chemical shift is averaged out by the fast tumbling of molecules and only the isotropic chemical shift remains. In solid state NMR, the chemical shielding anisotropy gives rise to broadening of the spectrum. In many cases, this interaction is so large that the resonance is too broad to observe. High resolution spectra can be obtained using techniques such as magic angle spinning (MAS). A brief introduction of MAS will be given in section 1.3.1.

1.2.4 Dipole-Dipole Interaction

A nuclear spin can also experience a local magnetic field generated by nearby spins. This interaction is strongly dependent on the distance between the nuclear spins and the internuclear vector with respect to the direction of the applied magnetic field. The dipolar Hamiltonian for two spins I and S can be written as

$$\mathcal{H}_D = \mathbf{I} \cdot \mathbf{D} \cdot \mathbf{S} = hD_{IS}\left(3(\mathbf{I} \cdot \mathbf{r_{IS}})(\mathbf{S} \cdot \mathbf{r_{IS}})/r_{IS}^2 - \mathbf{I} \cdot \mathbf{S}\right) \tag{1.22}$$

where **D** is a symmetric and traceless tensor, called the dipolar coupling tensor, $\mathbf{r}_{IS}$ is the dipolar vector between spins I and S. D_{IS} is the dipolar coupling constant, which can be expressed as

$$D_{IS} = -\left(\frac{\mu_0}{4\pi}\right)\frac{\gamma_I \gamma_S \hbar}{r_{IS}^3} \tag{1.23}$$

where r_{IS} is the internuclear distance between spin I and S and μ_0 is the permeability constant. The magnitude of the dipolar coupling constant is inversely proportional to the cube of the internuclear distance. Hence, the internuclear distance in a rigid system can be determined by the measurement of the dipolar coupling constant.

The direct dipolar Hamiltonian is often expressed, in terms of spherical polar coordinates, as

$$\mathcal{H}_D = hD_{IS}(A + B + C + D + E + F) \tag{1.24}$$

where

$$A = (3\cos^2\theta - 1)I_z S_z$$

$$B = -\frac{1}{4}(3\cos^2\theta - 1)\left[I_+ S_- + I_- S_+\right]$$

$$C = \frac{3}{2}\sin\theta\cos\theta e^{-i\phi}\left[I_+ S_z + I_z S_+\right]$$

$$D = \frac{3}{2}\sin\theta\cos\theta e^{i\phi}\left[I_- S_z + I_z S_-\right]$$

$$E = \frac{3}{4}\sin^2\theta e^{-2i\phi}\left[I_+ S_+\right]$$

$$F = \frac{3}{4}\sin^2\theta e^{2i\phi}\left[I_- S_-\right] \tag{1.25}$$

in which I_z, I_+, I_-, S_z, S_+ and S_- are nuclear spin operators, and θ and Φ are the polar angles describing the relative orientation of the dipolar vector $\mathbf{r_{IS}}$ with respect to the

external magnetic field (Figure 1.7). The raising (+) and lowing (-) operators are defined as

$$O_{\pm} = O_x \pm iO_y \quad ; \quad O = I, S \quad . \tag{1.26}$$

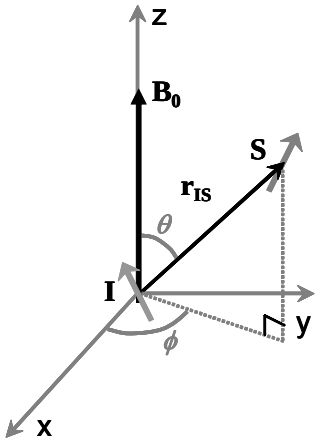

Figure 1.7 Spherical coordinates of a coupled spin pair (**I** and **S**) in a magnetic field $\mathbf{B_0}$, in which r_{IS} represents distance and θ and ϕ are the polar angles describing the orientation of the dipolar vector $\mathbf{r_{IS}}$ with respect to the laboratory frame.

In Equation 1.25, term *A* is referred to as the secular dipolar coupling which can be treated as a perturbation in the Zeeman Hamiltonian resulting in a broadening of the spectrum due to its orientation-dependent nature. Term *B* contains the flip-flop term, ($I_+S_- + I_-S_+$), only connecting spin states that differ in the polarization of the two spins. In the homonuclear dipolar interaction, the spin pairs may exchange energy in a flip-flop process by the mutual reorientation of the magnetization vectors. This flip-flop process is energy conserving and occurs with non-negligible probability when the difference in

resonance frequencies between two spins is smaller than the dipolar strength. Terms *C* and *D* are single quantum terms, while terms *E* and *F* are double quantum terms. They all lead to mixing of the Zeeman states.

In the high field approximation, if all the time dependent terms (containing ϕ), in the rotating frame are neglected, the Hamiltonian can be simplified as

$$\mathcal{H}_D = hD_{IS}(3\cos^2\theta - 1)\left(I_Z S_Z - \frac{1}{4}(I_+ S_- + I_- S_+)\right) \qquad (1.27)$$

In heteronuclear spin systems a further simplification occurs due to the weak coupling by dropping all terms that involve transverse spin operators (the operators related to I_+ and I_-):

$$\mathcal{H}_D = hD_{IS}(3\cos^2\theta - 1)I_Z S_Z \qquad (1.28)$$

Since the dipolar interaction is angular dependent, and the dipolar vectors in solids are randomly orientated with respect to the magnetic field, the dipole-dipole interaction causes a distribution of resonance frequencies. This dipolar broadening of NMR signal often prevents the observation of the chemical shifts of chemically distinct spins. Therefore, in order to eliminate this anisotropic broadening and obtain high resolution NMR spectra, MAS is usually applied. However, the dipolar interaction can provide useful information on spin connectivities. Many double resonance techniques can reintroduce the dipolar interaction under MAS conditions and will be briefly reviewed in section 1.3.3 and 1.3.4.

1.2.5 Quadrupolar interaction

Quadrupolar nuclei have a spin > 1/2, and an asymmetric distribution of nucleons giving rise to a non-spherical positive electric charge distribution; this is in contrast to spin-1/2 nuclei, which have a spherical distribution of positive electric charge. The asymmetric charge distribution in the nucleus is described by the nuclear electric quadrupole moment, eQ, which is an intrinsic property of the nucleus, and remains as a constant regardless of the environment. The interaction between the quadrupole moment and the electric field gradient (EFG) is called the quadrupolar interaction. EFG is caused by surrounding electrons distribution and can be represented by a symmetric traceless Cartesian tensor **V**, described by only three components V_{XX}, V_{YY} and V_{ZZ}, in its principal axis system (PAS). The magnitude these components follow $|V_{ZZ}| > |V_{YY}| > |V_{XX}|$ and $|V_{XX}| + |V_{YY}| + |V_{ZZ}| = 0$. The size of EFG is defined as

$$eq = V_{ZZ} \tag{1.29}$$

The shape of the tensor can be represented by an asymmetry parameter η, which is written as

$$\eta = (V_{XX} - V_{YY}) / V_{ZZ} \tag{1.30}$$

Thus, η ranges from 0, corresponding to axial symmetry, to 1. Determination of the value of η may give the information of the local symmetry of the nucleus in study. The size of

the quadrupolar interaction is usually represented by quadrupole coupling constant (*QCC*), defined as

$$QCC = eqeQ / h \tag{1.31}$$

in units of Hz. Since the quadrupole moment, *eQ*, is a constant for a given quadrupolar nucleus, the size of the QCC is often used as a measure of the local distortion around the nucleus.

The Hamiltonian of the quadrupolar interaction is written as

$$\mathcal{H}_Q = \frac{eQ}{2I(2I-1)h}\mathbf{I}\cdot\mathbf{V}\cdot\mathbf{I} \tag{1.32}$$

In the PAS, it can be described conveniently by

$$\mathcal{H}_Q = \frac{1}{6}\omega_Q\left[(3I_Z^2 - I(I+1) + \eta(I_X^2 - I_Y^2)\right] \tag{1.33}$$

where ω_Q is the quadrupole frequency in units of Hz, and can be expressed as

$$\omega_Q = \frac{3e^2qQ}{2I(2I-1)h} = \frac{3(QCC)}{2I(2I-1)} \tag{1.34}$$

In NMR spectroscopy, the quadrupolar interaction can often be treated as a small perturbation of the Zeeman interaction provided $\omega_Q << \omega_0$. The quadrupolar Hamiltonian, is then rearranged into a form with components commuting with the Zeeman spin operator $\omega_0 I_Z$, and is described as

$$\mathcal{H}_Q = \mathcal{H}_Q^{(1)} + \mathcal{H}_Q^{(2)} \tag{1.35}$$

where $\mathcal{H}_Q^{(1)}$ and $\mathcal{H}_Q^{(2)}$ are the first- and second-order quadrupolar Hamiltonians.

The $\mathcal{H}_Q^{(1)}$ term can be written as

$$\mathcal{H}_Q^{(1)} = \frac{1}{2} Q^{'}(\theta,\phi)\left[I_z^2 - \frac{1}{3} I(I+1) \right] \tag{1.36}$$

where $Q^{'}$, the first-order quadrupolar splitting, is a function of θ and ϕ,

$$Q^{'} = \frac{1}{2}\omega_Q(3\cos^2\theta - 1 + \eta\sin^2\theta\cos 2\phi) \tag{1.37}$$

where θ and ϕ are the polar angles define the relative orientation of the EFG tensor with respect to B_0. The full expression for the more complicated second-order quadrupolar Hamiltonian term $\mathcal{H}_Q^{(2)}$ is given elsewhere.[34] In general, the transition frequency between energy states *m* and *m*-1 for a quadrupolar nucleus can be written as

$$\omega_{m-1,m} = \omega_0 + \omega_{m-1,m}^{(1)} + \omega_{m-1,m}^{(2)} \tag{1.38}$$

where $\omega_{m-1,m}^{(1)}$ and $\omega_{m-1,m}^{(2)}$ represent the frequency change induced by the first- and second-order quadrupolar interactions, respectively.

The discussion below about the first-order interaction will focus on the case $\eta = 0$, when the term $\eta\sin^2\theta\cos 2\phi$ vanishes. The effects of the first-order quadrupolar interaction between energy states *m* and *m*−1 is then given by

$$\omega_{m-1,m}^{(1)} = \frac{1}{4}\omega_Q(3\cos^2\theta - 1)(1-2m) \tag{1.39}$$

Therefore, the central transition connecting the m=+1/2 and m= -1/2 states is not affected by the first-order quadrupolar interaction. However, all the satellite transitions are affected and 2*I* resonances are observed separated by $Q^{'}$ in the NMR spectrum. In

addition, the resonances are broadened since the term for $\omega_{m-1,m}^{(1)}$ is now angle-dependent. Figure 1.8 shows the effect of the quadrupolar interaction on the energy state of a spin-5/2 nucleus (e.g., ^{17}O).

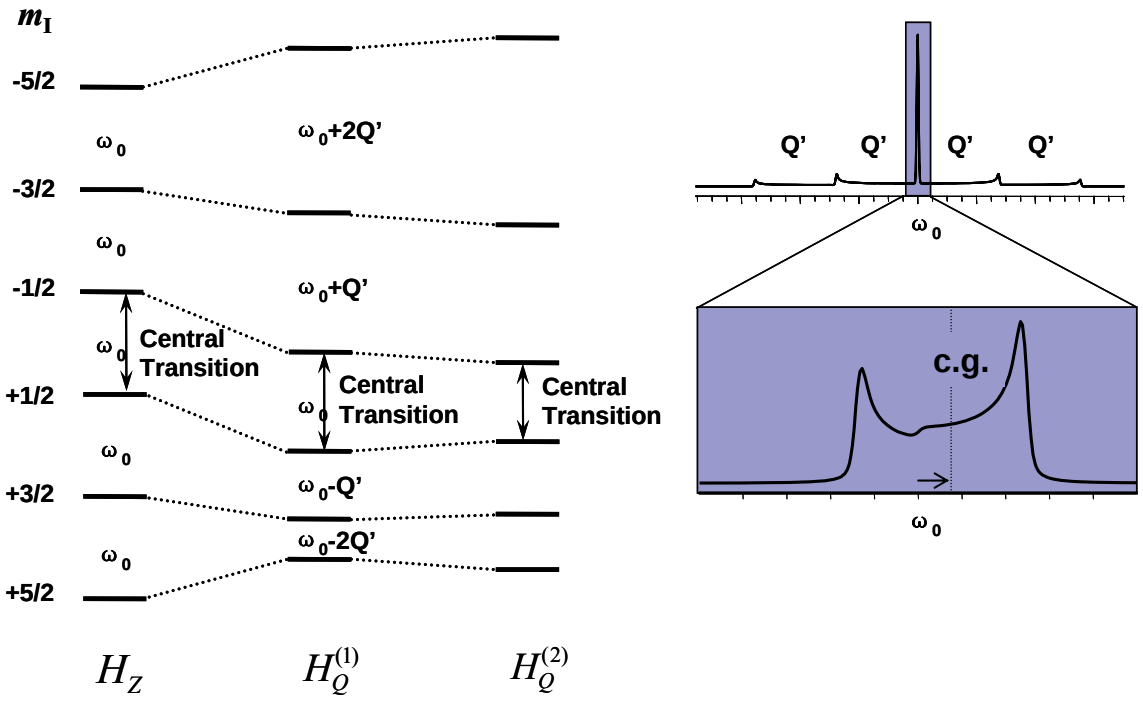

Figure 1.8 (a) Effects of the first- and second-order quadrupolar interactions on a spin-5/2 nucleus with negative γ. The shifts caused by the second-order quadrupolar interaction are exaggerated here. (b) Schematic NMR spectra of a spin-5/2 nucleus in a single crystal showing effect of the first-order quadrupolar interaction.

The second-order quadrupolar interaction is smaller than the first-order quadrupolar interaction by 2 to 3 orders of magnitude. However, if the quadrupolar

interaction is very large, the second-order quadrupolar interaction can affect the central transition significantly. As a result, the resonance is broadened and the center of gravity of the peak is shifted away from the isotropic chemical shift. This is known as the second-order quadrupolar induced shift. The induced shift caused by the second-order quadrupolar interaction of the central transition resonance, when $\eta = 0$, is given by

$$\omega^{(2)}_{½,-½} = \frac{\omega_Q^2}{16\omega_0}\left[I(I+1) - \frac{3}{4}\right](3\cos^2\theta - 1)(1 - 9\cos^2\theta) \qquad (1.40)$$

This effect is proportional to the square of ω_Q and inversely proportional to the Larmor frequency ω_0. Thus, the effect of the second-order quadrupolar interaction can be reduced by acquiring the spectrum at a higher external magnetic field. The second-order quadrupolar interaction cannot be completely averaged by MAS, resulting in broad anisotropic lineshapes in the spectra, making the interpretation of the spectra difficult. In the past two decades, many techniques have been developed to obtain high-resolution spectra by removing the second-order quadrupolar line broadening. Currently, the most widely used techniques are double-rotation (DOR)[35], dynamic angle spinning (DAS)[36] and multiple-quantum magic angle spinning (MQMAS).[37] Recently, satellite transition magic angle spinning (STMAS)[38] NMR has also attracted a lot of attention. The MQMAS technique will be discussed briefly in section 1.3.3.

1.2.6 Scalar Coupling

Scalar coupling is an indirect interaction between two nuclear spins mediated through the bonding electrons. In contrast to the through-space dipole-dipole interaction, scalar coupling is a through-bond interaction, which is also referred to as spin-spin coupling, indirect coupling or J-coupling. The mechanism could be thought of as one nucleus perturbing the surrounding electrons which then produces an additional magnetic field in the second nucleus. The Hamiltonian for the interaction is given by,

$$H_J = \mathbf{I} \cdot \mathbf{J} \cdot \mathbf{S} \tag{1.41}$$

where the **J** tensor defines the relative orientation of the J-coupling with respect to the magnetic field. The **J** tensor is axially symmetric with the unique component coincident with $\mathbf{r_{IS}}$.

The J-coupling between spins I and S results in splitting of the peak in the spectrum of spin I into 2S+1 evenly spaced lines without considering the quadrupolar interaction. Unlike the dipole-dipole interaction, J-coupling can not be averaged out by fast random motion. The source of the scalar coupling could be spin-orbital, spin-dipolar and Fermi contact interactions. As shown in Equation 1.41, there is no B_0 dependence on the coupling.

1.3 Introduction to Solid-State NMR Techniques

In this part, I will first briefly introduce the most fundamental solid-state NMR techniques: Magic Angle Spinning (MAS) and Cross Polarization (CP). Then a few two-dimensional or double resonance techniques tightly involved with the research work in this dissertation will be discussed.

1.3.1 Magic Angle Spinning (MAS)

In solution NMR, fast molecular motion effectively removes the anisotropic interactions and narrow resonances can be observed. In solid-state NMR spectroscopy, the lack of molecular motion leads to broadening of the resonances. Therefore, efforts have been made to develop techniques to acquire high resolution NMR spectra.

E. R. Andrew introduced the revolutionary technique, magic angle spinning (MAS),[39] which involves rotating the sample at a 'magic angle' of 54.74° with respect to the external magnetic field, to eliminate anisotropic interactions such as the chemical shielding interaction, heteronuclear dipolar coupling and first-order quadrupole coupling (Figure 1.9). It is clear that there is an angular dependence of $(3\cos^2\theta - 1)$ in the anisotropic interactions mentioned above (Equation 1.25 and 1.39). When θ is set to 54.74°, the term $(3\cos^2\theta - 1)$ vanishes and high resolution NMR spectra are obtained. When the spinning frequency is faster than the size of the anisotropic interaction, only a

single resonance is observed; otherwise, the powder pattern is split into an isotropic resonance with spinning sidebands separated at intervals of the spinning frequency.

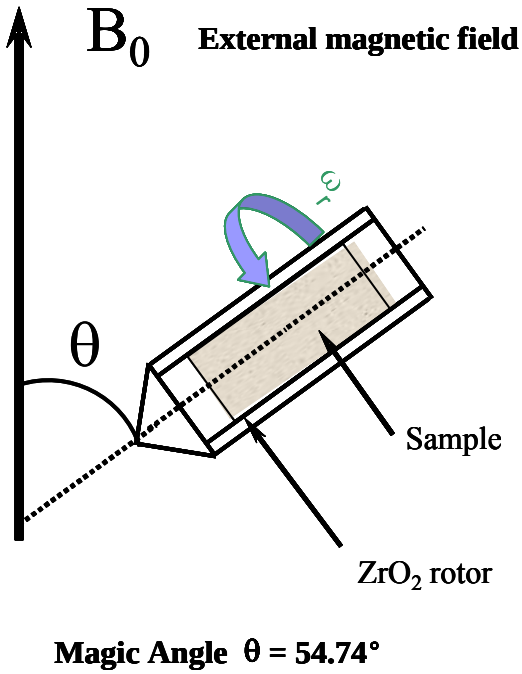

Figure 1.9 Schematic representation of a sample spinning at magic angle θ = 54.74° with respect to the external magnetic field.

1.3.2 Cross Polarization (CP)

In systems containing two nuclei I and S, one with more abundant spins than the other, cross polarization (CP)[40] is routinely used in solid-state NMR to enhance the sensitivity of dilute S spins by transferring polarization from abundant I spins. The signal intensity can increase by a factor of γ_I/γ_S. In addition, the longitudinal relaxation time (T_1) of the abundant spin I determines the recycle delay of the experiment. This time is

usually much shorter than the T_1 of the dilute spin S, thus a greater number of scans can be collected in the same time period.

The transfer of polarization from the more abundant nucleus I to the less abundant nucleus S is implemented by irradiating both nuclei at their correct Larmor frequencies in fulfillment of the following condition:

$$\omega_{1I} = \gamma_I B_{1I} = \gamma_S B_{1S} = \omega_{1S} \tag{1.42}$$

which is known as the Hartmann-Hahn condition.[41] This irradiating period is called the contact time in the CP experiment and usually is varied from tens of microseconds to hundreds of milliseconds. In the presence of spin-locking fields, the interaction of the I and S spins can be considered in the double rotating frame where rf fields become time-independent and the Zeeman splittings ($\omega_{1I} = \omega_{1S}$) are the same. Thus polarization transfer between I and S spin pairs is now allowed.

For CP experiments involving quadrupolar nuclear spins S, the Hartmann-Hahn condition is related to first-order quadrupole splitting, Q':[42]

$$\omega_{1I} = \omega_{1S} \quad \text{for} \quad \omega_{1S} >> \left|Q'\right| \tag{1.43}$$

$$\omega_{1I} = (S + \frac{1}{2})\omega_{1S} \quad \text{for} \quad \omega_{1S} << \left|Q'\right| \tag{1.44}$$

In the intermediate regime when ω_{1S} and Q' is comparable, the Hartmann-Hahn match is very difficult to meet.

For CP under MAS condition, the dipolar interaction becomes time dependent. The best match is usually at:[40,43]

$$\omega_{1I} = \omega_{1S} + n\omega_r \qquad n = \pm 1,2, \quad \text{for} \quad \omega_{1S} >> \left|Q^{'}\right| \qquad (1.45)$$

$$\omega_{1I} = (S + \frac{1}{2})\omega_{1S} + n\omega_r \quad n = \pm 1,2, \quad \text{for} \quad \omega_{1S} << \left|Q^{'}\right| \qquad (1.46)$$

where ω_r is the spinning rate. Equation 1.42 also applies for two sets of spin-1/2 nuclei. In practice, the Hartmann-Hahn condition is usually optimized using a model compound with a good signal to noise ratio.

1.3.3 Multiple Quantum Magic Angle Spinning (MQMAS)

The second-order quadrupolar line broadening can be eliminated by using Multiple Quantum MAS (MQMAS) NMR[44]. In 1995, Frydman and Harwood[37] introduced the MQMAS experiment, which provides 2D high-resolution NMR spectra of quadrupole nuclei with half-integer spin in solids, by refocusing the fourth-rank elements of the second-order quadrupole interaction in spin space. In this 2-D NMR method, an isotropic dimension, free of second-order quadrupolar line broadening, is obtained in addition to the normal anisotropic dimension. This technique does not require special probe hardware, thus it has attracted great interest. A lot of variations have been developed to improve the performance of MQMAS. The pulse sequence and coherence pathway of a standard z-filtered MQMAS NMR[45] are shown in Figure 1.10(a). The multiple-quantum coherence (MQ) evolves during t_1. This is followed by a 2nd hard pulse, which converts the MQ coherence to zero-quantum order. A soft pulse follows the z-filter and converts the zero-quantum coherence to single-quantum coherence (central

transition) for observation during t_2. The basic idea of this method is the anisotropic line broadening term under multiple quantum evolution during t_1 can be chosen to have opposite sign to that under single quantum evolution in t_2; thus a pure isotropic echo can be formed in t_2.

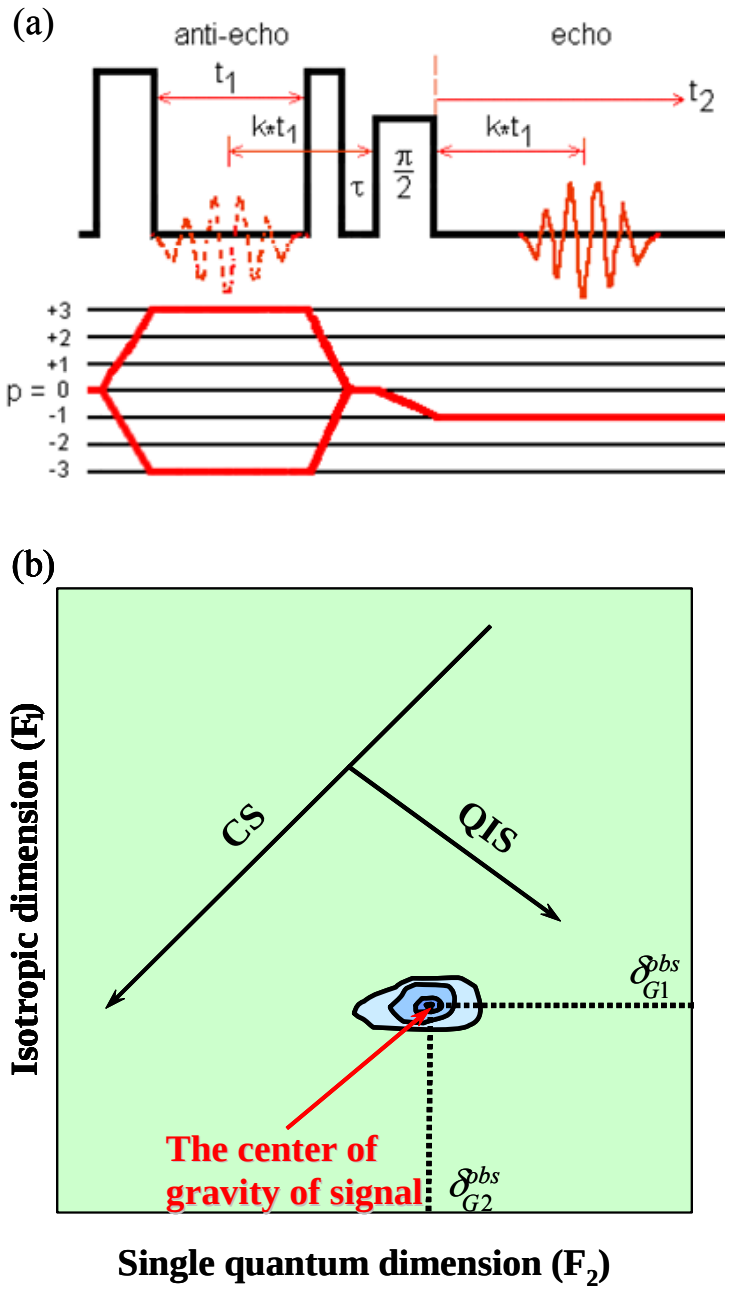

Figure 1.10 (a) Pulse sequences and coherence pathway for 2-D, z-filtered MQMAS NMR; (b) schematic 2D-MQMAS NMR spectrum. CS and QIS show the directions of chemical shift and quadrupolar induced shift, respectively.

A schematic MQMAS NMR spectrum is shown in Figure 1.10(b). F_2 is the normal anisotropic dimension while F_1 is the high resolution isotropic dimension obtained after a shear. The Isotropic chemical shift δ_{CS}^{iso} and quadrupole induced shift (QIS) can be obtained from the data conveniently. The latter contains the information concerning the quadrupolar parameters, QCC and η, which can be extracted by simulating slices performed along F_2. In this dissertation, the convention proposed by J.-P. Amoureux and C. Fernandez will be used,[46] which gives

$$\delta_{CS}^{iso} = \frac{10}{27}\delta_{G2}^{obs} + \frac{17}{27}\delta_{G1}^{obs}, \tag{1.47}$$

$$P_Q = \frac{4S(2S-1)\nu_0}{1000}\sqrt{\frac{170(\delta_{G1}^{obs} - \delta_{G2}^{obs})}{81[4S(S+1)-3]}}, \tag{1.48}$$

$$P_Q = QCC\sqrt{1+\frac{\eta^2}{3}}, \tag{1.49}$$

for triple-quantum MAS NMR spectrum acquired for spin-5/2 nucleus, where P_Q is, quadrupolar effect parameter, δ_{G1}^{obs} and δ_{G2}^{obs} are observed chemical shift of the center of gravity in isotropic dimension and in anisotropic dimension, respectively.

1.3.4 Transfer of Population Double-Resonance (TRAPDOR) NMR

Figure 1.11 shows the pulse sequence of TRAPDOR NMR, which was developed by Grey[47,48], Veeman[47] and Vega[48]. The experiment is designed to measure dipolar coupling involving one spin ½ and one quadrupolar nuclei, by making use of the population transfers that occur between the Zeeman levels of a quadrupolar nucleus under

conditions of slow MAS and continuous rf irradiation of the quadrupolar nucleus. Two separate NMR experiments are performed. The control experiment is the normal spin-echo experiment. The double resonance experiment applies a long pulse on the S (quadrupolar nucleus) spins during the dephasing time before the π pulse on the I spin. In the case of half integer quadrupolar nucleus, for example, the population of |±m> states of the S spin can be transferred to |±1/2> states through adiabatic passages. This will prevent the refocusing of the signal from the dipolar coupled I spin. The population transfer efficiency, can be measured by adiabicity parameter, which is defined as

$$\alpha' = \frac{\omega_1^2}{\omega_r \omega_Q} \tag{1.50}$$

Most of the passages occur adiabatically if the value of α' is larger than 1. Thus slow spinning speeds and high rf power for the S-spin irradiation are used. The value of *QCC* can also be measured by mapping the TRAPDOR fraction as a function of irradiation frequency offset. This is based on the fact that a TRAPDOR effect can only be determined if the S-spin irradiation frequency lies within the S-spin first-order quadrupole spectrum. As the offset increases, the TRAPDOR fraction decreases. The cutoff offset, where the TRAPDOR fraction drops to 0, occurs at $2\nu_Q = 0.3QCC$ for a spin 5/2 nuclei

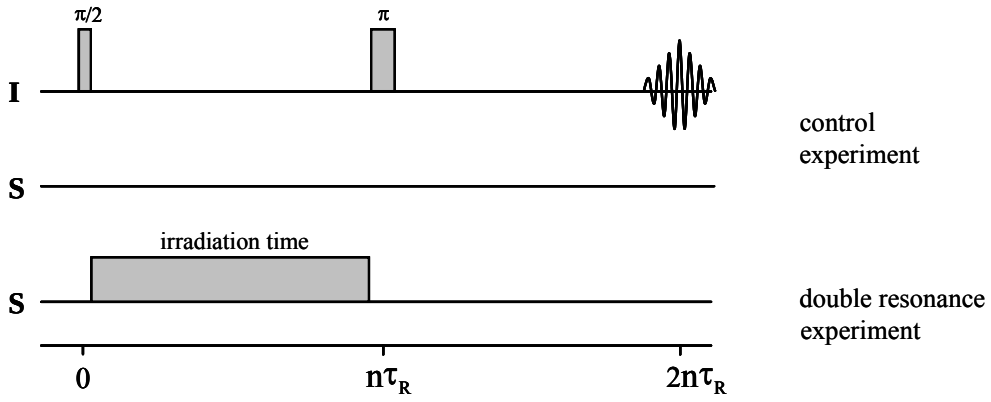

Figure 1.11 Schematic illustration for the pulse sequence of TRAPDOR NMR.

1.3.5 Rotaional Echo Double Resonance (REDOR) NMR

As illustrated in section 1.3.1, MAS removes the anisotropic interactions, including the dipolar interaction. Dipolar coupling, however, contains information about the internuclear distance because of its r_{IS}^{-3} dependence. Thus, many double resonance NMR techniques have been developed to reintroduce the dipolar coupling into the MAS experiments, to combine high resolution with distance measurements, to explore the structural information.

REDOR NMR was developed by Gullion and Schaefer.[49] The pulse sequence of REDOR NMR is shown in Figure 1.12. It consists of two separate experiments: the first is a control experiment, Figure 1.12 (a), which is a common spin-echo experiment. The second experiment, or double resonance experiment, Figure 1.12 (b), involves a train of π pulses applied to the S spins every half rotor period, which can prevent the magnetization of I from refocusing if I is coupled to S. Hence a decrease in signal

intensity at the echo shows the through space proximity between I and S spins. The effect of π pulses depends on the dipolar coupling strength. Experiments are performed as a function of the rotor period and the intensities of double resonance experiments S_f and control experiment S_0 are measured which can be used to obtain internuclear distances.

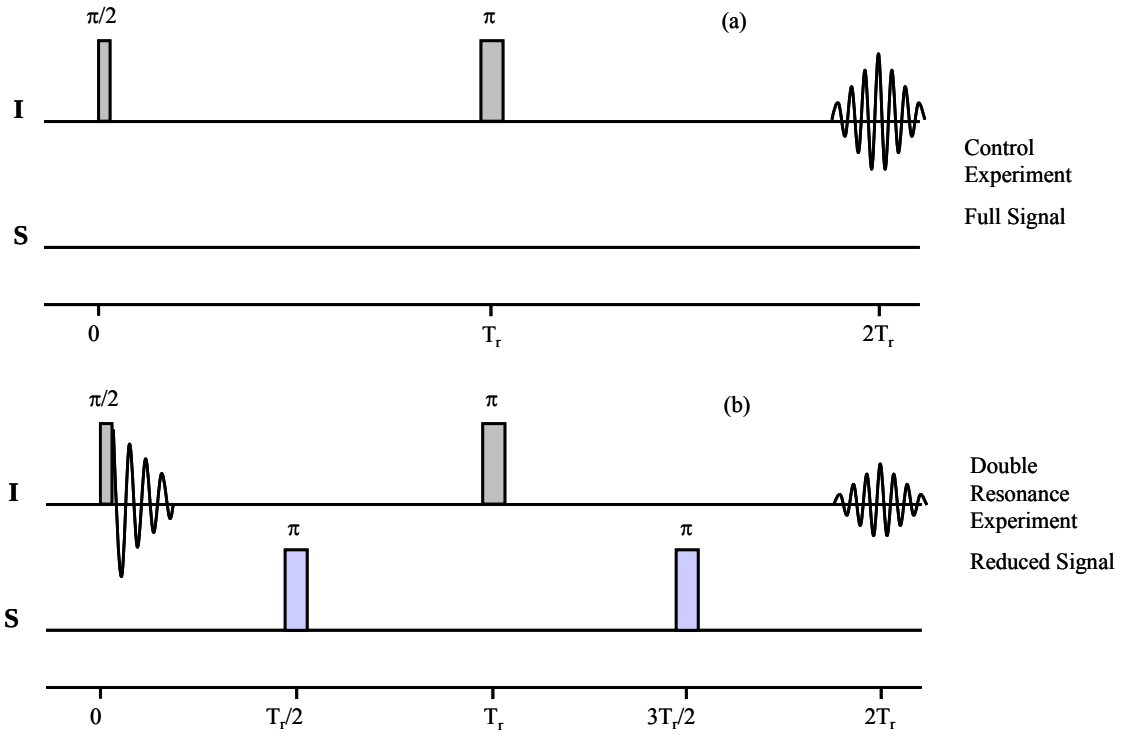

Figure 1.12 Schematic illustration for the pulse sequence of REDOR NMR: (a) control and (b) double resonance experiments.

1.3.6 Heternuclear Correlation (HETCOR) NMR

HETCOR NMR is a 2-D version of CP experiment and more powerful in testing the through space connectivity. The pulse sequence of the simplest version of HETCOR

is shown in Figure 1.13 (a). The transverse magnetization is generated for spin I and allowed to evolve at its characteristic frequency in time t_1. The remaining magnetization is then transferred to the other spin S in a cross-polarization step, and an FID collected in time t_2. Fourier transformation in t_1 and t_2 results in a two-dimensional frequency spectrum with cross peaks between I and S spin signals indicating that cross-polarization took place between the corresponding spins, and therefore that these spins are close in space. As shown in Figures 1.13 (b), a HETCOR spectrum shows spatial correlations between two heteronuclear spins.

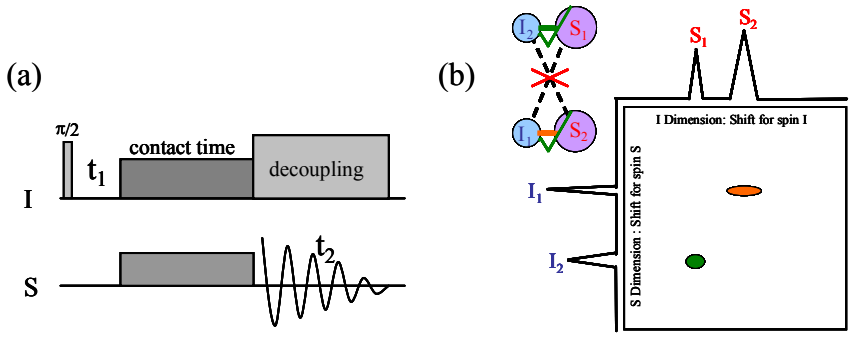

Figure 1.13 (a) Schematic illustration of the pulse sequence of HETCOR NMR. (b) Schematic 2-D NMR spectrum of HETCOR NMR, the signals due to the close proximities of the spin pairs I_1-S_2 and I_2-S_1 can be observed.

1.4 Multinuclear Solid-State NMR Studies of Zeolites

NMR has been widely applied in the characterizations of zeolite structure, acidity, binding sites and the catalytic reactions of sorption processes occur within the cavities of zeolites. NMR is a probe of short range local structure and provides complementary information to diffraction techniques, which mainly study the long-range order in materials. NMR spectroscopy can also be used to follow the catalytic reaction, gas sorption and hydrothermal synthesis processed in both in-situ and ex-situ fashions. The time scale of the interactions that can be probed by NMR spectroscopy is close to the time scale of many motional processes, hence, NMR spectroscopy is a powerful tool in the studies on the dynamics of the sorbate molecules and longer range diffusion processes. In this section, a brief review will be given on a few nuclei, which are widely applied in the NMR studies on zeolites and also closely involved in the research presented in this dissertation.

1.4.1 ^{29}Si MAS NMR Studies on Zeolites

1.4.1.1 ^{29}Si MAS NMR

In the early ^{29}Si MAS NMR studies on aluminosilicate type zeolites, Lippmaa, Engelhardt and coworkers[50,51] showed that the ^{29}Si MAS NMR contain well resolved ^{29}Si resonances with chemical shift dependence on the number of aluminum atoms in the second coordination sphere of silicon, i.e., Si(4Al,0Si), Si(3Al,1Si), Si(2Al, 2Si), Si(1Al,

3Si) and Si(0Al, 4Si). The typical chemical shift of a Si (0Al, 4Si) site is about -102 to -110 ppm, replacing each Si-O-Si linkage by Si-O-Al will cause a change of 5-6 ppm in chemical shift value from this original position. Generally speaking, the substitution of Al into the framework follows the "Loewenstein's rule"[52] that no Al-O-Al linkages are formed in the framework. Therefore the framework silicon/aluminum ratio can be extracted from the intensities of the five resonances mentioned above using the equation below:

$$n(Si)/n(Al) = \frac{\sum_{x=0}^{4} I_{Si(OAl)_x(OSi)_{4-x}}}{\sum_{x=0}^{4} 0.25xI_{Si(OAl)_x(OSi)_{4-x}}} \qquad (1.51)$$

where I and x stand for the intensity of a resonance and the number of silicon atoms substituted by aluminum in a tetrahedron, respectively. The aluminum framework content determined by this method is more accurate than that determined by analytical methods (ICP), since the latter cannot distinguish between the framework and extraframework aluminum.

^{29}Si MAS NMR is also widely applied in the estimation of Si-O-Si bond angles,[53-55] quantifying the number of crystallographic sites and identification of space group or symmetry, and measure of crystallinity. [56]

1.4.1.2 ^{1}H to ^{29}Si cross-polarization experiments

^{1}H to ^{29}Si CP experiment can provide not only improvement in sensitivity but also additional structural information, since the silicon atoms in closest proximity to protons are preferentially enhanced at short contact time. Chuang and coworkers refined a model of silanol bonding at the surface of silica gel, based on the enhancement in the intensities of Q_2 and Q_3 sites (bonded to hydroxyl groups) over the Q_4 site (non-bonded to hydroxyl groups) by comparing the results obtained in non-CP and CP experiments.[57] One point that needs to be emphasized here is that the data from ^{1}H to ^{29}Si CPMAS experiments should be regarded as qualitative rather than quantitative. In the case where quantification is required, strict precautions should be taken to ensure that the signal is not saturated.

1.4.2 ^{27}Al MAS NMR Studies on Zeolites

The applications of ^{27}Al MAS NMR studies on zeolites have mostly focused on aluminum silicates and aluminum phosphates (AlPO). In principle, ^{27}Al is a favorable nucleus for NMR studies because of the 100% natural abundance and the large chemical shift range of about 500 ppm. ^{27}Al is a spin-5/2 quadrupolar nucleus with a moderately large quadrupole moment. ^{27}Al spectra show distinct chemical shift ranges for four-, five- and six-coordinate environments, making it a good tool to distinguish between aluminum framework and extraframework species. However, a couple of practical difficulties in

^{27}Al NMR should be addressed here. First, the dehydrated, acidic forms of many zeolites contain highly distorted aluminum local environments. These distorted sites are consequently associated with large EFGs, all the ^{27}Al signals of which might not detected, especially in the single pulse spectra obtained at low fields. For example, a QCC of 15.3 MHz for the "invisible" framework aluminum atoms in dehydrated zeolite HY has been indirectly detected by Grey and coworkers using ^{1}H/^{27}Al TRAPDOR NMR[48]. Second, the contribution of the quadrupole induced-shift to the overall isotropic chemical shift cannot be neglected for environments with large QCCs, and at low magnetic fields. In order to extract an accurate value of chemical shift, acquiring spectra at different field strengths is recommended.

In the studies of zeolites, the most widely used ^{27}Al NMR techniques include: two-dimensional ^{27}Al MQMAS, and ^{27}Al/^{31}P, ^{1}H/^{27}Al, ^{27}Al/^{15}N (^{14}N) and ^{13}C/^{27}Al double resonance techniques, for instance, SEDOR, TRAPDOR, REDOR, REAPDOR, etc..

1.4.3 ^{1}H MAS NMR Studies on Zeolites

Solid state ^{1}H MAS NMR is a powerful tool to study the Brønsted acid sites in zeolites. Earlier studies have largely been performed at lower magnetic fields and spinning speeds than now available, and do not necessarily yield the highest possible resolution. Resonances at 6.5-7.0, 3.6-5.2, 2.6-3.6 and 1.3-2.3 ppm are generally resolved and assigned to ammonium ions, bridging hydroxyl protons (the Brønsted acid site), Al-OH groups and silanol protons, respectively.[58-60] Brunner and coworkers pointed out

that the line broadening of the ^{1}H resonances in zeolites can be reduced significantly by using a ^{1}H Larmor frequency of 500 MHz (11.7 T) and a spinning speed higher than 10 kHz.[61] The resulting residual line broadening presumably arises from distributions in local environments in the solid.

The analysis of the ^{1}H NMR spectra in many materials is often complicated by motion. The proton mobility in zeolites has been investigated in earlier ^{1}H MAS NMR studies that measured the relaxation, line width, and spinning sideband intensities of the protonated species [62-65].

1.4.4 ^{17}O MAS NMR Studies on Zeolites

As the major component and the ion with largest ionic radius in typical zeolite structure, oxygen is intimately involved in the adsorption and catalytic processes. ^{17}O, the only NMR active oxygen isotope, is a spin 5/2 quadrupolar nucleus with a very large chemical shift range (>1000 ppm). The electric field gradient (EFG) tensor at oxygen nucleus is directly related to the charge distribution at the oxygen atoms and the nearby atoms or ions [66-69]. Therefore, ^{17}O NMR spectra can provide considerable information concerning the local structure. However, the application of ^{17}O NMR in the investigation of zeolites has been hindered by the low natural abundance of ^{17}O (approx. 0.037%) and the large quadrupolar interactions which significantly broaden the NMR resonances. With the development of ^{17}O isotopic enrichment methods and high magnetic field NMR instruments with high speed magic angle spinning (MAS) capabilities, high resolution

^{17}O NMR spectra have been collected for a variety of zeolites [66,70-78]. In our previous work on zeolites HY and HZSM-5, we demonstrated that the ^{17}O signals from the oxygen atoms directly bound to Brønsted acid sites, which are not directly visible in the simple one-pulse experiments, can be detected and partially resolved by one-dimensional (1-D) and two-dimensional (2-D) $^{17}O/^{1}H$ double resonance techniques with optimized contact times, such as $^{1}H \rightarrow {}^{17}O$ cross-polarization (CP) NMR, ^{17}O-^{1}H CP rotational echo double resonance (CP-REDOR) NMR and ^{1}H-^{17}O heteronuclear correlation (HETCOR) NMR[1]. The resonances due to Si-O-Al and Si-O-Si sites in the zeolite framework, which overlap in ^{17}O 1-pulse NMR, can be readily distinguished in ^{17}O multiple-quantum MAS (MQMAS) NMR spectra. [70]

1.5 Reference

(1) Peng, L.; Huo, H.; Liu, Y.; Grey, C. P. *J. Am. Chem. Soc.* **2007**, *129*, 335

(2) Breck, D. W. *Zeolite Molecular Sieves: Structure, Chemistry, and Use.* ; Wiley-Interscience: New York, N.Y., 1974.

(3) Wielers, A. F. H.; Vaarkamp, M.; Post, M. F. M. *J Catal.* **1991**, *127*, 51.

(4) Farneth, W. E.; Gorte, R. J. *Chem. Rev.* **1995**, *95*, 615.

(5) Zecchina, A.; Spoto, G.; Bordiga, S. *Phys. Chem. Chem. Phys.* **2005**, *7*, 1627.

(6) Bevilacqua, M.; Alejandre, A. G.; Resini, C.; Casagrande, M.; Ramirez, J.; Busca, G. *Phys. Chem. Chem. Phys.* **2002**, *4*, 4575.

(7) Heeribout, L.; Semmer, V.; Batamack, P.; Doremieuxmorin, C.; Fraissard, J.; Antos, G. *J. Chem. Soc. Faraday T.* **1995**, *91*, 3933.

(8) Kentgens, A. P. M.; Iuga, D.; Kalwei, M.; Koller, H. *J. Am. Chem. Soc.* **2001**, *123*, 2925.

(9) Peng, L. M.; Liu, Y.; Kim, N. J.; Readman, J. E.; Grey, C. P. *Nat. Mater.* **2005**, *4*, 216.

(10) Peng, L.; Huo, H.; Grey, C. P. *In preparation*.

(11) Simperler, A.; Bell, R. G.; Foster, M. D.; Gray, A. E.; Lewis, D. W.; Anderson, M. W. *J. Phys. Chem.B* **2004**, *108*, 7152.

(12) Farcasiu, D.; Leu, R.; Corma, A. *J. Phys. Chem.B* **2002**, *106*, 928.

(13) Juamain, D.; Su, B. L. *Catal. Today* **2002**, *73*, 187.

(14) Olson, D. H. *Atlas of Zeolite Framework Types*; Elsevier, 2001.

(15) Breck, D. W. *Zeolite Molecular Sieves: Structure, Chemistry, and Use*; John Wiley & Sons, Inc., 1974.

(16) Kokotailo, G. T.; Lawton, S. L.; Olson, D. H.; Olson, D. H.; Meier, W. M. *Nature* **1978**, *272*, 437.

(17) Vankoningsveld, H.; Jansen, J. C.; Vanbekkum, H. *Zeolites* **1990**, *10*, 235.

(18) Vankoningsveld, H. *Acta Crystallogr. B* **1990**, *46*, 731.

(19) Olson, D. H.; Reischman, P. T. *Zeolites* **1996**, *17*, 434.

(20) vanKoningsveld, H.; Jansen, J. C. *Microporous Mater.* **1996**, *6*, 159.

(21) vanKoningsveld, H.; Jansen, J. C.; vanBekkum, H. *Acta Crystallogr. B* **1996**, *52*, 140.

(22) VanKoningsveld, H.; Koegler, J. H. *Microporous Mater.* **1997**, *9*, 71.

(23) Vankoningsveld, H.; Tuinstra, F.; Vanbekkum, H.; Jansen, J. C. *Acta Crystallogr. B* **1989**, *45*, 423.

(24) Wu, E. L.; Lawton, S. L.; Olson, D. H.; Rohrman, A. C.; Kokotailo, G. T. *J. Phys. Chem.***1979**, *83*, 2777.

(25) Chaudhuri, S. Solid State NMR and Atomistic Molecular Dynamics Simulation Study of Ionic Conductors, Catalysts and Perovskites. Ph. D. Dissertation, State University of New York at Stony Brook, 2003.

(26) Du, L. S. Application and Theoretical Study of Solid-State NMR to Inorganic Fluorides and Oxyfluorides. Ph. D. Dissertation, State University of New York at Stony Brook, 2000.

(27) Duer, M. J. *Introduction to Solid-State NMR Spectroscopy*; Blackwell Publishing Ltd: Oxford, 2004.

(28) Ernst, R. R.; Bodenhausen, G.; Wokaun, A. *Principles of Nuclear Magnetic Resonance in One and Two Dimensions*; Oxford University Press: Oxford, 1987.

(29) Kao, H. M. Probing the Bronsted and Lewis Acid Sites in Zeolite Y with Probe Molecules and Solid-State Double Resonance NMR. Ph. D. Dissertation, State University of New York at Stony Brook, 1998.

(30) Levitt, M. H. *Spin Dynamics: Basics of Nuclear Magnetic Resonance*; John Wiley & Sons, Ltd: Chichester, 2001.

(31) Liu, H. M. Structural and Functional Characterization of Inorganic Materials by Solid-State NMR and Diffraction Techniques. Ph. D. Dissertation, State University of New York at Stony Brook, 2001.

(32) Mehring, M. *Principles of High Resolution NMR in Solids*; Springer-Verlag: Berlin Heidelberg New York, 1983.

(33) Stejskal, E. O.; Memory, J. D. *High Resolution NMR in the Solid State*; Oxford University Press, Inc.: New York, 1994.

(34) Man, P. P. Quadrupolar Interactions. In *Encyclopedia of Nuclear Magnetic Resonance*; Grant, D. M., Harris, R. K., Eds.; Wiley: Chichester, 1996; pp 3838.

(35) Samoson, A.; Lippmaa, E.; Pines, A. *Molecular Physics* **1988**, *65*, 1013.

(36) Mueller, K. T.; Sun, B. Q.; Chingas, G. C.; Zwanziger, J. W.; Terao, T.; Pines, A. *J. Magn.c Reson.* **1990**, *86*, 470.

(37) Frydman, L.; Harwood, J. S. *J. Am. Chem. Soc.* **1995**, *117*, 5367.

(38) Gan, Z. H. *J. Am. Chem. Soc.* **2000**, *122*, 3242.

(39) Andrew, E. R.; Bradbury, A.; Eades, R. G. *Nature* **1958**, *182*, 1659.

(40) Pines, A.; Gibby, M. G.; Waugh, J. S. *J. Chem. Phys.* **1973**, *59*, 569.

(41) Hartmann, S. R.; Hahn, E. L. *Phys. Rev.* **1962**, *128*, 2042.

(42) Vega, A. J. *Solid State Nucl. Magn. Reson.* **1992**, *1*, 17.

(43) Stejskal, E. O.; Schaefer, J.; Waugh, J. S. *J. Magn. Reson.* **1977**, *28*, 105.

(44) Iuga, D.; Morais, C.; Gan, Z. H.; Neuville, D. R.; Cormier, L.; Massiot, D. *J. Am. Chem. Soc.* **2005**, *127*, 11540.

(45) Amoureux, J. P.; Fernandez, C.; Steuernagel, S. *J. Magn. Reson. A* **1996**, *123*, 116.

(46) Amoureux, J. P.; Fernandez, C. *Solid State Nucl. Magn. Reson.* **1998**, *10*, 211.

(47) Grey, C. P.; Veeman, W. S. *Chem. Phys. Lett.* **1992**, *192*, 379.

(48) Grey, C. P.; Vega, A. J. *J. Am. Chem. Soc.* **1995**, *117*, 8232.

(49) Gullion, T.; Schaefer, J. *J. Magn. Reson.* **1989**, *81*, 196.

(50) Lippmaa, E.; Magi, M.; Samoson, A.; Engelhardt, G.; Grimmer, A. R. *J. Am. Chem. Soc.* **1980**, *102*, 4889.

(51) Lippmaa, E.; Magi, M.; Samoson, A.; Tarmak, M.; Engelhardt, G. *J. Am. Chem. Soc.* **1981**, *103*, 4992.

(52) Loewenstein, W. *Am. Mineral.* **1954**, *39*, 92.

(53) Thomas, J. M.; Klinowski, J.; Ramdas, S.; Hunter, B. K.; Tennakoon, D. T. B. *Chem. Phys. Lett.* **1983**, *102*, 158.

(54) Smith, J. V.; Blackwell, C. S.; Hovis, G. L. *Nature* **1984**, *309*, 140.

(55) Smith, J. V.; Blackwell, C. S. *Nature* **1983**, *303*, 223.

(56) Fyfe, C. A.; Feng, Y.; Grondey, H.; Kokotailo, G. T.; Gies, H. *Chem. Rev.* **1991**, *91*, 1525.

(57) Chuang, I. S.; Maciel, G. E. *J. Phys. Chem.B* **1997**, *101*, 3052.

(58) Hunger, M.; Freude, D.; Frohlich, T.; Pfeifer, H.; Schwieger, W. *Zeolites* **1987**, *7*, 108.

(59) Freude, D.; Hunger, M.; Pfeifer, H.; Schwieger, W. *Chem. Phys. Lett.* **1986**, *128*, 62.

(60) Hunger, M.; Freude, D.; Pfeifer, H.; Schwieger, W. *Chem. Phys. Lett.* **1990**, *167*, 21.

(61) Brunner, E. *J. Chem. Soc. Faraday T.* **1990**, *86*, 3957.

(62) Baba, T.; Kumasito, N.; Ono, Y.; Sugisawa, H.; Takahashi, T. *Micropor. Mesopor. Mater.* **1998**, *22*, 203.

(63) Baba, T.; Kumasito, N.; Ono, Y. *J. Phys. Chem. B* **1998**, 804.

(64) Sarv, P.; Tuherm, T.; Lippmaa, E.; Keskinen, K.; Root, A. *J. Phys. Chem.* **1995**, *99*, 13763.

(65) Baba, T.; Ono, Y. *Applied Catalysis a-General* **1999**, *181*, 227.

(66) Bull, L. M.; Cheetham, A. K. *Stud. Surf. Sci. Catal.* **1997**, *105*, 471.

(67) Grandinetti, P. J.; Baltisberger, J. H.; Farnan, I.; Stebbins, J. F.; Werner, U.; Pines, A. *J. Phys. Chem.* **1995**, *99*, 12341.

(68) Grey, C. P. Nuclear Magnetic Resonance Studies of Zeolites. In *Handbook of Zeolite Science and Technology*; Auerbach, S. M., Carrado, K. A., Dutta, P. K., Eds.; Marcel Dekker, 2003; pp 205.

(69) Mueller, K. T.; Wu, Y.; Chmelka, B. F.; Stebbins, J.; Pines, A. *J. Am. Chem. Soc.* **1991**, *113*, 32.

(70) Amoureux, J. P.; Bauer, F.; Ernst, H.; Fernandez, C.; Freude, D.; Michel, D.; Pingel, U. T. *Chem. Phys. Lett.* **1998**, *285*, 10.

(71) Bull, L. M.; Bussemer, B.; Anupold, T.; Reinhold, A.; Samoson, A.; Sauer, J.; Cheetham, A. K.; Dupree, R. *J. Am. Chem. Soc.* **2000**, *122*, 4948.

(72) Bull, L. M.; Cheetham, A. K.; Anupold, T.; Reinhold, A.; Samoson, A.; Sauer, J.; Bussemer, B.; Lee, Y.; Gann, S.; Shore, J.; Pines, A.; Dupree, R. *J. Am. Chem. Soc.* **1998**, *120*, 3510.

(73) Freude, D.; Loeser, T.; Michel, D.; Pingel, U.; Prochnow, D. *Solid State Nucl. Magn. Reson.* **2001**, *20*, 46.

(74) Loeser, T.; Freude, D.; Mabande, G. T. P.; Schwieger, W. *Chem. Phys. Lett.* **2003**, *370*, 32.

(75) Neuhoff, P. S.; Shao, P.; Stebbins, J. F. *Micropor. Mesopor. Mat.* **2002**, *55*, 239.

(76) Pingel, U. T.; Amoureux, J. P.; Anupold, T.; Bauer, F.; Ernst, H.; Fernandez, C.; Freude, D.; Samoson, A. *Chem. Phys. Lett.* **1998**, *294*, 345.

(77) Readman, J. E.; Kim, N.; Ziliox, M.; Grey, C. P. *Chem. Commun.* **2002**, 2808.

(78) Stebbins, J. F.; Zhao, P. D.; Lee, S. K.; Cheng, X. *Am. Mineral.* **1999**, *84*, 1680.

Chapter 2

Probing Brønsted acid sites in zeolite HY and HZSM-5 with low temperature ^{17}O - ^{1}H Double Resonance MAS NMR spectroscopy

Abstract

Brønsted acid sites play a key role in controlling the catalytic performances in acidic catalysts. A determination of the structure of the acid site, in particular, the O-H bond length, is fundamental to the understanding of its acid strength. The O-H distances in zeolite HY and HZSM-5 extracted from ^{17}O-^{1}H REDOR NMR data acquired at room temperature are noticeably longer than the results from *ab-initio* calculations due to the presence of some restricted motions at room temperature, such as zeolite framework vibrations and O-H librational motion. We present here our ^{17}O-^{1}H REDOR NMR results of zeolite HY and HZSM-5 at a lower temperature of 183 K, where some of these motions are frozen out. By comparing the line shapes of simulation results from the SIMPSON package with the experimental data, an O-H distance of about 0.97 ~ 0.98 Å was obtained for zeolite HY, which is consistent with the previous *ab-initio* calculation results. The results demonstrate that low temperature REDOR NMR can provide more accurate estimates of the O-H distance, which should prove useful in understanding zeolite structure and acidity.

2.1 Introduction

Zeolites are microporous aluminosilicates with widespread industrial applications, which include their use as catalysis, in separations, ion exchange, and even in medical applications.[1-3] The catalytic activity and selectivity of the protonic forms of zeolites mainly depend on their unique porous structures and the acidity of the bridging hydroxyl groups, Si-OH-Al, which function as Brønsted acid sites [4,5]. The factors that control the Brønsted acidity of these materials continue to be debated but are generally believed to be influenced by a number of often interrelated factors. These include the local (Si-O(H)-Al and T-O-T bond angles, OH distances), and intermediate (shapes and sizes of the rings and pores that form the zeolite) structures and also the proximity between acid sites. The different factors manifest themselves in very different acidities, proton mobility[6] and catalytic activities. We have been using a wide range of NMR techniques in order to understand how local structure varies between structures, in order to help assess the relative importance of the different structural features in controlling zeolite function. Our recent studies have focused on a detailed characterization of the ^{17}O NMR parameters (chemical shift, quadrupolar coupling constant, ^{17}O-^{1}H dipolar couplings) that characterize of the local environment of the oxygen atom bound to the Brønsted acid site, in order to explore the sensitivity of this nucleus to structure and acidity. Here we explore the use of ^{17}O-^{1}H double resonance methods to determine structure and examine the effect of mobility on the NMR spectra.

Two zeolites with different structures and Si/Al ratios have been selected for the study reported here: zeolite HY with a low Si/Al ratio of 2.6 and zeolite HZSM-5 with a higher Si/Al ratio of 25. The structures of these two types of frameworks have been explained in Chapter 1.

In our previous work on zeolites HY and HZSM-5, the ^{17}O signals from the framework (Si-O-Al and Si-O-Si linkages) as well as the oxygen atoms directly bound to Brønsted acid sites have been successfully resolved and characterized [7,8]. We applied one-dimensional (1-D) and two-dimensional (2-D) $^{17}O/^{1}H$ double resonance techniques, such as $^{1}H \rightarrow {}^{17}O$ cross-polarization (CP) NMR and ^{17}O-^{1}H rotational echo double resonance (REDOR) NMR to detect Brønsted acid sites which are not directly visible in the simple one-pulse experiments. Different Brønsted acid sites associated with different ^{17}O quadrupolar coupling parameters were resolved by using ^{1}H-^{17}O heteronuclear correlation (HETCOR) NMR. The ^{17}O-^{1}H REDOR method was used to measure the ^{17}O-^{1}H dipolar coupling constant. In a rigid system, comprising isolated (^{17}O-^{1}H) spin pairs, this dipolar coupling constant can then be converted directly into an internuclear distance, r_{IS}, since the latter is directly proportional to r_{IS}^{-3}. However, any motion present in the system, if occurring on a timescale that is shorter than the size of the dipolar coupling will result in partial, or in some cases, complete averaging of the dipolar coupling, leading to longer apparent internuclear distances. This was the case for the zeolitic systems at room temperature, where the O-H distance in zeolite HY extracted from the room temperature ^{17}O-^{1}H REDOR NMR data was longer than the results from

ab-initio calculations and from neutron diffraction. Weaker ^{17}O-^{1}H dephasing was observed for zeolite HZSM-5 in comparison to that of HY, which is consistent with longer O-H distance and/or increased proton mobility. The reduction of the dipole-dipole coupling was ascribed to the framework vibrational and/or O-H librational averaging of the through-space dipole-dipole coupling. The one-pulse ^{17}O MAS NMR spectrum of HY at 173 K showed more a distinct second-order quadrupole line shape than the 293 K data, indicating of these motions may be significantly reduced at lower temperature [7]. Thus, it may be possible to obtain more accurate O-H distances from REDOR NMR spectroscopy data acquired at low temperature. Thus, the aims of this work are to extract the O-H distance from low temperature ^{17}O-^{1}H REDOR NMR of zeolites HY and HZSM-5 and investigate the mechanism of the proton mobility in zeolite HZSM-5 by variable temperature 1-D and 2-D ^{1}H MAS NMR spectroscopy.

2.2 Experimental Section

2.2.1 Materials Preparation

NaZSM-5 was prepared from NH_4ZSM-5 (Si/Al=25; Zeolyst) by ion exchange (repeated three times) with a 1 M $NaNO_3$ solution. The slurry was held at room temperature for 12 h, whereupon the solid was filtered, washed with distilled water, and then dried at ambient temperature. NaY (Si/Al=2.6; Strem Chemicals) and the as-prepared NaZSM-5 samples were enriched as described previously [9], by heating a dehydrated sample in $^{17}O_2$ gas (59.6% enriched $^{17}O_2$; Isotec, Inc.) at 853 K for 12 h. ^{17}O-enriched zeolite NH_4Y was prepared by ion exchange with a 1 M NH_4NO_3 solution at ambient temperature for 12 h (repeated five times). ^{17}O-enriched zeolite NH_4ZSM-5 was prepared by ion exchange with a 1 M NH_4NO_3 solution at 353K for 12 h (repeated three times). ^{17}O-enriched H-form zeolites was prepared by heating ^{17}O-enriched NH_4-form zeolites under vacuum with a step of 0.2 K/min to 383 K, and then 0.4 K/min to 673 K, after that the temperature was held at 673 K for 12 h. NH_4ZSM-5 was heated following the same procedure described above to prepare non-enriched HZSM-5. The samples were stored and packed into NMR rotors in the N_2 glove box, prior to the NMR experiments.

2.2.2 Solid-state NMR Spectroscopy

MAS NMR spectra were obtained with Bruker Avance 600 with 89 mm wide-bore 14.1 T superconducting magnet, in 4 mm rotors at 81.4 MHz. A rotor cap with an o-ring was used to avoid the adsorption of water during the NMR measurements. The rotors were spun using dry nitrogen gas in order to avoid contamination by H_2O molecules in the air and any undesired ice formation during low temperature experiments. Both ^{17}O and ^{1}H chemical shifts are referenced to H_2O (0.0 ppm). The Hartmann-Hahn condition for the CP-REDOR NMR experiments was set by using the ^{17}O-enriched zeolite HY sample. The NMR pulse sequence is shown in Figure 2.1. This 'mirror-symmetric' pulse sequence was used, due to the large dipolar couplings present in this system. NMR line shape simulations were performed with the SIMPSON package developed by Nielsen and co-workers [10]. *Rf* field strengths of $\omega_1(^{17}O)/2\pi$ =28 kHz and $\omega_1(^{1}H)/2\pi$ =70 kHz were used.

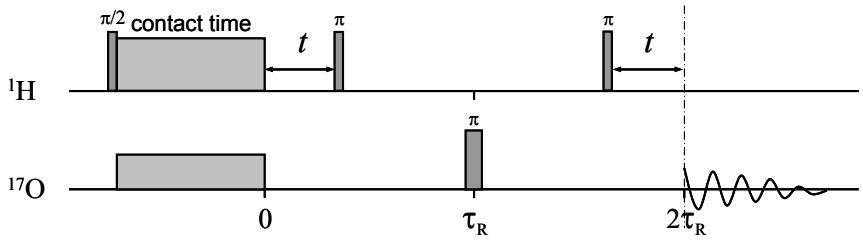

Figure 2.1 NMR pulse sequence: $^{1}H \rightarrow {}^{17}O$-$^{1}H$ CP-REDOR with shifted π pulses.

2.2.3 NMR Simulation Details

NMR line shape simulations were performed with the SIMPSON package developed by Nielsen and co-workers.[10]

The 'direct' method ('direct calculation by chronological time integration')[10] was used for all the SIMPSON simulations. The spin system comprised a single oxygen spin coupled to a proton. The following ^{17}O NMR parameters were used: δ_{CS} = 21, QCC = 6.0 MHz and η = 1.0 for zeolite HY at room temperature. Only the evolution of central transition coherence (|+1/2> - |–1/2>, was considered since this is the dominant coherence excited in the CP preparation period. Simulations were performed by varying 't', the time between the end of the contact time and the ^{1}H π pulse. S_0 and S were obtained by integrating the isotropic resonances control and double resonance spectra, respectively.

The Euler angles (α, β, γ) used in the simulation to describe the relative orientations between the principal axis frame of the dipolar / quadrupolar tensors and the crystal fixed frame was set to (30.3°, 0°, 0°) and (166.3°, 89.7°, 122.1°), respectively, according to the electric field gradient (EFG) tensor calculated for site O_1 in zeolite HY, where the values of QCC and η are reported in an earlier work.[8] Note, in the convention used by SIMPSON, α and γ are defined as rotations about the z-direction of the crystal fixed frame; β is about the y axis. The coordinates of the atoms around Brønsted acid sites (Si-O_1H-Al) in the crystal fixed frame are listed as the following:

O (0.00, 0.00, 0.00), H (0.00, 0.00, 0.83), Si (1.34, -0.78, -0.64), Al (-1.34, 0.79, -0.63)

2.3 Results and Discussion

2.3.1 Low temperature $^{1}H \rightarrow {}^{17}O$-$^{1}H$ CP-REDOR NMR of zeolite HY

$^{1}H \rightarrow {}^{17}O$-$^{1}H$ CP-REDOR NMR experiments of HY were carried out at a temperature of 183 K. As in our previous study [7], a 'mirror-symmetric' pulse sequence (Figure 2.1) was used [11-13], rather than the pulse sequence often used for quadrupolar nuclei [14,15], due to the large dipolar couplings present in this system. The REDOR fractions, defined as $(1 - S/S_0)$, where S and S_0 were obtained by integrating the signal intensities in double resonance and control spectra, were measured as a function of time t, which represents the time between the end of the contact time and the ^{1}H π pulse, *i.e.,* the shift of the pulse (Figure 2.1). t = 1/2 rotor period (i.e., about 34.4 μs for a spinning speed of 13 kHz) corresponds to the maximum evolution time for the ^{17}O spins, under the influence of the ^{1}H dipolar coupling. The data acquired without the two dephasing π pulses were used as the control experiment. The REDOR fractions were obtained by integrating the whole spectra and the CP-REDOR fractions of zeolite HY at 298 K (17.6 T) [7] and 183 K (14.1 T) are shown in Figure 2.2 (a). The REDOR fractions increase with increasing value of time t and reach a maximum when t is around 30 and 25 μs for the data acquired at 298 K and 183 K, respectively. The more rapid dephasing observed for

the data acquired 183 K indicates that the average O-H dipolar coupling at low temperature is larger than at room temperature. This is further supported by the fact that the maximum REDOR fraction in the data acquired at 183 K (~0.95) is larger than the one obtained at 293 K (~0.90).

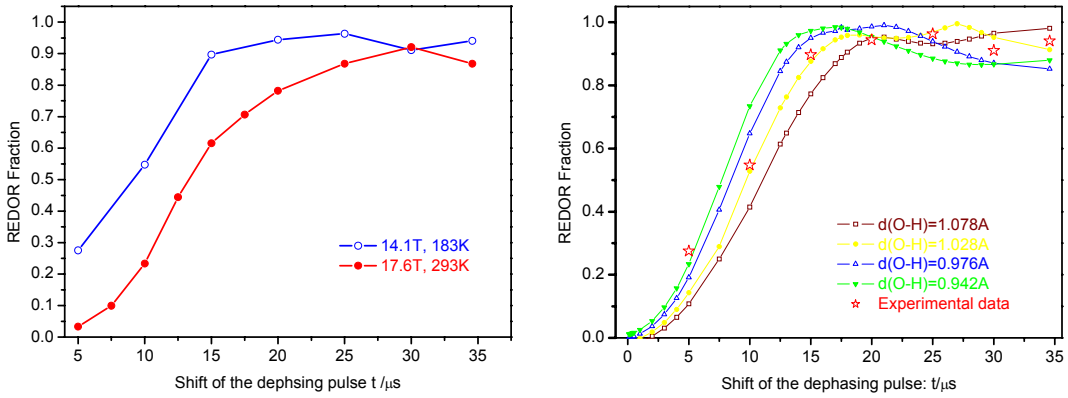

(a) (b)

Figure 2.2 (a) $^{1}H \rightarrow {}^{17}O\text{-}^{1}H$ CP-REDOR NMR fraction ($1 - S/S_0$) measured as a function of the shift of the first dephasing pulse (time, t) without ^{1}H decoupling during the acquisition period at two different conditions. (b) comparison of the REDOR fractions obtained from experimental data with the SIMPSON simulation results. The dipolar coupling constants used in these simulations are 13.0, 15.0, 17.5 and 19.5 kHz, corresponding to O-H distances of 1.078, 1.028, 0.976 and 0.942 Å. Spinning speed, 13 kHz; recycle delay, 1 s; ^{1}H π pulse, 6.2 μs (17.6 T) or 6.0 μs (14.1 T).

Numerical simulations with several chosen O-H distances using SIMPSON package [10] are compared to the low temperature experimental REDOR fractions of zeolite HY in Figure 2.2 (b). The simulations were performed by calculating the total intensities of the ^{17}O spectrum obtained following a REDOR dephasing sequence. The Euler angles used in the simulation, which define the relative orientations between the principal axis system (PAS) of the dipolar and quadrupolar tensors with respect to the crystal fixed frame, were obtained from our *ab-initio* calculations, reported earlier [7,8]. However, it is important to note that the theoretical REDOR dephasing curve should not, to a first approximation, depend on the relative orientation of the quadrupolar and dipolar tensors. This assumption was confirmed in simulations performed in our earlier study.[7] The calculated data qualitatively fit the experimental data. The whole dephasing behavior of the calculated curve is most similar to the experimental data for an O-H distance of 1.028 Å, while the initial rise of the experimental REDOR fraction curve is closer to that seen in the calculated 0.976 Å curves. The fact that fitting the initial rise of the experimental data gives a shorter O-H distance is similar to the room temperature observations [7]. However, unlike the simulated REDOR fraction curves, the experimental REDOR fraction at 183 K still does not reach 1.0, and no pronounced oscillations in the REDOR fractions are observed. These effects are both presumably due to the presence of residual motion that persists even at this low temperature, but may also be due to spin-diffusion processes between the proton species which could cause similar changes to the REDOR fraction curves.[16]

As demonstrated in previous studies, the dephasing is not constant for the whole second-order quadrupolar lineshape [7,17]. The CP-REDOR spectra of zeolite HY obtained at low temperature (183 K, 14.1 T) are shown in Figure 2.3(f) and the room temperature (293 K, 17.6 T) data [7] are shown in Figure 2.3(b) for comparison. The control spectra were phased properly with 0-order phasing only. All the double resonance spectra were phased with the same number of 0-order phasing as that used for corresponding control spectrum. As seen in the room temperature data, the intensities of the major discontinuities at 183K decrease with increasing time t and then increase, while the behaviors of these oscillations are very different. For example, the intensity of the middle, most intense discontinuity at approximately -28 ppm drops with increasing time t and reaches a minimum which is close to zero when t is about 20 μs. A similar behavior can be seen for the intensity at approx -8 ppm, which is between the high frequency discontinuity at 14 ppm and the middle discontinuity. However, when t is longer than 20 μs, the intensity at -28 ppm increases again while the intensity at -8 ppm continues to decrease and reach the minimum at about 25 to 30 μs, then increases to almost zero when t = 34.6 μs. These differences in the dephasing behavior across the line shapes can be ascribed to the fact that the various components of the 2nd-order quadrupolar lineshape arise from different parts of the powder which are associated with different effective dipolar coupling constants.

The line shape of the low temperature CP-REDOR NMR spectra of HY (acquired without ^{1}H decoupling, Figure 2.3 (e), (g), (h)) was simulated in order to extract the O-H

distance. As was the case for the room temperature data of HY, where a surprisingly good fit with an O-H distance of 0.98 to ~1.01 Å was observed (Figure 2.3 (a), (c), (d)), the low temperature data were also well simulated, with a O-H distance of 0.975 ± 0.025 Å (Figure 2.3 (g)), consistent with the calculated values [18-20].To get a perfect fit of the line shape, simulations were performed using various QCC values in a range of 6.0-6.2 MHz (see Figure 2.4). The QCC value of 6.0 MHz, which has been used for the room temperature simulations, is obviously smaller and cannot totally fit the line shape at low temperature. The results of simulations indicate that QCC= 6.175MHz gives the best fit. The increase of the QCC value at low temperature is presumably ascribed to a more rigid environment around the oxygen at the Brønsted acid site, which is due to the slower motion of both the hydroxyl group and the framework. As in the room temperature data, a slightly shorter distance is extracted from the simulations of the lineshape data than in the REDOR fraction data, but this effect is now much less pronounced than in the room temperature data, where distances of approx. 1.04 and 1.01 Å were obtained with the two approaches. In order to assess the best fits to the lineshapes, we examined the frequency of the oscillations in intensity of the different discontinuity, as well as their intensities. This approach appears to be less sensitive to the effects of motion, and may reflect the fact that different parts of the powder are associated with different average dipolar coupling constants (due to differences in the relative orientations of the O-H dipolar tensors and the rotor axis). However, more detailed simulations are required in order to understand this fully.

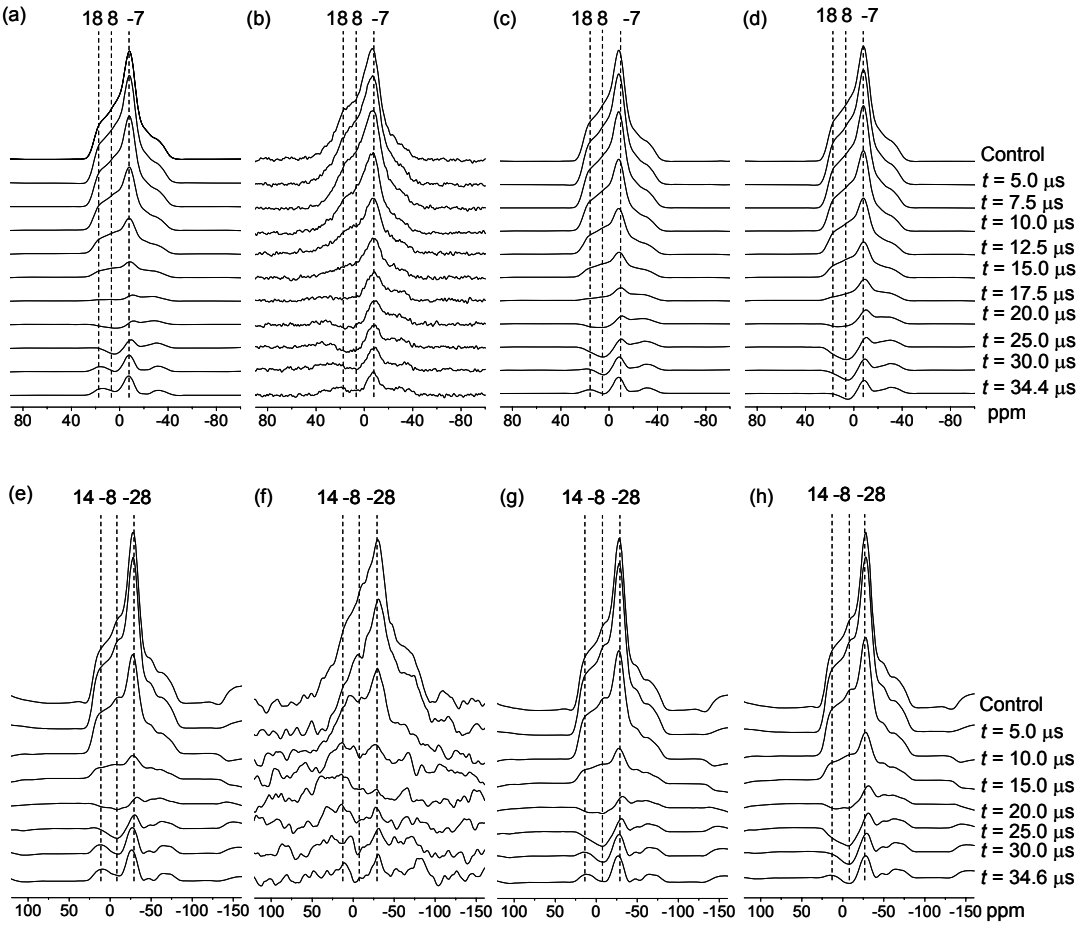

Figure 2.3 (b) Experimental $^{1}H \rightarrow {}^{17}O\text{-}^{1}H$ CP-REDOR NMR spectra, acquired without ^{1}H decoupling, as a function of the shift of the first dephasing pulse (time, *t*) at 17.6 T at 298 K and (a, c, d) simulations performed with dipolar coupling constants of 19000, 17308 and 15811 Hz, corresponding to O-H distances of 0.95, 0.98 and 1.01 Å, respectively, and no ^{1}H decoupling [7]. NMR parameters used are δ_{CS} = 21, QCC = 6.175 MHz, and η = 1. (f) $^{1}H \rightarrow {}^{17}O\text{-}^{1}H$ CP-REDOR NMR spectra at 14.1 T at 183 K and (e, g, h) simulations performed with dipolar coupling constants of 19000, 17576 and 16291 Hz, corresponding to O-H distances of 0.95, 0.975 and 1.00 Å, respectively, and no ^{1}H decoupling. NMR parameters used are δ_{CS} = 21, QCC = 6.175 MHz, and η = 1.

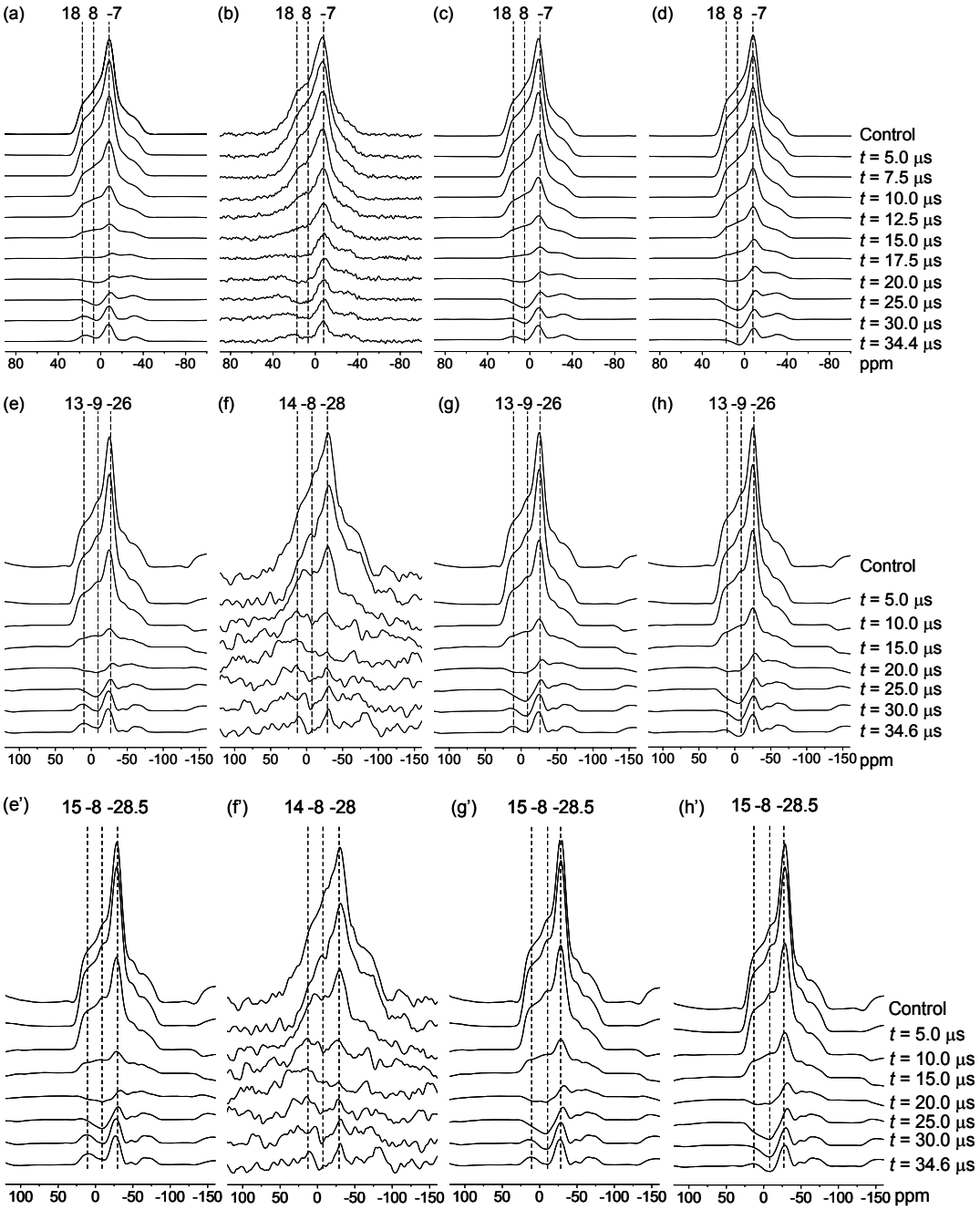

Figure 2.4 (b) Experimental $^{1}H \rightarrow {}^{17}O$-$^{1}H$ CP-REDOR NMR spectra, acquired without ^{1}H decoupling, as a function of the shift of the first dephasing pulse (time, *t*) at 17.6 T at 298 K and (a, c, d) simulations performed with dipolar coupling constants of 19000, 17308 and 15811 Hz, corresponding to O-H distances of 0.95, 0.98 and 1.01 Å,

respectively, and no ^{1}H decoupling [7]. NMR parameters used in all simulations are δ_{CS} = 21, QCC = 6.0 MHz, and η = 1. (f) Experimental ^{1}H → ^{17}O-^{1}H CP-REDOR NMR spectra at 14.1 T at 183 K and (e, g, h) simulations performed with dipolar coupling constants of 19000, 17576 and 16291 Hz, corresponding to O-H distances of 0.95, 0.975 and 1.00 Å, respectively, and no ^{1}H decoupling. NMR parameters used in all simulations are δ_{CS} = 21, QCC = 6.0 MHz, and η = 1. (e', g', h) simulations performed with dipolar coupling constants of 19000, 17576 and 16291 Hz, corresponding to O-H distances of 0.95, 0.975 and 1.00 Å, respectively, and no ^{1}H decoupling. NMR parameters used in all simulations are δ_{CS} = 21, QCC = 6.2 MHz, and η = 1.

2.3.2 Low temperature $^{1}H \rightarrow {}^{17}O$-$^{1}H$ CP-REDOR NMR of zeolite HZSM-5

Low temperature $^{1}H \rightarrow {}^{17}O$-$^{1}H$ CP-REDOR NMR data of zeolite HZSM-5 data is difficult to acquire due to the low framework aluminum content of this material. Compared to the high Si/Al ratio zeolite HY sample (Si/Al = 2.6), this low Si/Al ratio zeolite HZSM-5 sample (Si/Al=25) only possesses 1/10 Al atoms in the structure, which directly leads to a low proton concentration system and a greatly reduced the CP signal of HZSM-5. Additionally, the longer ^{1}H T_1 relaxation of zeolite HZSM-5 at 183K increased the experiment time dramatically. (About 2s at room temperature and 10s at 183K)

Figure 2.5 (a) shows the $^{1}H \rightarrow {}^{17}O$-$^{1}H$ CP-REDOR NMR spectra of HZSM-5 at 14.1 T, 183K. A slower spinning speed of 8 kHz was used in order to improve the efficiency of the CP transfer process. A faster dephasing rate is observed for the discontinuity at 16 ppm, compared with the one at -12ppm. The CP-REDOR fractions of zeolite HZSM-5 at 298 K (17.6 T) [7] and 183 K (14.1 T) are shown in Figure 2.5(b). The REDOR fraction of room temperature dataset was obtained by integrating the whole spectra; for the low temperature dataset, only the central transition and the first spinning sidebands have been included in the integral to avoid the errors resulting from the low signal to noise ratio. Error bars were added by estimating the possible error caused by the choice of the range over which to perform the integral. Larger error bars were added to the last to data points to include the possibly bigger errors due to the relatively low signal intensity. The REDOR fractions increase with increasing value of time t and reach a

maximum when t is around 30 and 20 μs for the data acquired at 298 K and 183 K, respectively. The maximum REDOR fraction in the data acquired at 183 K (~0.93) is noticeably larger than the one obtained at 293 K (~0.70), but again, does not reach 1.0 even at low temperature. Both the more rapid dephasing observed for the data acquired 183 K and the higher REDOR fraction indicate that the average dipolar coupling at low temperature is larger than at room temperature. The low maximum REDOR fraction at room temperature is ascribed to a motion. The simulations of REDOR curves using the universal equation in the original publication of REDOR NMR spectroscopy[15] were performed with Mathcad software instead of the SIMPSON simulations, because of the less explored structures of the Brønsted acid sites and insufficient information about the relative orientation of the CSA tensors and quadrupolar tensors. To compare the experimental data with the universal REDOR fraction curve, a total dephasing time was calculated by multiplying the first dephasing pulse time t by a factor of 4. The REDOR fraction curve obtained from the experimental data at 183K gives a surprisingly good fit with the universal REDOR fraction curve using a dipolar coupling constant of 17.5 kHz, which corresponds to a O-H distance of 0.976 Å.

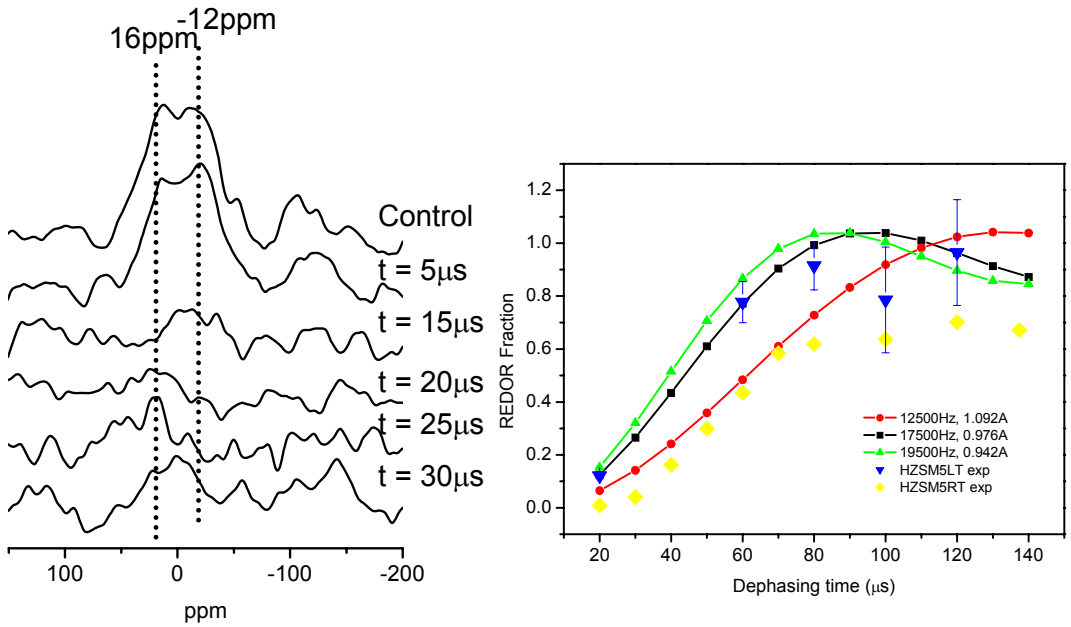

Figure 2.5 (a) $^{1}H \rightarrow {}^{17}O\text{-}^{1}H$ CP-REDOR NMR spectra of HZSM-5 acquired with ^{1}H decoupling, as a function of the shift of the first dephasing pulse (time, t), at 183K, 14.1 T, spinning speed, 8 kHz; recycle delay, 2 s; ^{1}H π pulse, 6.2 μs. (b) $^{1}H \rightarrow {}^{17}O\text{-}^{1}H$ CP-REDOR NMR fraction ($1 - S/S_0$) measured as a function of the shift of the dephasing time (4 times of the first dephasing pulse time, t). Spinning speed, 13 kHz; recycle delay, 1 s; ^{1}H π pulse, 6.2 μs (293K, 17.6 T). Comparison of the REDOR fractions obtained from the experimental data with the simulated universal REDOR fraction curves. The dipolar coupling constants used in the simulations are 12.5kHz, 17.5kHz and 19.5kHz, corresponding to the O-H distance of 1.092Å, 0.976 Å and 0.942 Å, respectively.

2.4 Conclusions

Low temperature ^{17}O-^{1}H REDOR NMR experiments at 183 K were employed in order to reduce the motional processes present in these materials and measure the O-H bond lengths in zeolites HY and HZSM-5. The REDOR dephasing is more rapid at low temperature than the room temperature, indicative of a larger effective dipolar coupling. By comparing the experimental data with the line shape simulations of zeolite HY, a bond length of 0.975 ± 0.025 Å has been extracted. This value is shorter than that obtained from room temperature data, and is consistent with the bond length of 0.97 Å predicted by *ab-initio* calculations.

The REDOR data indicates that the motion has been significantly reduced at low temperatures. The maximum REDOR fraction is still less than 1 and the REDOR oscillations are less pronounced than predicted theoretically, implying that there are still residual motions and/or spin diffusion processes at l83 K. Finally, the error bars associated with the O-H measurements indicate that very small changes in O-H distances may be difficult to quantify with the experimental methodology reported here, but the larger changes that result from for example the formation of strong hydrogen bonding to probe molecules, or possibly to different nearby framework sites, should result in detectable changes in O-H distances.

2.5 References

(1) Corma, A.; Rey, F.; Rius, J.; Sabater, M. J.; Valencia, S. *Nature* **2004**, 431, 287.

(2) Greaves, G. N.; Meneau, F.; Majerus, O.; Jones, D. G.; Taylor, J. *Science* **2005**, 308, 1299.

(3) Paillaud, J. L.; Harbuzaru, B.; Patarin, J.; Bats, N. *Science* **2004**, 304, 990.

(4) Corma, A. *Chem. Rev.* **1995**, 95, 559.

(5) Karge, H. G.; Hunger, M.; Beyer, H. K. Characterization of zeolites - infrared and nuclear magnetic resonance spectroscopy and X-ray diffraction. In Catalysis and Zeolites: Fundamentals and Applications; Weitkamp, J., Puppe, L., Eds.; Springer: New York, 1999; pp 198.

(6) Sarv, P.; Tuherm, T.; Lippmaa, E.; Keskinen, K.; Root, A. *J. Phys. Chem.* **1995**, 99, 13763.

(7) Peng, L.; Huo, H.; Liu, Y.; Grey, C. P. *J. Am. Chem. Soc.* **2007**, 129, 335

(8) Peng, L.; Liu, Y.; Kim, N.; Readman, J. E.; Grey, C. P. *Nature Mater.* **2005**, 4, 216.

(9) Readman, J. E.; Kim, N.; Ziliox, M.; Grey, C. P. *Chem. Commun.* **2002**, 2808.

(10) Bak, M.; Rasmussen, J. T.; Nielsen, N. C. *J. Magn. Reson.* **2000**, 147, 296.

(11) Goetz, J. M.; Wu, J. H.; Yee, H. F.; Schaefer, *J. Solid State Nucl. Magn. Reson.* **1998**, 12, 87.

(12) Gullion, T. *Magn. Reson. Rev.* **1997**, 17, 83.

(13) Wu, J. H.; Xiao, C. D.; Yee, A. F.; Goetz, J. M.; Schaefer, J. *Macromolecules* **2000**, 33, 6849.

(14) Fyfe, C. A.; Mueller, K. T.; Grondey, H.; Wong-Moon, K. C. *J. Phys. Chem.* **1993**, 97, 13484.

(15) Gullion, T.; Schaefer, J. *J. Magn. Reson.* **1989**, 81, 196.

(16) Chan, J. C. C.; Eckert, H. *J. Magn. Reson.* **2000**, 147, 170.

(17) Zeyer, M.; Montagne, L.; Jaeger, C. *Solid State Nucl. Magn. Reson.* **2003**, 23, 136.

(18) Fois, E.; Gamba, A.; Tabacchi, G. *J. Phys. Chem. B* **1998**, 102, 3974.

(19) Larin, A. V.; Vercauteren, D. P. *J. Mol. Catal. A-Chem.* **2001**, 168, 123.

(20) Xue, X.; Kanzaki, M. *J. Phys. Chem. B* **2001**, 105, 3422.

Chapter 3

Low Temperature ^{1}H MAS NMR Spectroscopy Studies of Proton Motion in Zeolite HZSM-5

Abstract

Low temperature ^{1}H MAS NMR spectroscopy is used to study protonic motion in zeolite HZSM-5, in both samples that have been dried using procedures that are standard in the literature, and samples that have been more carefully dehydrated. A significant enhancement of proton mobility is seen for the "standard" dehydrated HZSM-5 sample, in comparison to that seen for the much drier sample. This is ascribed to a vehicle-hopping mechanism involving the residual water that is present in these zeolites. A gradual change of the framework structure is observed on cooling to approx. 213 K, as monitored via the change in ^{1}H chemical shift values of the Brønsted acid resonances and by X-ray diffraction. A more sudden change in structure is seen by differential scanning calorimetry (DSC) and NMR, at approx. 220 - 230 K, which is associated with changes in both the mobility and the modes of binding of the residual water to the Brønsted acid sites and the zeolite framework.

3.1 Introduction

Solid state ^{1}H MAS NMR is a powerful tool with which to study the Brønsted acid sites in zeolites. Earlier studies of HZSM-5 have largely been performed at lower fields and spinning speeds than now available, and do not necessarily show the highest possible resolution. Only resonances at 4.0, 2.9 and 1.8 ppm are generally clearly resolved and assigned to bridging hydroxyl protons (the Brønsted acid site), Al-OH groups and silanol protons, respectively.[1-3] Brunner and coworkers pointed out that the line broadening of the ^{1}H resonances in this material can be reduced significantly by using a ^{1}H Larmor frequency of 500 MHz (11.7 T) and a spinning speed higher than 10 kHz.[4] The resulting residual line broadening presumably arises from distributions in local environments in the solid. A broad signal at 6.1-7.0 ppm is often observed and has attracted considerable research interest. In 1994, Haw and co-workers reported that this broad feature was more pronounced at 123K and assigned it to a second type of Brønsted acid site.[5,6] Alternative assignments have also been proposed, for instance, water adsorption on Lewis acid sites, Brønsted acid sites located in Si $(OAl)_2$ T sites, hydroxyl protons on the surfaces of the zeolite particles, Si-OH-Al proton weakly hydrogen bonded to neighboring framework oxygen, Brønsted acid protons exchanging between several oxygen positions, and finally, residual NH_4^+ ions.[6-12]

The analysis of the ^{1}H NMR spectra in many materials is often complicated by motion. For example, in our previous ^{1}H- ^{17}O CP/REDOR NMR study of HZSM-5 with

Si/Al= 25 we observed REDOR fractions that were much lower than predicted at room temperature, assuming typical O-H distances,[11] which we ascribed to rapid protonic motion. This proton mobility in zeolites has been investigated in earlier ^{1}H MAS NMR studies that measured the relaxation, line width, and spinning sideband intensities of the protonated species [13-16]. Sarv *et al.* reported that the activation energy of protonic motion in zeolite HZSM-5 (Si/Al=39), extracted from a high temperature ^{1}H MAS NMR study of the spinning sideband intensities, is 45 kJ/mol.[15] Baba *et al.* studied the line widths of the isotropic resonances of a series of zeolite HZSM-5 samples with various Si/Al ratios using high temperature ^{1}H MAS NMR, and, in contrast, reported a much lower activation energy of 11 kJ/mol for their sample with a Si/Al ratio of 21. For the samples with Si/Al ratio from 39 to 106, they found that the activation energy remained constant at around 17-20 kJ/mol[14,17]. The lineshape analysis of Baba *et al*. is complicated by the overlap of the 6.1-7.0 ppm broad feature with the main Brønsted acid resonance, particularly at higher temperatures; this may result in errors in estimation of the line width, possibly accounting for the differences between the numbers reported by these two groups. In spite of these large discrepancies, it appears that HZSM-5 zeolites with Si/ Al < 30 appear to show lower activation energies for proton motion, compared to lower aluminum content HZSM-5 samples or, counter to this trend, other zeolites with lower Si/Al ratios, for instance, H-mordenite and HY.[15] Sarv *et al.* suggested that the motion measured by these experiments only involved the proton-hopping between oxygen atoms around the same aluminum (T) atom (intrasite motion), translational motion between

Brønsted sites (intersite motion) involving a much larger activation energy.[15] In the most recent study of the proton mobility in ammonia- and water-loaded zeolite HZSM-5 and HY samples, Freude and coworkers showed that small loadings of water increased the proton mobility significantly.[18] They ascribed the motion in this system to intersite motion involving a proton vehicle mechanism, where H_2O/H_3O^+ is the vehicle in the wet materials, and intersite hops involving H^+ ions in the drier samples. Surprisingly, they suggested that the intrasite hops were too fast to be detected by NMR. Furthermore, the activation energy of the mobility decreased noticeably as a function of the activation temperature of the zeolite, samples with fewer residual water molecules/NH_4^+ ions showing noticeably lower activation energies, even though motion should be enhanced by a vehicle mechanism in these samples.

Franke and Simon studied the proton mobility in HZSM-5 by impedance spectroscopy and proposed that there is both proton intrasite motion (involving hops between oxygen around the same T atoms) and inter-site motion (between neighboring T atoms)[19,20]. The inter-site motion is strongly affected by the hopping distance between two adjacent Brønsted sites, and thus, the Si/Al ratio. It is clear that an improved understanding of the mechanisms of this protonic motion process is still required, if only to explain the noticeable discrepancies between the results from the different groups. It is important to stress that is not easy to distinguish between a rotation + a translation, and a rotational motion only using standard NMR spectroscopy experiments (in contrast to pulse-field gradient experiments).

The zeolite HZSM-5 samples used in most of the NMR and impedance studies reviewed above are prepared following the same procedure, namely by calcining the commercial NH_4ZSM-5 under vacuum at a temperature around 673K, a procedure which is generally considered to remove all the residual water. The products were then stored and measured in dry nitrogen atmosphere or sealed in glass capsule, ensuring no subsequent contamination by water.

The aim of this present work is to examine the effect of two different activation procedures on proton motion in a relatively high aluminum content (Si/Al = 25) zeolite HZSM-5 sample. The sample was calcined under vacuum following the reported standard procedure [5,15,17] and is labeled HZSM-5-V. In order to rule out the assignment of the broad ^{1}H signal around 6-7 ppm to residual NH_4^+ or water, we prepared a second sample by dehydrating the HZSM-5 sample under helium gas flow (HZSM-5-He). This method is thought to help remove trace water and NH_3 molecules. Variable temperature ^{1}H MAS NMR experiments were performed at around and below room temperature to monitor the motional process in both these samples. The experiments were performed at high field strength (14.1 T) with spinning speeds (8-9 kHz) that are sufficient to eliminate most of the broadening due to ^{1}H homonuclear dipolar coupling in these systems, at least at room temperature.

3.2 Experimental Section

3.2.1 Materials Preparation

HZSM-5-V was prepared by heating NH_4ZSM-5 (Si/Al=25; Zeolyst) under vacuum, with a step size of 0.2 K/min to 383 K, and then at 0.4 K/min to 673 K; after that the temperature was held at 673 K for 12 h. HZSM-5-He was prepared by heating the NH_4ZSM-5 in a tube furnace under helium gas flow, with the same heating program. The sample was quickly transferred into N_2 glove box and loaded in a tube that could be attached to the vacuum line. To remove the surface water absorbed during sample transportation, a second dehydration process was carried out by heating this sample under vacuum with a step of 0.2 K/min to 473K, holding at 473K for 5 h. The samples were stored and packed into NMR rotors prior to the NMR experiments in the N_2 glove box.

3.2.2 Solid-state NMR Spectroscopy

MAS NMR spectra were obtained with Bruker Avance 600 and Varian Infinityplus 360 spectrometers, with 89 mm wide-bore 14.1 and 8.45 T superconducting magnets, respectively, in 4 mm rotors. A rotor cap with an o-ring was used to avoid the adsorption of water during the NMR measurements. The rotors were spun with dry nitrogen gas in order to avoid contamination by H_2O molecules in the air and any undesired ice formation during low temperature experiments. The ^1H chemical shift is referenced to $CHCl_3$ (7.26 ppm).

The spin-lattice, T_1, relaxation time was measured by using the inversion-recovery (T1IR) pulse sequence. The pulse sequence consists of a 180° pulse and a 90° pulse separated by a variable time interval, τ. Data acquisition commences right after the 90° pulse.

The $^1H/^{27}Al$ TRAPDOR experiments were carried out by using the pulse sequence proposed by Grey and Veeman[21]. A rotor synchronized spin-echo pulse was applied on ^1H channel, and a dephasing pulse was continuously irradiated on ^{27}Al channel during the delay period in between the ^1H 90° and 180° pulses.

3.2.3 X-ray powder diffraction

X-ray powder diffraction data of the HZSM-5-V sample at 290 and 200K were collected at the X16c line of the National Synchrotron Light Source (NSLS), at

Brookhaven National Laboratory, using a sealed 0.7mm glass capillary and a wavelength of 0.69793 Å. Diffraction patterns were collected over the 2θ range of 1-30°. The variation of lattice parameters at the two different temperatures was determined by Rietveld refinement (with the GSAS program)[22] of the room temperature monoclinic[23] zeolite HZSM-5 structure .

3.2.4 Differential scanning calorimetry (DSC)

Differential scanning calorimetry analysis of HZSM-5-V was carried out in a temperature range of 213 - 298K under a dry N_2 atmosphere in a Perkin Elmer DSC-7 calorimeter. The heating/ cooling ramp rate was 2K/min.

3.2.5 Elemental analysis

Nitrogen elemental analysis has been performed on both HZSM-5-V and HZSM-5-He samples by Galbraith Laboratories, Inc. The samples were dissolved in a concentrated NaOH solution, in a distillation flask. The distillation flask was immediately attached to a distillation apparatus and all ammonia was distilled into a 3% boric acid solution. This solution was then analyzed by Ion Specific Electrode according to Galbraith procedure E7-6.

3.3 Results and Discussion

3.3.1 Variable temperature ^{1}H MAS NMR of HZSM-5-He

Figure 3.1 shows the variable temperature ^{1}H MAS NMR spectra of HZSM-5-He, the sample prepared under helium gas flow. The sample was cooled down to 153K and held at this temperature for 5h to equilibrate, before starting to acquire the NMR data as a function of increasing temperature. Two groups of resonances are seen at 3.9-4.2 ppm and 1.6-1.9 ppm, which are assigned to Brønsted acid site and silanol groups, respectively. The absence of the 6-7 ppm broad feature in these spectra confirms that this resonance, when present, is associated with a residual species that can be completely removed by helium gas flow. The N elemental analysis results indicate that the upper limit for the NH_3 content in this sample is 600 ppm (~ 0.2 NH_3/unit cell (u.c.), u.c. weight = 5760), confirming that the content of NH_4^+ ions in the samples is very small, if not nonexistent.

The chemical shift of the Brønsted acid site remains constant at 4.2 ppm between 153 and 213K. A gradual shift to 3.9 ppm on further heating to 293K is then observed. This change of ^{1}H chemical shift is ascribed to a slight change of the framework structure and T-O-T angles, which takes place above 213K, presumably driven by increased amplitudes and frequencies of the vibrations of the silicate framework[24]. No obvious change in chemical shifts was observed for the two silanol peaks at 1.6 and 1.9 ppm, and

the terminal silanol groups do not appear to be affected by any change of framework structure. Spin-lattice (T_1) times were measured at various temperatures, the 1.6 ppm peak showing the longest T_1 relaxation times of 14 and 10s at 153 and 293K, respectively. The T_1 relaxation of the 1.9 ppm peak is faster, and is 8 and 5s at 153 and 293K, respectively. The 1.6 ppm peak is ascribed to a more isolated/more rigid silanol environment than that of the 1.9 ppm peak. The increase in the T_1 relaxation times suggests that the SiOH groups become more rigid at lower temperatures. The two resonances from the silanol groups narrow with increasing temperature. This can be ascribed to more extensive vibrations or rotations of the hydroxyl groups around their equilibrium positions. Some ^{1}H exchange among the two same species is possible, but, since no evidence for any coalescence of the 2 resonances is seen, this ^{1}H exchange cannot be occurring on a timescale shorter than the inverse of the frequency separation between the two resonances (about 180Hz at 14.1 T; i.e., <5.5 ms).

A small amount of dealumination has occurred, which results in the sharp AlOH resonance at 2.3 ppm. The relatively high concentration of silanol groups in this sample is ascribed to the method used to make this commercial sample, higher concentrations being observed in HZSM-5 samples synthesized with a template, in comparison to the template-free method.[3,25] Our results are consistent with other ^{1}H NMR for similar samples presented in prior literature.[14,15,17]

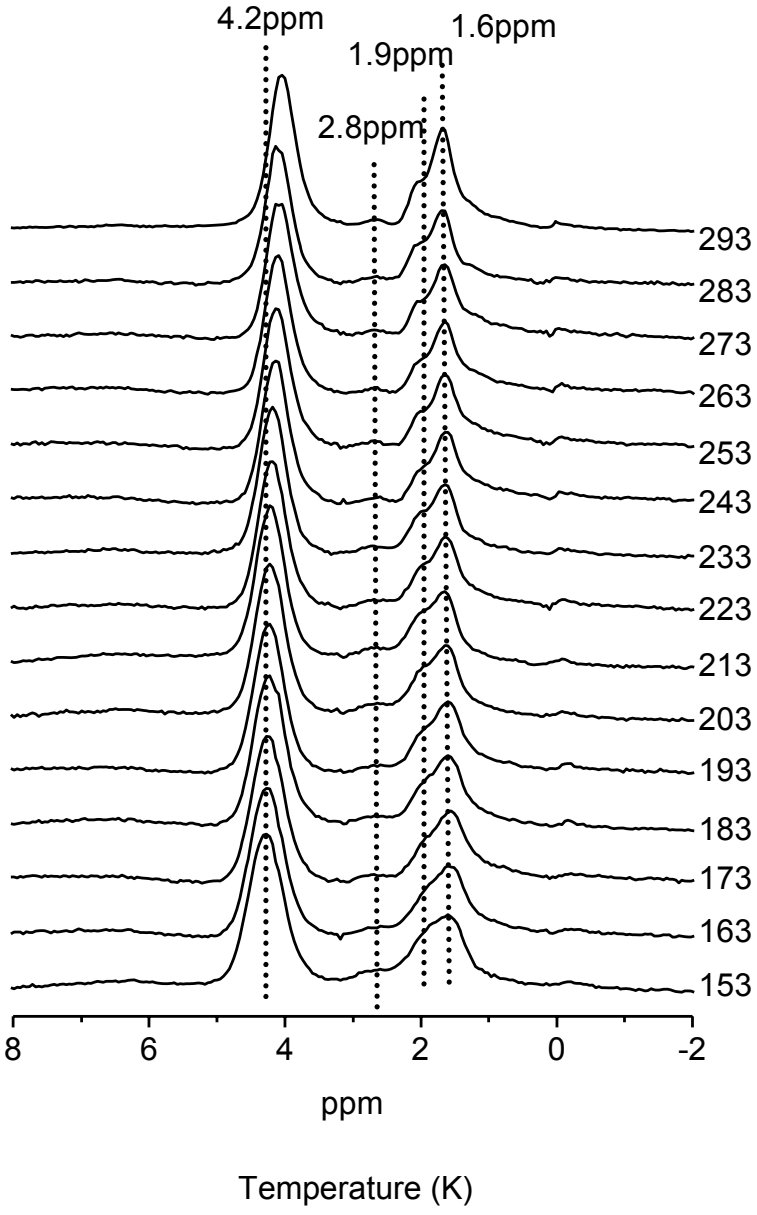

Figure 3.1 Variable temperature ^{1}H MAS NMR spectra of HZSM-5-He at 14.1 T; single pulse spectra; spinning speed =8 kHz.

3.3.2 Variable temperature ^{1}H MAS and low temperature $^{1}H/^{27}Al$ TRAPDOR NMR of HZSM-5-V

The variable temperature ^{1}H MAS NMR of the sample dehydrated under vacuum by using standard dehydration methods, HZSM-5-V, is shown in Figure 3.2. Similar resonances are observed on cooling (Figure 3.2 (a)) to those seen for HZSM-5-He in the chemical shift regions for the Brønsted acid, AlOH and silanol groups. However, unlike the HZSM-5-He sample, a broad signal centered at 6.1-7.0 ppm is now observed, which is coincident with the previously reported broad shoulder downfield of the Brønsted acid peak[3,4,10,26]. On decreasing the temperature (Figure 3.3 (a)), this broad feature gets narrower and finally a more distinct resonance at 6.2-6.5 ppm is observed. The change in the chemical shift of the Brønsted acid site is slightly greater than that seen for HZSM-5-He, shifting from 3.9 to 4.5 ppm from 293 to 213K, remaining at 4.5 ppm on further cooling.

In order to obtain unambiguous assignments of all the resonances seen at low temperatures, $^{1}H/\ ^{27}Al$ TRAPDOR NMR experiments were carried out at 203K. The results (Figure 3.3) confirm the previous assignments of the resonances at 5-2.9 ppm to the bridging (Brønsted acid site) hydroxyl protons (4.0-5.0 ppm) and Al-OH protons (2.9 ppm)[7]. No TRAPDOR effect is seen for the 1.9 and 1.6 ppm silanol peaks consistent with their assignments. The peak at 6.2-6.5 ppm does not show a noticeable $^{1}H\ /\ ^{27}Al$ TRAPDOR effect, which indicates that these protonated species are not strongly dipolar

coupled to Al atoms, and that this signal, at least in our samples, is not from a bridging hydroxyl proton (i.e., a Brønsted acid site). On this basis, we previously suggested that this resonance was due to residual ammonium cations,[11] although the assignment of this peak to residual water H-bonded to a Brønsted acid site was also suggested as a plausible assignment. The N elemental analysis (NH_3 content is 293 ppm, ~ 0.1 NH_3/u.c.) confirms that the zeolite contains only a trace amount of residual nitrogen. We thus assign the peak at 6.2-6.5 ppm to residual water associated with a Brønsted acid site. This residual "water" is either due to water molecules H-bonded to Brønsted acid sites, or to H_3O^+ ions (or both). It is non-trivial to distinguish between these two species based solely on their ^1H chemical shift, as discussed in earlier work.[10] The exact nature of the species that give rise to this (these) resonance(s) is explored further below. A pronounced loss of intensity of this 6.2-6.5 ppm peak, with increasing delay time between the $\pi/2$ and π pulses in the echo spectra (compare Figure 3.3(a) and (b)), shows that these environments are associated with relatively short spin-spin relaxation time (T_2), in comparison to all the other resonances.

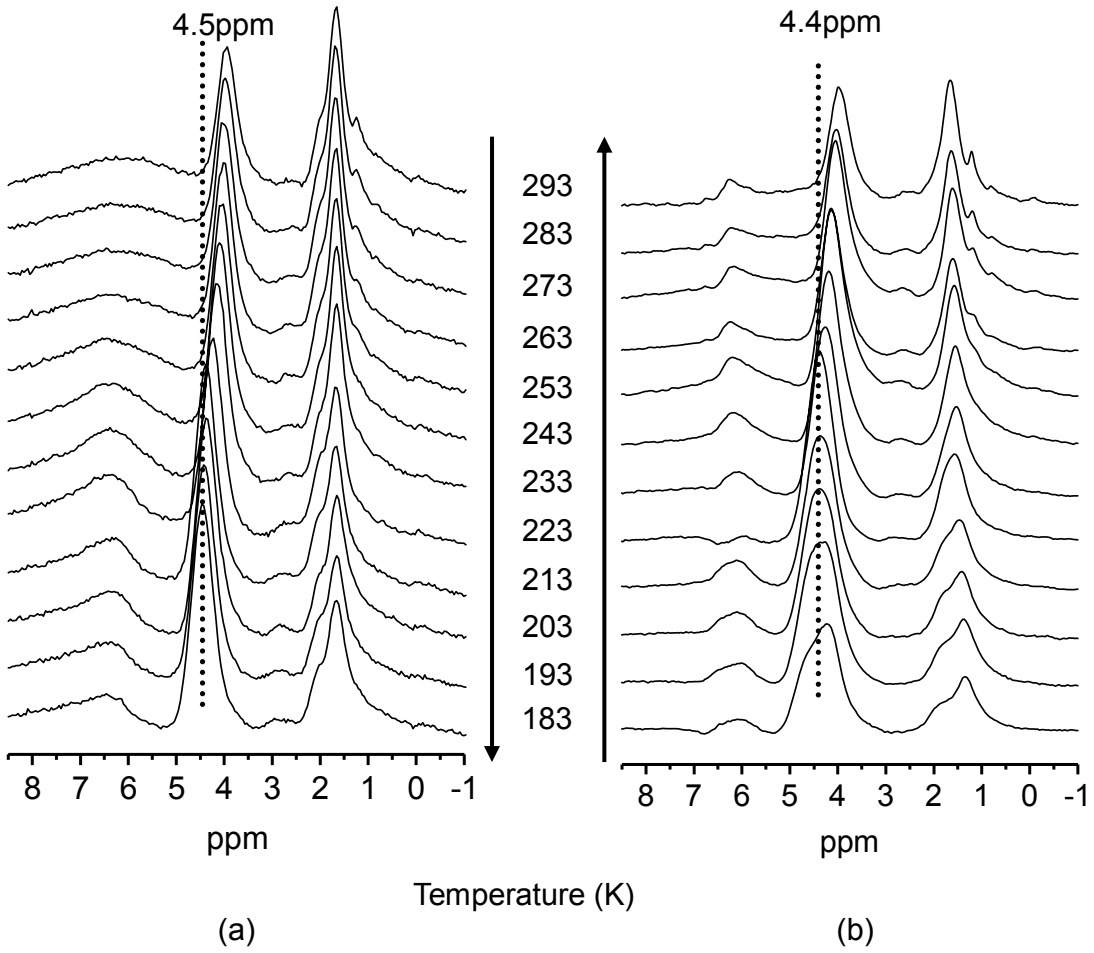

Figure 3.2 Variable temperature ^{1}H MAS NMR spectra of HZSM-5-V at 14.1 T, single pulse, spinning speed =8 kHz.

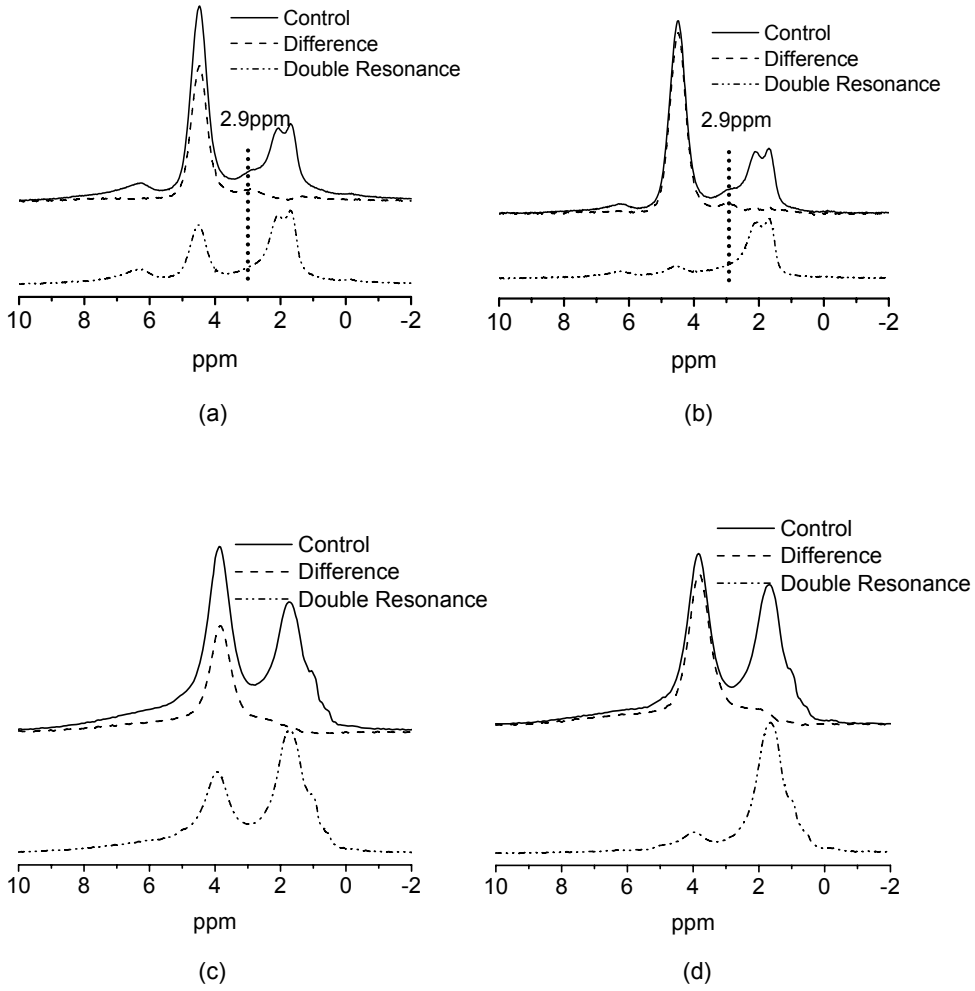

Figure 3.3 $^{1}H/^{27}Al$ TRAPDOR NMR of HZSM-5-V. Low temperature data were acquired at 203K, at 14.1 T, spinning speed = 8 kHz, with ^{27}Al irradiation times of (a) 2 (250μs) and (b) 8 rotor periods (1000μs). Room temperature data were acquired at 298K, at 8.45 T, spinning speed=5 kHz, with irradiation times of (c) 1 (200 μs) and (d) 5 rotor periods (1000μs). A loss of intensity on applying ^{27}Al irradiation (the double resonance experiment) indicates that the ^{1}H species is near Al.

Since the performance of an NMR probe may vary with temperature, particularly in so-called lossy samples that contain mobile species (see below), it is difficult to compare the absolute intensity of the different resonances (even after accounting for the Boltzmann factor). We have, therefore, used the intensity of silanol groups, $I_{SiOH,}$ (integral over 2.3- 0.5 ppm) as an internal standard. This was assumed to be a reasonable assumption as most of the silanol groups in zeolite HZSM-5 do not undergo rapid chemical exchange with any of the other proton species, as confirmed by the two-dimensional (2D) NMR experiments described in the next section. Thus, the relative intensity of silanol groups should not be significantly affected by the proton motional processes involving the other groups of the system. The Brønsted acid proton integrated intensity, I_{acid}, was assumed to correspond to the intensity of the peak(s) between 3.9 to 4.6 ppm. The ratio I_{acid}/ I_{SiOH} increases noticeably from 0.9 at 293 K to 2.1 at 183 K. In contrast, if an integral is taken over the larger chemical shift range of 8.3 to 3.0 ppm at each temperature, $I_{8.3\text{-}3.0ppm}$, the $I_{8.3\text{-}3.0ppm} / I_{SiOH}$ ratio stays constant over the whole temperature range from 183 K to room temperature. For comparison, the same integrations were performed for the HZSM-5-He spectra, and the I_{acid}/ I_{SiOH} ratio stays approximately the same from 293 to 153K. According to this intensity analysis, the intensity of the broad signal in HZSM-5-V is anti-correlated with the intensity of the Brønsted acid site resonance. A proton motional process involving exchange between the residual water and a subset of the Brønsted acid protons appears to be occurring at room temperature, which gives rise to the broad peak. This motion can be slowed down with

decreasing temperature, leading to a more distinct resonance at around 6.2 – 6.5 ppm and a noticeable gain in the intensity at Brønsted acid site resonance.

The sample was held at low temperatures for more than 48 hours to equilibrate and the spectrum shown at the bottom of Figure 3.2 (b) was then taken. A significant broadening of all the resonance indicates that the proton motional processes (including vibrational and librational motions) have been further frozen out. Two distinct Brønsted acid site resonances can now be observed at 4.6 and 4.2 ppm, and the broader 6.2-6.5 ppm resonance now appears to consist of two more distinct features at approx. 6.1 and 6.4 ppm. The shift of the resonance at 4.2 ppm is identical to the Brønsted acid proton peak observed in the H-ZSM-5-He sample, and is thus ascribed to the bare Brønsted acid proton. The resonance at 4.6 ppm is then tentatively assigned to protons no longer undergoing chemical exchange with the residual water molecules. The more positive chemical shift value of this resonance, as compared to the bare Brønsted acid proton resonance, suggests that these Brønsted acid protons are very weakly hydrogen-bonded to the water molecules. This indicates that at least some of the residual "water" 6 – 7 ppm resonance at this temperature must be due to H_2O rather than H_3O^+, at least following equilibration at low temperatures.

The two Brønsted acid site resonances coalesce to form a resonance at around 4.4 ppm when the sample is heated up slightly from 193 to 203K. From 203K to 213K, the coalescenced peak becomes narrower. Above 213K, the resonance continues to sharpen and its chemical shift changes gradually from 4.4 to 3.9 ppm, indicating that the

framework change that occurs on cooling is reversible. A number of significant observations were made at around 213 - 223 K, which appear to be associated with a change of structure and mobility. First, a jump of about 3MHz in the ^{1}H channel tuning of the NMR probe was observed when the temperature was raised above 213 K (i.e., between 213 and 223K); a similar change in probe tuning was observed on cooling. This generally indicates a change in the dielectric (or electronic) properties of a material and is consistent with the sudden onset of a motional process. This change in the material's dielectric constant (and the detuning) was sufficient to result in a noticeable change in the ^{1}H nutation frequency of from 89 kHz above to 78 kHz below 213 K. The I_{acid}/ I_{SiOH} value remained constant below 213K but decreased gradually above 223K. Second, the 6.1/6.4 ppm broad resonance show unusual behavior at 223K: The intensity of this resonance decreases noticeably at this temperature, and the resonance appears to be distorted. This is tentatively ascribed to the interference of motion of the water molecules with MAS, so that the dipolar coupling is no longer removed, but it may also be due to the onset of other motional processes. Above 223K, a broad resonance emerges at approx. 5.2 ppm, in between the 6.1/6.4 ppm resonances and the Brønsted acid site peaks; the 6.1 ppm component of the 6.1/6.4 ppm resonance has now essentially disappeared. Thus we ascribe the broad resonance to protons undergoing chemical exchange between the Brønsted acid sites and a water resonance that gives rise to the 6.1 ppm signal. This is consistent with the decrease in the intensity of the Brønsted acid site signal in this temperature regime. Furthermore, this also indicates that the 6.1 ppm component must be

due to weakly H-bonded water, not H_3O^+ ions. We tentatively ascribe the coalescence of the two Brønsted acid sites at 4.2 & 4.6 ppm to the onset of the water motion, exchange occurring both between sites and with the H-bonded H_2O molecules. Note that the I_{acid}/ I_{SiOH} ratio observed at low temperature is not very different from that observed in the HZSM-5-He sample, indicating that the extent of dealumination in the two samples is similar.

Based on all of the above observations, it is clear that a significant increase in the proton motional process involving the residual water and part of the Brønsted acid protons occurs at around 213K-223K. The process is not completely reversible, on the timescale of these NMR experiments, since the spectra seen on heating are quite different from those seen on cooling. The broad resonance originally observed at 6-7 ppm at room temperature is not observed. Instead, a fraction of the intensity of the 6.4 ppm resonance remains, and this resonance is much sharper. However, if the sample is then examined at a later period (i.e., after a few hours to days), the spectrum resembles that seen initially, and the broad 6-7 ppm resonance returns.

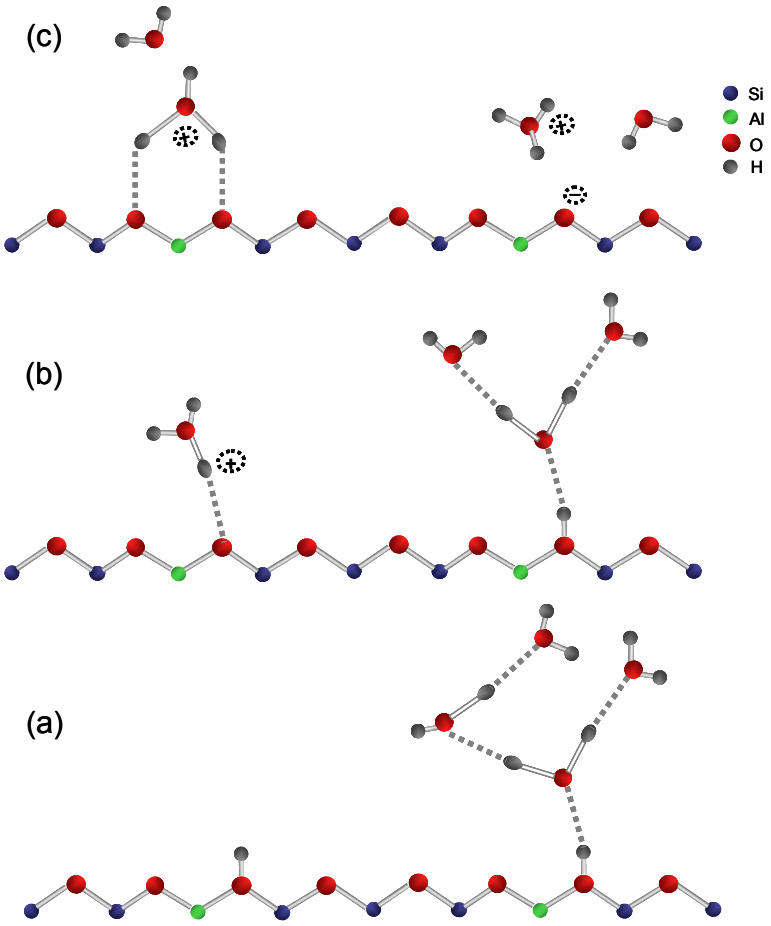

Figure 3.4 Schematic illustrations for the proton motion processes in sample HZSM-5-V upon heating from (a) 183K to (b) 213-223K and finally to (c) 293K.

The two resonances from the silanol groups also coalesce at a temperature slightly above 213K. The silanol region now resembles a typical SiOH region seen in previous HZSM-5 samples, where only one resonance at 1.8 ppm is typically observed.[5,6] The sharp resonance at about 1 ppm is presumably due to a more isolated silanol group. In HZSM-5-He sample, these two resonance do not coalesce even at room temperature, which suggests that the proton exchange between these two types of silanol groups is mediated by the presence of mobile H_2O/H_3O^+. Differences between our spectra and early NMR spectra of ^1H ZSM-5[5,6], may also be due to lower resolution of the spectra and possibly differences in the numbers and types of defect present in these samples.

To explore the effect of motion on TRAPDOR spectra, room temperature $^1H/^{27}Al$ TRAPDOR experiments were performed on the sample that had been relaxed for a few days. Figure 3.3 (c) and (d) show the control, double resonance and difference spectra obtained with ^{27}Al irradiation time of 200 μs and 1000 μs, respectively. As shown in Figure 3.3 (c), TRAPDOR effects can be observed for the 6.4, 3.9 and 2.5 ppm resonances, even with short ^{27}Al irradiation time of 200 μs. Surprisingly, the TRAPDOR effect for the broad resonance centered at 6.4-6.5 ppm is only slightly lower than that observed on the resonance of Brønsted acid protons at 3.9 ppm (see Figure 3.3 (c) and (d)). This result is consistent with the TRAPDOR effect observed on zeolite HZSM-5 for this resonance by other authors.[27,28] The 1.9 ppm resonance of silanol groups also shows a small TRAPDOR effect, when the ^{27}Al irradiation time is 1000μs or longer (Figure 3.3 (d)). The change of the dephasing behaviors of the 6.4 and 1.9 ppm resonances between

low and room temperatures is presumably caused by the different proton motional processes, and different H-bonding networks. At low temperature, we propose that the 6.1-6.4 ppm peak is due to larger H_2O (H_3O^+) clusters with only weak H-bonding to the Brønsted acid proton. This is consistent with the small shift seen for the 4.6 ppm Brønsted acid proton resonance, which has a shift very close to that of the bare Brønsted acid site. The dipolar coupling interaction between the protons of the water molecules and the framework Al is too weak to cause any significant dipolar dephasing in the TRAPDOR experiment. At higher temperatures, more mobile single water molecules/H_3O^+ ions or smaller clusters are present which give rise to the broad resonance. Since the clusters are smaller, these bind more strongly to the Brønsted acid site; (note that some of the intensity of this resonance arises from strongly H-bonded Brønsted acid sites/H_3O^+, consistent with this suggestion), causing the TRAPDOR effect. Furthermore, this result suggests that the sharper resonances seen at approximately 6.1 ppm on 1st returning the sample to room temperature (Figure 3.2) contains the larger clusters present at low temperatures. On the basis of the weak TRAPDOR effect for the 1.9 ppm, we assign this resonance to the internal SiOH defects created by the removal of organic template during calcination. Protons from these SiOH defects may be involved in the proton motional process at/ above room temperature.

3.3.3 2D-Magnetization Exchange NMR

The ^{1}H MAS 2D magnetization exchange experiments of HZSM-5 were performed to probe the exchange processes between the different species in the HZSM-5-V sample. The sample was cooled down and measured at 223K straight away, without leaving the sample for an extended period at lower temperatures. As shown in Figure 3.4 (a) and (b), strong cross-peaks are observed between the resonances at 4.6 and 6.2 ppm at 223K, when using a mixing time of 1 and 5ms. In comparison to the results observed by Haw and coworkers[5], who used a mixing time of 250 ms at 123K, the exchange rate at 223K is noticeably faster, which is consistent with the increase in H-H exchange rate between these two sites with temperature. A second component is seen for the broad line, which does not undergo exchange with the Brønsted acid sites, but gives rise to the narrow ridge on the diagonal with noticeable intensity spreading to as high a frequency as 8.5 ppm. Cross-peaks between the Brønsted acid site protons and silanol protons can only be observed with a longer mixing time of 500ms. The cross-peak only involves the 1.9 ppm silanol environment, which is consistent with the small TRAPDOR effect observed at this resonance in the $^{1}H/^{27}Al$ TRAPDOR experiment with long ^{27}Al irradiation time. No exchange is seen with the 1.6 ppm peak. The broader 6-7 ppm peak disappears when using these long mixing times, presumably due to its shorter T_1. Cross-peaks can be generated by two sources, spin-diffusion between proton species and actual chemical exchange. Exchange via both processes, however, does suggest that the

environments undergoing exchange are in reasonably close proximity. However, both processes can result in magnetization transfer over quite long distances (nm), either when very rapid motion is present, is mediated by mobile species, or for tightly coupled spin systems. The results are consistent with the location of the majority of the silanol protons on the zeolite surfaces, i.e., spatially separated from the Brønsted acid sites. These silanols give rise to the resonance at 1.6 ppm. The 1.9 ppm silanol resonances are either due to internal defects, or more acidic silanol groups (also at the surface), which can undergo exchange more readily with any mobile water in the samples. Slow exchange between the 2 main silanol peaks (1.9 & 1.6 ppm) and with the Brønsted acid site protons is seen at higher temperatures (303 K), which we ascribed to motion involving or mediated by H_2O. Long timescale of the exchange between the silanols and the rest of the spin system (i.e., the Brønsted acid sites and water), (approx. 500 ms at 223K) validates our use of the intensities of these groups (I_{SiOH}) as internal intensity standards. At 303 K this exchange appears to be more rapid, and may explain the loss of signal intensity seen in a 2D exchange experiment performed with a mixing time of 500 ms.

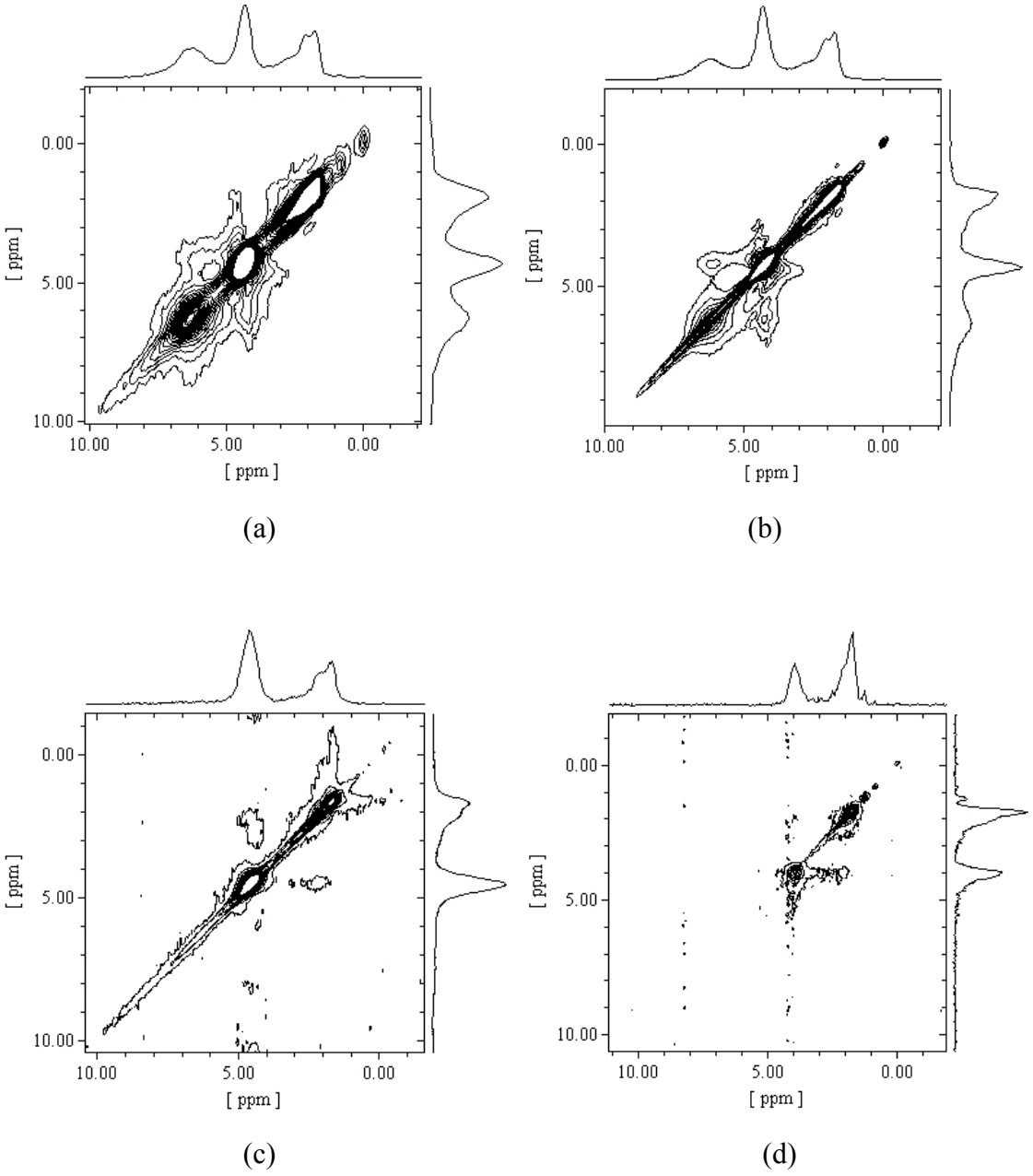

Figure 3.5 2D ^{1}H MAS magnetization exchange spectra of HZSM-5-V at 14.1 T with mixing times of (a) 1ms, (b) 5ms and (c) 500ms at 223K, spinning speed = 9kHz; (d) mixing time 500ms at 303K, spinning speed = 8kHz.

3.3.4 DSC

Figure 3.5 shows the DSC curve for sample HZSM-5-V. The sample was first cooled from room temperature to 213K. One exothermic event can be observed during this cooling process, the inflexion of which is located at around 228K. The sample was then held at 213K for 2h before being heated up to room temperature. During the heating process, an endothermic event starts at about 225K with an inflexion at around 233K. The result of DSC supports the argument that a change of framework or water structure occurs at around 220 - 230K. The transition temperature measured from DSC on heating is slightly higher than that measured by NMR, which is ascribed to the faster ramp rate used in the DSC experiment. Most striking is the irreversibility of the process, a significant hysteresis being observed. Unfortunately, we were not able to acquire a DSC plot for HZSM-5-He, because we were unable to ensure that the sample remained completely dry.

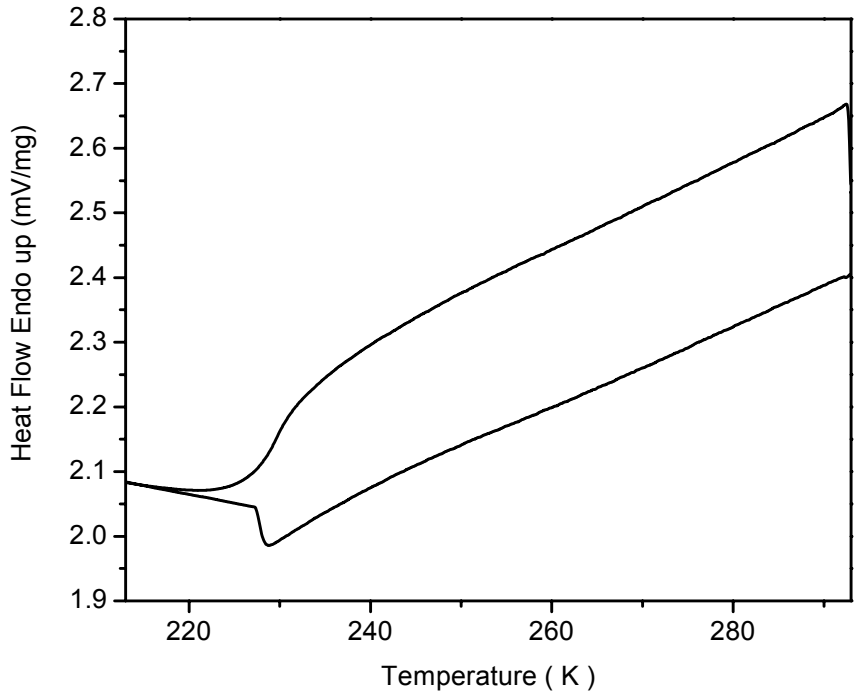

Figure 3.6 DSC curve for sample HZSM-5-V, acquired with a temperature ramp rate of 2K/min

3.3.5 XRD

The unit cell parameters of sample HZSM-5-V at 290 and 200K were determined by Rietveld refinement. The refinement results are shown in Figure 3.6 (a) (200K) and (b) (290K). The refined cell parameters are listed in Table 3.1. The unit cell shrinks at low temperature due to a contraction along *b* direction, but no change in space group ($P2_1/n.1.1$) was observed. This contraction along the *b* direction in turn leads to a distortion of a subset of T-O-T angles. Table 2 shows the comparison of 48 T-O-T angles at 200K and 290K. The center oxygen atoms of the most affected T-O-T angles (with differences of greater than 0.08°) are shown in Figure 3.7. All of the most affected angles are located in the double 10-rings of the sinusoidal channel along the *a* direction (Figure 3.7 (a)) or the intersection of the straight and sinusoidal 10-ring channels (Figure 3.7 (b)). The circles and arrows on Figure 3.7 (a) indicate the most affected oxygen atoms (Increasing and decreasing angles are labeled with red and green, respectively, which is consistent with the marks in Table 3.1) and the directions of the shifts of positions, respectively. The channels along the *a* direction have been flattened by the contraction of the framework along the *b* direction. Figure 3.7 (b) shows the structure from another angle of view with the straight 10-ring channel running along the b direction, and the affected oxygen atoms located around the intersection of the straight and sinusoidal 10-ring channels.

Table 3.1 Unit cell parameters of HZSM-5-V.

	a (Å)	b (Å)	c (Å)	α(°)	β(°)	γ(°)	V (Å^3)
290K	20.104	19.917	13.407	89.91	90.0	90.0	5368.18
200K	20.099	18.899	13.405	90.19	90.0	90.0	5361.45

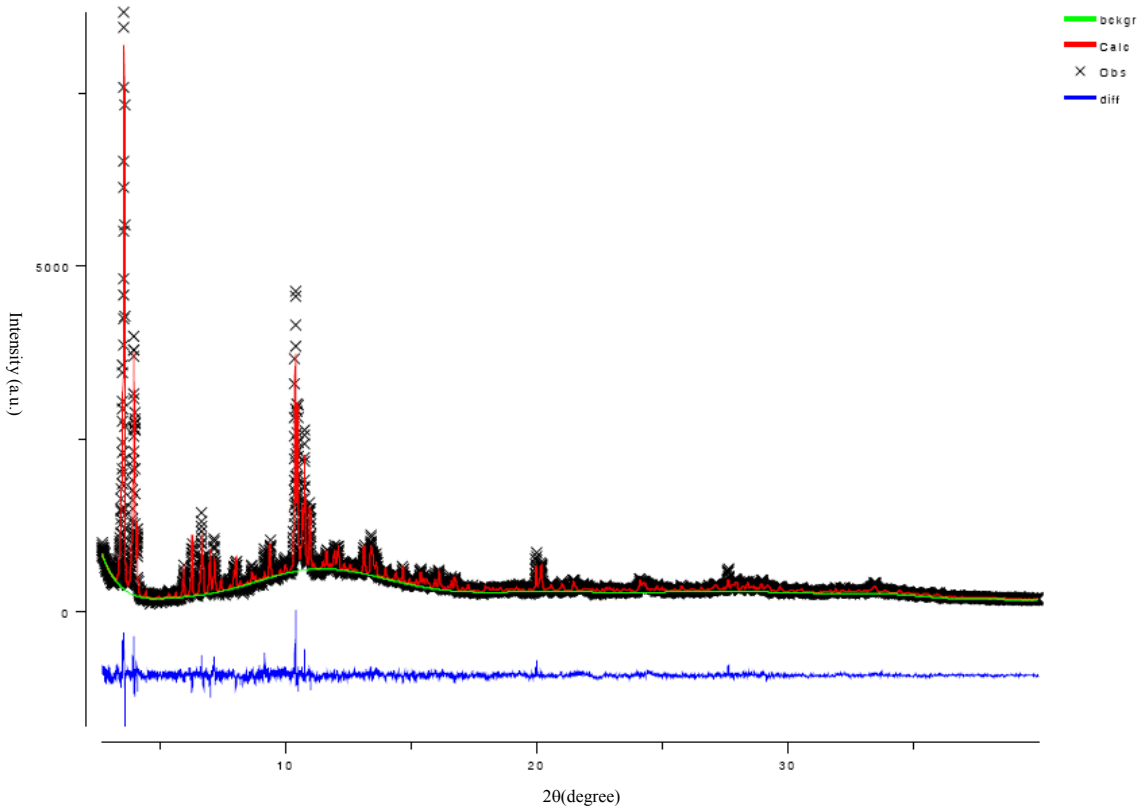

(a)

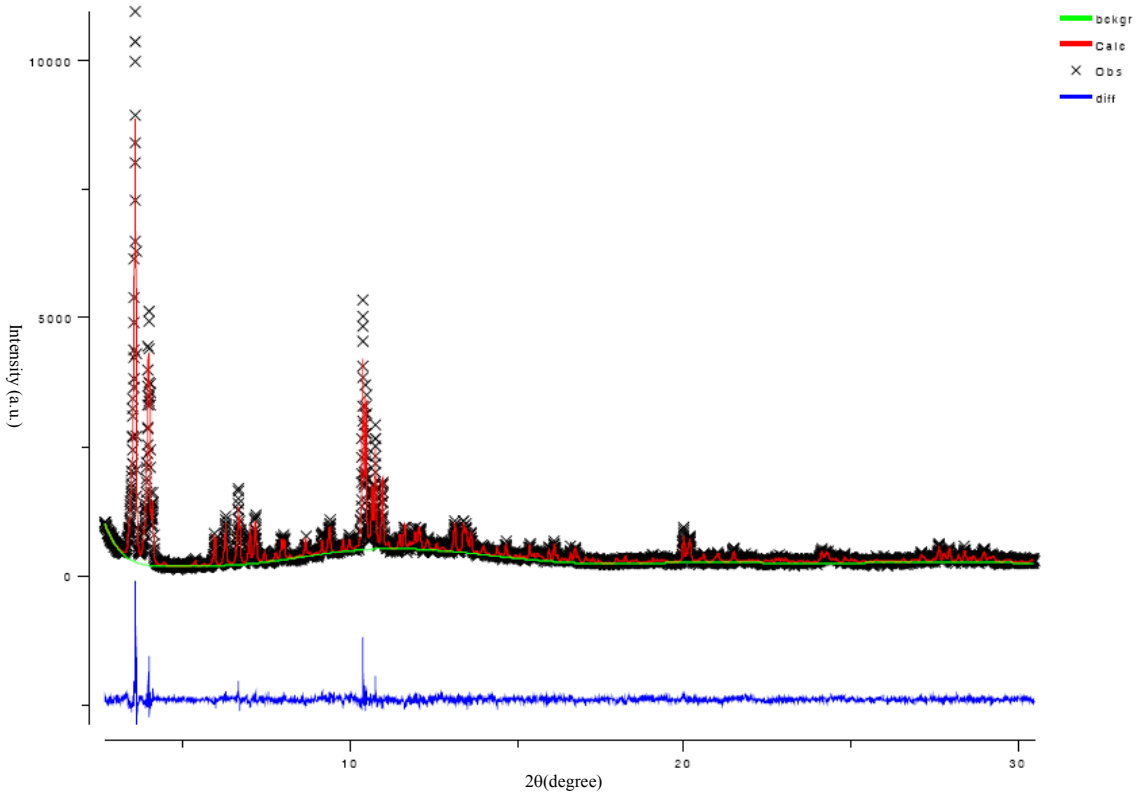

(b)

Figure 3.7 The Rietveld refinement (with the GSAS program) of the HZSM-5 structure with the XRD patterns obtained at two different temperatures (a) 200 and (b) 290 K, performed with the room temperature monoclinic zeolite HZSM-5 structure as a staring model.

Table 3.2 Comparison of T-O-T angles at 200K and 290K.

O	*T-O-T (°,200K)*	*T-O-T (°,290K)*	*O*	*T-O-T (°,200K)*	*T-O-T (°,290K)*
O_1	*144.78*	*144.69*	O_{25}	*150.98*	*150.99*
O_2	*145.13*	*145.15*	O_{26}	*145.26*	*145.28*
O_3	*158.11*	*158.10*	O_{27}	*153.24*	*153.29*
O_4	*147.03*	*147.08*	O_{28}	*148.94*	*148.91*
O_5	*148.93*	*148.93*	O_{29}	*157.11*	*157.07*
O_6	*162.78*	*162.75*	O_{30}	*155.52*	*155.50*
O_7	*158.27*	*158.31*	O_{31}	*147.70*	*147.68*
O_8	*150.90*	*150.84*	O_{32}	*156.73*	*156.77*
O_9	*150.57*	*150.56*	O_{33}	*149.19*	*149.13*
O_{10}	*154.46*	*154.39*	O_{34}	*146.11*	*146.15*
O_{11}	*156.00*	*156.00*	O_{35}	*150.00*	*149.93*
O_{12}	*167.16*	*167.15*	O_{36}	*158.57*	*158.59*
O_{13}	*159.01*	*159.03*	O_{37}	*153.79*	*153.80*
O_{14}	*157.35*	*157.36*	O_{38}	*152.92*	*152.83*
O_{15}	*150.02*	*149.92*	O_{39}	*163.62*	*163.64*

O_{16}	169.04	169.07	O_{40}	160.01	160.02
O_{17}	145.75	145.60	O_{41}	151.18	151.27
O_{18}	141.05	140.89	O_{42}	156.12	156.07
O_{19}	168.63	168.68	O_{43}	149.90	150.03
O_{20}	142.39	142.25	O_{44}	150.79	150.87
O_{21}	144.79	144.84	O_{45}	155.50	153.45
O_{22}	151.10	151.12	O_{46}	155.54	155.66
O_{23}	156.10	156.11	O_{47}	149.60	149.60
O_{24}	149.71	149.72	O_{48}	147.68	147.67

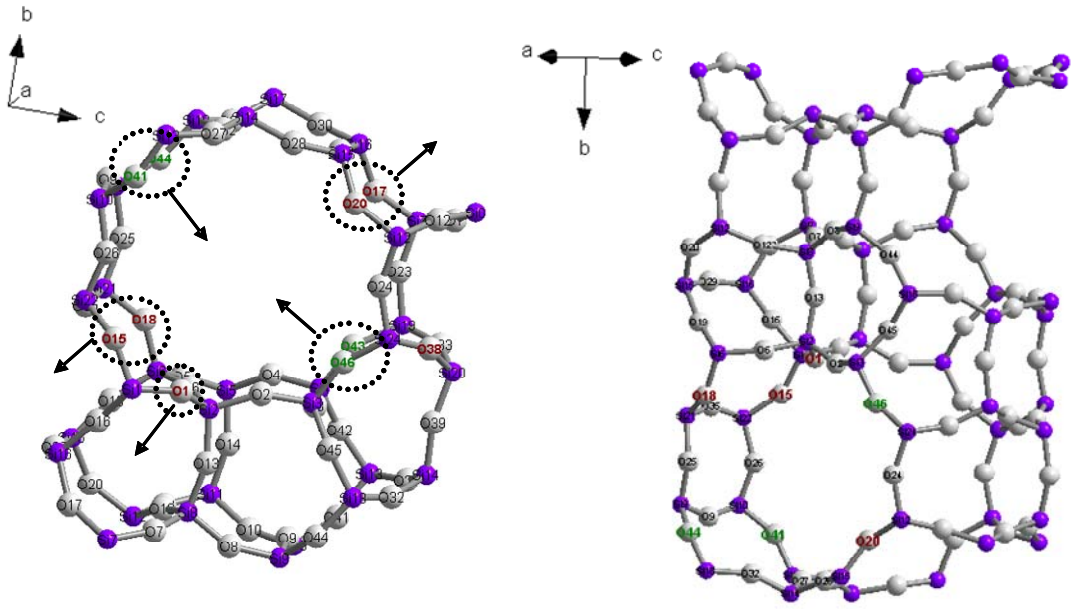

(a) (b)

Figure 3.8 The channel structure of HZSM-5, (a) double 10-ring sinusoidal channel along the *a* direction, (b) 10-ring straight channel viewed along the *b* direction. The center oxygen atoms of those T-O-T angles increase and decrease upon cooling are labeled in red and green, respectively.

3.3.6 Discussion

Before discussing the possible mechanisms for protonic motion, we analyze the structural changes that occur at low temperatures. The XRD results confirm that the framework contracts along the *b* direction at low temperature. DSC analysis indicates that a phase change appears to take place at around 225K. The process is not fully reversible, and some hysteresis is observed. This is consistent with the ^{1}H NMR spectra (and in particular, the "water" resonances), which are quite different on heating and cooling. In contrast, the chemical shift of the Brønsted acid resonance (3.9-4.2 ppm) shifts gradually from lower to higher frequency as the temperature is lowered. This process is reversible and a similar reversible shifting of the ^{1}H Brønsted acid resonances is seen for both the "wet" and dry (HZSM-5-He) zeolites. Thus, two processes seem to be occurring on lowering temperature. The first is a gradual contraction of the zeolite framework (mostly along the b-direction). This contraction will result in a change in the T-O-T bond angles and thus the ^{1}H chemical shift of the Brønsted acid site. A correlation between the experimental T-O-T angle and the proton acidity has been established in zeolite HZSM-5 based on quantum chemical studies.[29] The ^{1}H chemical shift of the Brønsted acid site was also proposed to be a measure of the O-H bond length, which is in turn related to the acidic strength. The increasing value of the ^{1}H chemical shift upon cooling is indicative of a longer O-H distance, which could be caused by an increase in the T-O-T angle. Since the same gradual chemical shift change is observed for the "wet" and "dry" samples, this

indicates that this is an intrinsic behavior of the zeolite upon cooling, not a change induced by water molecules. The second process that occurs at approximately 200 – 223 K is related to the water molecules, but it may also cause a structural change of the framework. This appears to a complex process involving both a slowing down of the motion and also a change in the nature of the H-bonding. The process is also associated with a large kinetic barrier, because an extremely large hysteresis is observed, the room temperature sample taking hours to equilibrate. This is somewhat surprising, given that we believe that the water molecules are mobile at this temperature. The most likely explanation is that the H_2O/H_3O^+ species and the Brønsted acid sites form complex H-bonded clusters. The exact nature of these clusters will vary with temperature due to (a) a change in mobility, and (b) a change in the framework structure. The latter will result in change in the shape and sizes of the pores and possibly in the acidity of the Brønsted acid sites, which will in turn affect the H-bonding networks formed by the H_2O/H_3O^+ and the extent of proton transfer from the Brønsted acid site to the H_2O molecule. At low temperatures, larger clusters appear to be present, which result in weaker H-bonding of the H_2O molecule to the Brønsted acid site. This is tentatively ascribed to the contraction of the pores, and the reduced mobility, which may favor multiple interactions with the oxygen atoms of the framework, rather than a single (likely stronger) interaction with the Brønsted acid site. At higher temperatures, the Brønsted acid sites increasingly undergo exchange with the H_2O/H_3O^+ species and different H-bonded clusters are formed. Since the concentration of water molecules is low (the ratio of Brønsted acid sites to water is 1:

0.07, based on the intensity of the two resonances at low temperature, and assuming that the 6.1 ppm is due to water only), and diffusion of the water is highly tortuous, involving 1D channels, we propose that it takes an extremely long time for equilibrium to be reached at the different temperatures.

The proton mobility/conductivity in zeolite HZSM-5 has been demonstrated to be strongly affected by the Si/Al ratio in both ^{1}H MAS NMR and impedance studies. This phenomenon has been ascribed to H^{+} hopping between oxygen atoms associated with the same T (Al) site, giving rise to a hopping length which is determined by the distance between two closest Si-O-Al oxygen atoms. This theory contradicts the lower extent of proton mobility that has been observed experimentally on zeolites H-mordenite and H-Y, both of which possess a much lower Si/Al ratio and hence shorter hopping length between different T sites. However this may reflect the lower acidity of these zeolites. As is clear from this current work, the residual water in this widely studied zeolite HZSM-5-V strongly influences that dynamics complicating the analysis of at least some of these previous studies.

The exact nature of residual water in acid zeolites remains unresolved in the literature. Previous ^{1}H NMR and infrared studies proposed two possible forms, hydrogen bonded water and hydroxonium ions, H_3O^{+}.[30-32] Sauer and coworkers studied the absorption of water in zeolites by both *ab initio* calculations and inelastic neutron scattering (INS).[33-35] According to their *ab initio* calculations[34,35] for a water, Brønsted acid site 1:1 complex, the hydrogen bonded structure represents the thermodynamic

minimum, the H_3O^+ cation occurring only as an intermediate transition state. The energy difference between both forms is only a few kJ/mol. The ion pair can be stabilized by adding a second water molecule. In the complex with a water to Brønsted acid site ratio 2:1, both $(H_2O)_2$ and $H_5O_2^+$ are energy minima. However, in their INS study on zeolite HZSM-5 (Si/Al= 12.5) with various loading level of water (3.5-35 H_2O/u.c.), hydroxonium ions were not observed even in sample with loading level as high as 6 H_2O molecules per acid site. This conflicts with the experimental results reported by Deng et al. who observed a ^1H resonance at 8.0 ppm, which they ascribed to "free" H_3O^+, for a water loading level of higher than 1.4 H_2O/u.c. in zeolite HZSM-5 (Si/Al=14).[28] It should be noted that Smith et al. reported both H_3O^+ and H_2O can be identified in zeolite HSAPO-34 by neutron powder diffraction at 10 K, when water molecules interact with Brønsted acid sites sitting in rings of different sizes.[36] Vega et al. studied the interaction of water molecules and zeolite H-RHO at various loading levels, but could not determine definitively whether the Brønsted acid protons remain on the framework or whether transfer to H_2O to form H_3O^+ occurs. More recently, Kanellopoulos *et al.*[18] have suggested that since hydroxonium species, non-H bonded water molecules and fully H-bonded water molecules show shifts of 7 – 19, 0.31 and 4.78 ppm, respectively, the cluster comprising three water molecules and hydroxonium ion should have an average shift of 8.3 ppm. On this basis they argue that a hydroxonium ion must contribute to the high frequency signal. Our results suggest that at least part of this signal is due to H_2O, but that the contribution of the two species can vary as a function of both temperature and

cooling/heating rates. What is clear from these previous studies, is that the addition of more water molecules to the system, and the formation of larger more extended H-bonded clusters of water, aids the transfer of H^+ from the zeolite, to form larger clusters of H_3O^+ ions H-bonded to more than one water molecule.

Protonic conduction in solid materials is generally explained by two classic mechanisms: the Grotthuss Mechanism and the Vehicle Mechanism[37,38].In the Grotthuss Mechanism, protons are hydrogen bonded to water molecules and transported through the reorientation of water molecules in an infinite network of hydrogen bonds. The Vehicle Mechanism does not require an infinite network of hydrogen bonds. According to this model, either H_3O^+ or H_2O plays the role of a vehicle. The proton motion in this case is related with the diffusion of the vehicles. Both of these two mechanisms will occur in system with a large content of water. Zeolite HZSM-5-V with Si/Al=25 only has 4 bridging Si-O(H)-Al sites in each unit cell, while the number of residual H_2O in each unit cell is even smaller (7% based on the intensities of the low temperature NMR spectra, assuming the approx. 7 ppm is water). Thus, we propose that motion in nominally dry zeolite HZSM-5-V occurs via a vehicle-hopping mechanism. This mechanism was also proposed to be important by Kanellopoulos *et al.*[18] in their recent study of HZSM-5 loaded with either H_2O or NH_3.

In a vehicle-hopping mechanism, protons can migrate either in the form of H_3O^+, the H_3O^+ cations hopping from one Si-O-Al to another, or as H_2O molecules, the H_2O molecules hopping from one Brønsted acid site to another. The former mechanism

requires that there are vacant T sites (i.e., T sites with bare O-atoms for the H_3O^+ to bind to), so that an H_3O^+ "hop" can occur. Alternatively, the motion can be concerted involving motion of more than one H_3O^+ (or H^+) ion at the same time. An intermediate mechanism can be envisaged whereby the H_3O^+ ion hops to bind to a bare O atom on a T site already containing an H-bonded H_3O^+ ion, to form a short-lived intermediate. This then results in an almost immediate hop of the second H_3O^+ ion to another T site, causing another H_3O^+ (or H^+) ion to hop. The second mechanism is simpler as the H_2O ions are free to hop from site to site without involving any concerted motion, which is generally easier. However, only motion involving H^+ or H_3O^+ ions contributes to the conductivity as measured by a.c. impedance methods, and thus H_3O^+ or H^+ motion must be occurring at least at high temperatures. The activation energies of these mechanisms may be reduced if additional H_2O/H_3O^+ species are nearby, additional H-bonding helping in the H^+ transfer processes. Even though the vehicle mechanism will be associated with a lower activation energy, it will still be influenced by the hopping length, consistent with the dependence of the activation energy on the Si/Al ratio.[19,20] Furthermore, we speculate that the lower activation energy seen previously for higher Al content HZSM-5 zeolites is a combination of the shorter hopping distance and the fact that they are more difficult to dehydrate completely and thus contain more residual water molecules.

Kanellopoulos *et al.*[18] in their recent paper observe a decreasing activation energy for proton mobility upon increasing the activation temperature, over a range of 573 ~723K, and an associated lowering of the onset of motional narrowing of the Brønsted

acid site. These authors suggested that the proton mobility of zeolite HZSM-5 activated at ≥ 673K was not influenced by residual water, however, they still observe the high frequency (6-7 ppm) resonance, which we believe is due to H_2O/H_3O^+. They also state that it is difficult to determine the absolute concentration of residual water molecules in these systems. We speculate that at lower activation temperatures, residual NH_4^+ ions are present, which are not as good "vehicles", while at higher temperatures, only a few water molecules remain, which can act as more effective vehicles. Furthermore, when more water is present, it is also possible that different water clusters and networks are present and that isolated H_2O/H_3O^+ species or small clusters may act as faster vehicles than slightly larger clusters, which may move more slowly along the zeolite channels. However, it is important to stress that the differences between the two studies results from slight differences in zeolites, which could arise from the synthesis and activation methods used to prepare the materials. This is unfortunately a phenomenon that plagues comparison between nominally similar materials, in this field. Clearly, more studies are required to investigate these complex phenomena.

3.4 Conclusions

The traditional "static" calcination procedure for making dehydrated H-form zeolite by heating the ammonium form zeolite under a vacuum does not remove all the water molecules in the HZSM-5 framework. The residual water, at least in our systems, is responsible for the resonance at 6 – 7 ppm, often seen in "dry" HZSM-5 systems. The

residual water can, however, be removed when the calcination is carried out under extra dry helium gas flow. The difficulty in removing the water may be related to the 1D channel structure of HZSM-5, combined with the small cages of the pentasil units, which could trap the water. The residual water molecules enhance the proton motional process considerably, and thus results from zeolites activated in a similar fashion cannot be used to discuss the relative ease of inter vs. intra site H^+ sites, particularly in HZSM-5 zeolites with Si/Al<30. A vehicle-hopping model has been proposed to explain the motion that occurs in the wet systems.

On cooling the temperature, the chemical shift value of the Brønsted acid sites in both the dry and wet samples shift to higher frequencies, which is ascribed to a gradual contraction of the zeolite framework, the XRD results showing that the largest change is seen along the b-direction of the cell. The DSC and NMR results indicate that a more sudden change occurs at approximately 200 – 220 K, which appears to be associated with a change in both proton mobility and the nature of H-bonding. This structural/motional change is associated with a significant hysteresis. The results indicate that considerable care is taken when interpreting the dynamics and double resonance (^{1}H-^{27}Al, ^{1}H-^{17}O) spectra of nominally dry zeolites.

3.5 References

(1) Hunger, M.; Freude, D.; Frohlich, T.; Pfeifer, H.; Schwieger, W. *Zeolites* **1987**, 7, 108.

(2) Freude, D.; Hunger, M.; Pfeifer, H.; Schwieger, W. *Chem. Phys. Lett.* **1986**, 128, 62.

(3) Hunger, M.; Freude, D.; Pfeifer, H.; Schwieger, W. *Chem. Phys. Lett.* **1990**, 167, 21.

(4) Brunner, E. *J. Chem. Soc. Faraday T.* **1990**, 86, 3957.

(5) Beck, L. W.; White, J. L.; Haw, J. F. *J. Am. Chem. Soc.* **1994**, 116, 9657.

(6) Brunner, E.; Beck, K.; Koch, M.; Heeribout, L.; Karge, H. G. *Microporous Mater.* **1995**, 3, 395.

(7) Hunger, M. *Solid State Nucl. Magn. Reson.* **1996**, 6, 1.

(8) Freude, D. *Chem. Phys. Lett.* **1995**, 235, 69.

(9) Hunger, M. Habilitation Thesis, University of Leipzig, 1991.

(10) Hunger, M.; Freude, D.; Pfeifer, H. *J. Chem. Soc. Faraday T.* **1991**, 87, 657.

(11) Peng, L.; Huo, H.; Liu, Y.; Grey, C. P. *J. Am. Chem. Soc.* **2007**, 129, 335

(12) Freude, D.; Ernst, H.; Wolf, I. *Solid State Nucl. Magn. Reson.* **1994**, 3, 271.

(13) Baba, T.; Kumasito, N.; Ono, Y.; Sugisawa, H.; Takahashi, T. *Micropor. Mesopor. Mater.* **1998**, 22, 203.

(14) Baba, T.; Kumasito, N.; Ono, Y. *J. Phys. Chem. B* **1998**, 804.

(15) Sarv, P.; Tuherm, T.; Lippmaa, E.; Keskinen, K.; Root, A. J. *Phys. Chem.* **1995**, 99, 13763.

(16) Baba, T.; Ono, Y. *Applied Catalysis a-General* **1999**, 181, 227.

(17) Baba, T.; Inoue, Y.; Shoji, H.; Uematsu, T.; Ono, Y. *Microporous Mater.* **1995**, 3, 647.

(18) Kanellopoulos, J.; Gottert, C.; Schneider, D.; Knorr, B.; Prager, D.; Ernst, H.; Freude, D. *J Catal.* **2008**, 255, 68.

(19) Franke, M. E.; Simon, U. *Solid State Ionics* **1999**, 118, 311.

(20) Franke, M. E.; Simon, U. *Phys. Status Solidi B* **2000**, 218, 287.

(21) Grey, C. P.; Veeman, W. S. *Chem. Phys. Lett.* **1992**, 192, 379.

(22) Larson, A. C.; VonDreele, R. B. "General Structure Analysis System," Los Alamos National Laboratory, 1985.

(23) Vankoningsveld, H.; Jansen, J. C.; Vanbekkum, H. *Zeolites* **1990**, 10, 235.

(24) Spearing, D. R.; Farnan, I.; Stebbins, J. F. *Phys. Chem. Miner.* **1992**, 19, 307.

(25) Hunger, M.; Freude, D.; Pfeifer, H. *Catal. Today* **1988**, 3, 507.

(26) Freude, D.; Klinowski, J. J. Chem. Soc. Chem. Comm. **1988**, 1411.

(27) Kalwei, M.; Koller, H. *Solid State Nucl. Magn. Reson.* **2002**, 21, 145.

(28) Deng, F.; Du, Y. R.; Ye, C. H.; Wang, J. Z.; Ding, T. T.; Li, H. X. *J. Phys. Chem.***1995**, 99, 15208.

(29) Redondo, A.; Hay, P. J. *J. Phys. Chem.* **1993**, 97, 11754.

(30)Batamack, P.; Doremieuxmorin, C.; Fraissard, J.; Freude, D. *J. Phys. Chem.***1991**, 95, 3790.

(31)Luz, Z.; Vega, A. J. *J. Phys. Chem.***1987**, 91, 374.

(32)Marchese, L.; Chen, J. S.; Wright, P. A.; Thomas, J. M. *J. Phys. Chem.***1993**, 97, 8109.

(33)Jobic, H.; Tuel, A.; Krossner, M.; Sauer, J. *J. Phys. Chem.***1996**, 100, 19545.

(34)Krossner, M.; Sauer, J. *J. Phys. Chem.***1996**, 100, 6199.

(35)Sauer, J. *Science* **1996**, 271, 774.

(36)Smith, L.; Cheetham, A. K.; Morris, R. E.; Marchese, L.; Thomas, J. M.; Wright, P. A.; Chen, J. *Science* **1996**, 271, 799.

(37)Kreuer, K. D. *Chem. Mater.* **1996**, 8, 610.

(38)Kreuer, K. D.; Rabenau, A.; Weppner, W. Angew Chem Int. Edit. **1982**, 21, 208.

Chapter 4

Probing Brønsted Acid Sites in Zeolite H-MOR with Trimethylphosphine Molecules and Solid State NMR Spectroscopy

Abstract

The use of ^{1}H single resonance and ^{1}H-observed double-resonance MAS NMR spectroscopy, combined with trimethylphosphine $(CH_3)_3P$ probe molecules to investigate the acidities and locations of Brønsted acid sites in zeolite H-MOR is demonstrated in this chapter. Variable temperature (293K-183K) ^{1}H MAS NMR indicated that the major motional processes in zeolite H-MOR are presumably framework vibration and O-H bond libration rather than the translational motion of Brønsted acid protons via a proton-vehicle mechanism as observed for zeolite HZSM-5. The probe molecule-framework interaction upon various loading level and sample preparation conditions has been discussed in detail. By controlling the availability of the Brønsted acid sites located in cavities confined by different aperture sizes to the probe molecules, the locations of Brønsted acid sites in 8-ring channel and the intersection of 12-ring channel and the side-pocket have been determined.

4.1 Introduction

Mordenite (MOR) type zeolites are important catalysts for many industrial applications. The acidic form, H-Mordenite, in particular, shows spectacular selectivity, for example, in the selective transalkylation and disproportionation of alkylbenzenes.[1,2] This selectivity mainly lies in the availability of the catalytically active sites, the Brønsted acid sites in acid-catalyzed reactions, located in the cavities with specific shapes and sites, which only allow reactants with suitable sizes and geometry configurations to access these sites.[3] A determination of the locations of Brønsted acid sites in acidic zeolites is essential if structure-reactivity relationships are to be developed.

The location of protons in H-MOR has been extensively studied by a variety of methods, including X-ray/neutron diffraction, FTIR spectroscopy and *ab initio* calculations, however, conflicting results have been reported and their locations are still under debate. Early X-ray diffraction studies on dehydrated H-MOR by Mortier and co-workers concluded that the probability of proton attachment to each oxygen site was equal.[4] Martucci *et al* studied deuterated zeolite mordenite by neutron diffraction and claimed that there are four different Brønsted acid sites. One is on framework oxygen O_6, at the entrance of the side pocket; another is on O_9, in the center of the 8-ring channel; the other two are on O_5 and O_{10}, pointing into the center of the 12-ring.[5] In the FTIR studies of zeolites H-MOR loaded with probe molecules, the assignments of the low frequency and high frequency ν(OH) bands to the OH groups in the constrained 8-ring and 12-ring

main channel, respectively, are widely agreed upon. Bevilacqua and coworkers further proposed that the low frequency OH group corresponds to the O_6 site, while the high frequency OH groups are due to Brønsted acid sites at O_2, O_5, O_3, O_7 and O_{10}[6,7]. In contrast, Marie et al. reported that there is a third type of Brønsted acid site corresponding to a ν(OH) band at an intermediate frequency and suggested possible positions for the three types of OH groups at O_2, O_7 and O_9[8]. *Ab initio* density function theory (DFT) calculations of zeolites H-MOR gave similar results, namely that the Brønsted acid sites are located at O_2-O_7-O_9[9] or O_2-O_7-O_9-O_{10}[9,10]. A recent DFT calculation study, however, demonstrated that main channel and side pocket hydroxyls are not energetically different because of the confinement effect from the framework environment[11].

To determine the locations of Brønsted sites unambiguously using state-of-the-art solid-state NMR spectroscopic methods is the main motive of this present study. Solid-state NMR spectroscopy has been demonstrated as a very useful tool with which to investigate the properties, local structures and interactions of zeolites. ^{1}H, ^{27}Al and ^{29}Si NMR spectroscopy have been widely used to probe acidity and to quantify the number of different crystallographic sites, silicon to aluminum n(Si)/n(Al) ratio and coordination numbers of the aluminum species [12,13], while the interactions between zeolites and adsorbed species have been explored with ^{1}H, ^{13}C, ^{15}N and ^{31}P NMR spectroscopy[14-17].

4.2 Experimental Section

4.2.1 Materials Preparation

Zeolite Na-Mordenite (Na-MOR) with framework *n*(Si)/*n*(Al) ratio of 8.8 (HSZ-642NAA) was obtained from Tosoh Corporation. Zeolite NH_4-MOR was prepared by ion exchange with a 1 M NH_4NO_3 solution at ambient temperature for 12 hours (repeated three times). Zeolite H-MOR was prepared by heating NH_4MOR under vacuum from room temperature to 383 K in 7 h, and then to 673 K in 12 h where the temperature was held at 673 K for a further 12 h. The samples were stored and then packed into NMR rotors in the N_2 glove box, prior to the NMR experiments.

TMP (99%, Alfa) and d_9-TMP (Sigma-Aldrich) were adsorbed at liquid nitrogen temperature on the H-MOR sample pre-packed in a 5 mm rotor. The loading levels are determined by the drop of pressure upon exposure of TMP to the sample, in a previously calibrated vacuum line. The samples were then left at room temperature or 323 K for over 4 hours for equilibrium.

4.2.2 Solid-state NMR Spectroscopy

MAS NMR spectra were obtained with Varian Infinityplus 360, Bruker Avance 600 and 750 spectrometers, with 89 mm wide-bore 8.45, 14.1 and 17.6 T superconducting magnets, respectively, in 5 mm and/or 4 mm rotors. Rotor caps with o-rings or rotor spacers with screws were used to avoid adsorption of water during the NMR measurements. ^{31}P and ^{1}H chemical shifts are referenced to 85% H_3PO_4 and $CHCl_3$ (0.0 and 7.26 ppm, respectively). $^{1}H \rightarrow {}^{31}P$ and $^{31}P \rightarrow {}^{1}H$ CP experiments were performed with short contact times (0.1 ms), to select for P atoms directly bound to H.

The ^{1}H spin-echo pulse sequence used here is composed of 90° and 180° pulses separated by a time interval of 1 rotor cycle. The waiting time between the 180° pulse and the data acquisition is also rotor-synchronized. The 180° pulse is applied to refocus the precessing ^{1}H magnetizations

The $^{1}H/^{27}Al$ TRAPDOR experiments were carried out by using the pulse sequence proposed by Grey and Veeman[18]. A rotor synchronized spin-echo pulse was applied on ^{1}H channel, and a dephasing pulse was continuously irradiated on ^{27}Al channel during the delay period in between the ^{1}H 90° and 180° pulses.

4.3 Results and Discussion

4.3.1 Preliminary Assignments of ^{1}H MAS NMR Spectra

Generally speaking, ^{1}H MAS NMR spectra of acidic zeolites can rarely provide unambiguous information about different types and locations of the Brønsted acid protons. The ^{1}H MAS NMR of zeolite H-MOR, shown in Figure 4.1 (a), can be taken as a typical example of the problem. Only two resonances at 3.9 and 1.8 ppm are resolved, which can be assigned to Brønsted acid protons and silanol group protons, respectively. The samples when packed in normally air-tight NMR rotors can adsorb trace amount of water upon long time exposure to atmosphere leading to an addition resonance at approximately 6.2 ppm due to a H_2O / Brønsted acid complex, as shown in Figure 4.1 (b). This sample is ^{17}O-enriched and had been stored in a rotor for an extended period due to the consideration of the high cost of ^{17}O enrichment.

4.3.2 Variable Temperature ^{1}H MAS NMR and ^{1}H/^{27}Al TRAPDOR NMR

Figure 4.2 shows the variable temperature ^{1}H MAS NMR spectra of non-^{17}O-enriched zeolite H-MOR as a function of decreasing temperature. The sample was gradually cooled down to 183K by a step size of 10K and held at each temperature for 30 min to equilibrate, before starting to acquire the NMR data. Resonances at 3.9-4.4 and 1.7 ppm are assigned to Brønsted acid site and silanol groups, respectively. The appearance of the small resonance at around 6.3 ppm in the spectrum of this sample is

presumably due to trace amount of residual H_2O or NH_4^+. The chemical shift of the Brønsted acid site remains constant at 3.9 ppm between 293 and 223K. A gradual shift to 4.4 ppm on further cooling to 183K is then observed. As discussed in the previous chapter, this change of ^1H chemical shift is similar to what has been observed for zeolite HZSM-5 and can be ascribed to a slight change of the framework structure and T-O-T angles, which takes place below 223K, presumably driven by decreased amplitudes and frequencies of the vibrations of the silicate framework[19]. No obvious change in chemical shifts was observed for the two silanol peaks at 1.7 ppm, and the terminal silanol groups do not appear to be affected by any change of framework structure. After being held at 183K for 2 hours, the sample was then heated back to room temperature, as shown in the top spectrum of Figure 4.2. The chemical shift value of the resonance due to Brønsted acid protons changed back to 3.9 ppm, which indicates the reversibility of this structure change upon heating and cooling. In contrast to the results obtained on zeolite HZSM-5, no strong proton motional processes involving the Brønsted acid protons and residual H_2O were observed.

In order to obtain unambiguous assignments of all the resonances seen at low temperatures, ^1H/ ^{27}Al TRAPDOR NMR experiments were carried out at 183K. The result (Figure 4.3) confirms the assignment of the resonances at 4.4 ppm to the bridging (Brønsted acid site) hydroxyl. No TRAPDOR effect is seen for the 1.7 ppm silanol peak consistent with the assignment. The resonance at around 6.3 ppm splits into two resonances with different behavior upon irradiation on the ^{27}Al channel. One of the

resonances is centered at 6.6 ppm, which shows strong ^{1}H / ^{27}Al TRAPDOR effect similar to the resonance associated with the Brønsted acid protons. The other resonance centered at around 6.3 ppm does not show a noticeable ^{1}H / ^{27}Al TRAPDOR effect, which indicates that these protonated species are not strongly dipolar coupled to Al atoms. Similar to the assignments of zeolite HZSM-5,[20] these resonances can be assigned to residual ammonium cation and/or water H-bonded to a Brønsted acid site. The motional processes involving both residual species and the Brønsted protons are complicated. Two possible explanations can be proposed. (a) At the temperature the $^{1}H/^{27}Al$ TRAPDOR experiments were performed (183K), the water molecule can be localized on a Brønsted acid site with H-bonding. The resonance at 6.6 ppm is ascribed to Brønsted acid proton H-bonded to water molecule; while the resonance at 6.3 ppm with an $^{1}H/^{27}Al$ TRAPDOR effect is tentatively assigned to protons in a water molecule. (b) As demonstrated in Figure 4.1 (a), the small resonances in this 6.3-6.6 ppm area are absent in the dry ^{17}O-enriched sample, and appear upon the adsorption of trace amount of water. However, this sample used for the $^{1}H/^{27}Al$ TRAPDOR experiments is a freshly prepared non-^{17}O-enriched sample. The appearance of this resonance can be ascribed to residual NH_4^+ and H_2O, assuming that the ^{17}O enrichment can cause some change in the framework structure and hence ease the removal of NH_4^+ and H_2O.

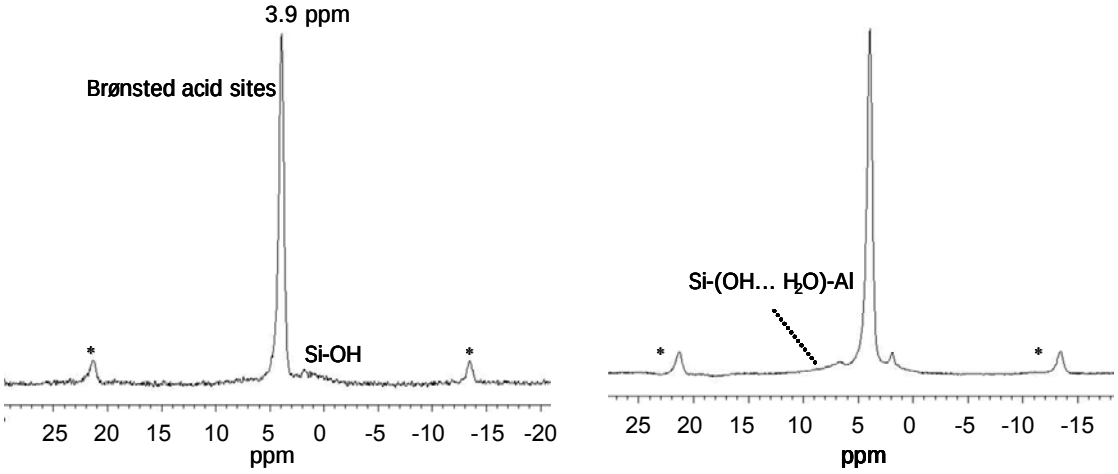

(a) (b)

Figure 4.1 ^{1}H MAS NMR of (a) dry zeolite H-MOR and (b) a zeolite H-MOR that contains a trace amount of water, at 17.6 T, spinning speed = 13kHz. Spinning sidebands are denoted by *. Both these samples are samples that were previously ^{17}O-enriched as described.

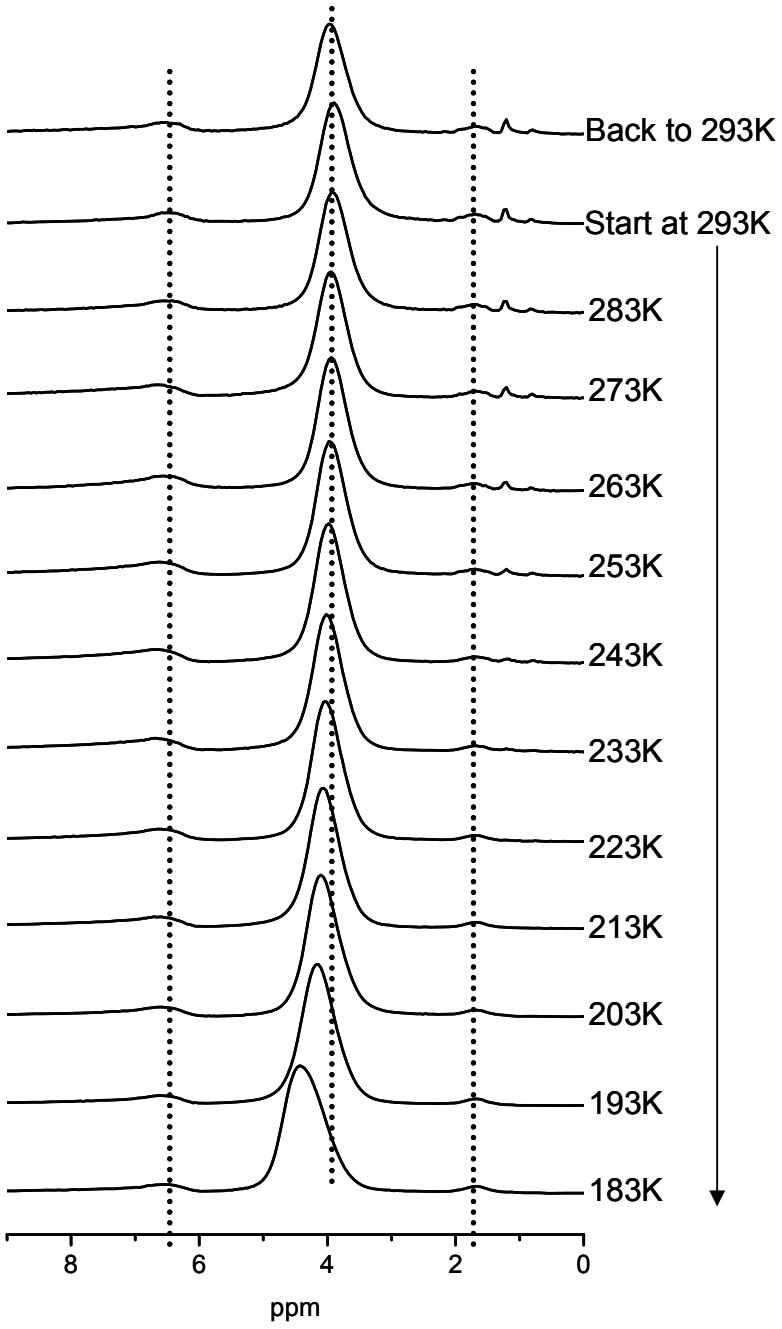

Figure 4.2 Variable temperature ^{1}H MAS NMR spectra of H-MOR at 14.1 T, single pulse, spinning speed =8 kHz.

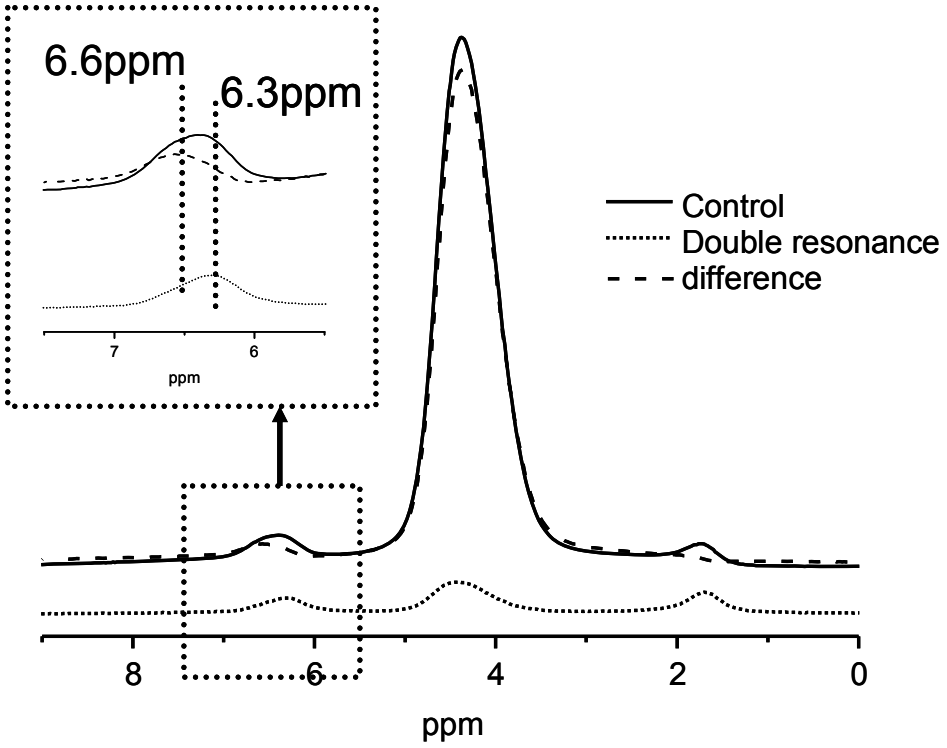

Figure 4.3 Low temperature $^{1}H/\ ^{27}Al$ TRAPDOR NMR of H-MOR acquired at 183K, at 14.1 T, spinning speed = 8 kHz, with ^{27}Al irradiation for 8 rotor periods (1000μs). A loss of intensity on applying ^{27}Al irradiation (the double resonance experiment) indicates that the ^{1}H species is nearby Al. Spinning speed = 8 kHz.

4.3.3 Properties of the Probe Molecules

In order to extract more information about Brønsted acid protons from ^{1}H MAS NMR spectroscopy, trimethylphosphine (TMP) has been employed as a basic probe molecule that can interact with a Brønsted acid proton to form either a neutral-hydrogen-bonded or an ion-pair complex[21]. The measurement of the side pocket 8-ring window connecting the 12-ring and the 8-ring channels is 3.4 × 4.8 Å (Figure 4.4 (a)), while the estimated diameter of a TMP molecule obtained by measuring the distance between two distant hydrogen atoms in the $–CH_3$ groups is 5.5 Å (Figure 4.4 (b)). Thus, TMP molecules can not readily pass through the 8-ring window of the side pocket to access the 8-ring channel due to the spatial hindrance arising from the three methyl groups. However, protons located inside the side pocket can presumably be accessed by a TMP molecule partially by the phosphorus atom entering the side-pocket first, the methyl groups remaining in the large cage.

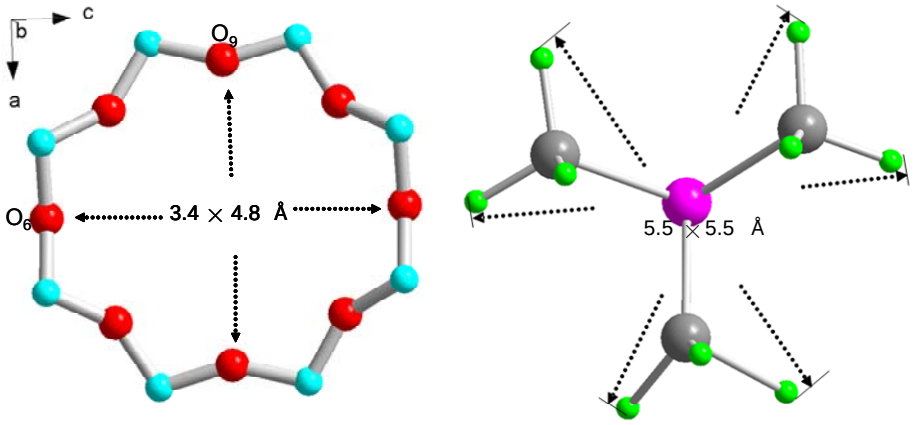

(a) (b)

Figure 4.4 Measurements of (a) side pocket 8-ring of zeolite H-MOR and (b) the TMP molecule

4.3.4 ^{1}H MAS NMR of TMP/ zeolite H-MOR complexes

As shown in Figure 4.5 (a), at a loading level of 2 TMP per unit cell (u.c.) and equilibrium temperature of 293 K, three resonances at 6.8, 4.0 and 2.1 ppm are observed corresponding to TMP/Brønsted acid complexes, Brønsted acid sites and methyl groups, respectively. The small sharp resonance at around 0 ppm is presumably due to the probe background. Figure 4.5 (b) shows the ^{1}H MAS NMR spectrum of the sample with the same nominal loading level but which was equilibrated at 323 K during the sample preparation. Integrals of the resonances at 6.8 and 4.0 ppm were taken to quantify the numbers of the Brønsted acid sites that interact with TMP. The sum of the two is denoted as the total amount of acidic protons (TA), while the integral of the 4.0 ppm peak is denoted as the residual amount of acidic protons (RA). The ratio of RA/TA can be used as a measure of the inaccessible Brønsted acid sites. The calculated ratio for the room temperature equilibrated sample is 25%; the value decreases slightly to 20% when the sample was equilibrated at 323 K. To eliminate the strong resonance due to methyl group protons and simplify the ^{1}H NMR spectrum, deuterated d_9-TMP was employed instead of normal TMP to prepare the samples with higher loading levels. As shown in Figure 4.5 (c) and (d), the RA/TA ratios are 25% and 55% for the samples at loading levels of 3.5 and 10 TMP/ u.c., respectively. In summary, about 20~25% of the Brønsted acid protons never interact/bond with TMP whatever the loading level. These protons are assigned to Brønsted acid sites located in the small pocket.

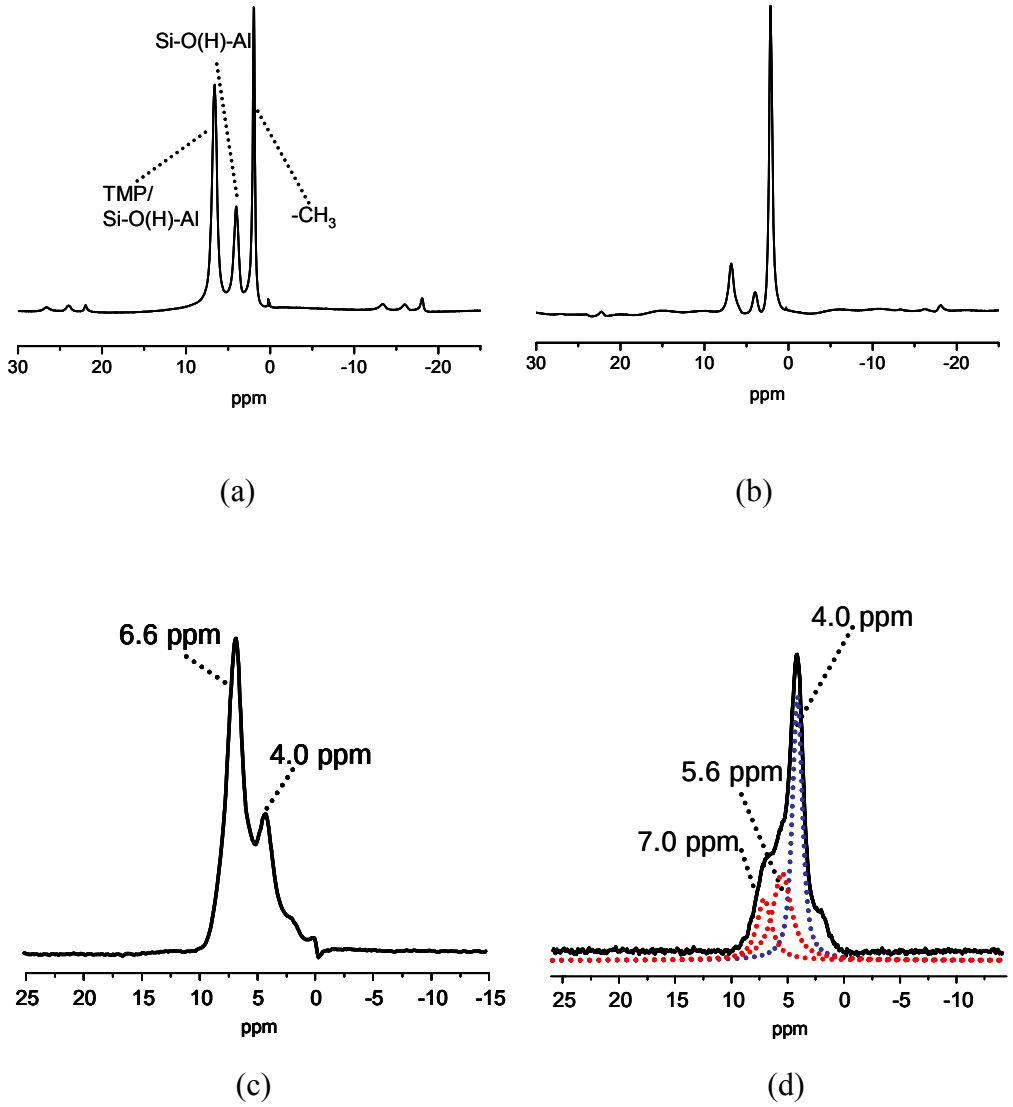

Figure 4.5 ^{1}H MAS NMR of TMP/ zeolite H-MOR complexes with a loading level of 2 TMP/ u.c., sample equilibrium temperature: (a) 293 and (b) 323K. Room temperature ^{1}H MAS csecho NMR spectra of deuterated d_9-TMP/H-MOR complexes with loading levels of (c) 3.5 and (d) 10 d_9-TMP/u.c., sample equilibrium temperature: 323K. The dashed lines show the deconvoluted components. All spectra were acquired at 8.47T, with a recycle delay 2 s, at room temperature.

4.3.5 The $^{31}P \rightarrow {}^{1}H$ / $^{1}H \rightarrow {}^{31}P$ CP-MAS NMR and Deconvolution Details

In Figure 4.5 (d), an asymmetric doublet due to P-H through bond J-coupling at 7.0 and 5.6 ppm was observed on the sample adsorbed with 10 TMP/u.c.. The separation of 1.4 ppm between the two peaks corresponds to a J-coupling constant of about 500 Hz, which is consistent with previous reports[14]. This unambiguously confirms that the 7.0+5.6 ppm resonances are due to $TMPH^+$. In contrast, no J-coupling was seen in the $TMPH^+$ resonances in the samples with lower loading levels. However, as shown in Figure 4.6, a doublet can be seen in the spectra of the $^{31}P \rightarrow {}^{1}H$ and $^{1}H \rightarrow {}^{31}P$ CP MAS NMR for samples with the loading levels of both 3.5 and 10 TMP/u.c..

To investigate the nature of the TMP/HMOR complexes with different loading levels in more detail, the chemical shift value and linewidth of each deconvoluted resonance are listed in Table 4.1. In the ^{1}H MAS NMR spectrum obtained on the sample with 2 TMP/u.c., the resonance due to the TMP/ Brønsted acid complex is centered at 6.8 ppm with a relatively narrow linewidth of about 280 Hz. For the sample with 3.5 TMP/u.c., this resonance is centered at 6.7 ppm with a much broader linewidth of ~530 Hz. For the sample with the loading level of 10 TMP/u.c., doublet centered at 5.6 and 7.0 ppm with linewidth of 560~600 Hz is observed. However, the $^{31}P \rightarrow {}^{1}H$ CP-MAS NMR spectra obtained on samples with both loading levels (3.5 and 10 TMP/ u.c.) show constant linewidths for each peak in the doublet.

The overall lineshape observed in the ^{1}H single-pulse or csecho experiment can be considered as the sum of two subsets: (a) Brønsted protons H-bonded to TMP which experience the hopping of TMP molecules from one binding site to another; hence, no H-P J-coupling can be observed. (b) The rigid $TMPH^{+}$ cation. In this case, an H-P covalent bond has been formed upon complete H-transfer from the Brønsted acid oxygen to the phosphorus in TMP, which leads to the observable doublet due to J-coupling. Presumably CP selects the subset of the rigid $TMPH^{+}$ molecules only. At the loading level of 2 TMP/u.c. (Figure 4.5 a&b), the former is the dominant component and gives rise to a narrow singlet resonance. At the loading level of 10 TMP/u.c. (Figure 4.5 d), most of the Brønsted acid protons accessible to TMP molecules exist as rigid $TMPH^{+}$ cations corresponding to the 7.0+5.6 ppm doublet. The broad singlet resonance observed for the sample with the loading level of 3.5 TMP/u. c. (Figure 4.5 c) is due to the coexistence of these two species with comparable amounts.

4.3.6 Stabilization effect of the framework on the probe molecules

Kao and co-workers reported DFT calculations of the interaction between $TMPH^{+}$ ion-pair and the zeolite framework.[22] The positive charge of $TMPH^{+}$ is partially delocalized over the whole cation. Hence the cation can be stabilized by electrostatic interactions between the negatively charged framework and the protons from both methyl groups and the P-H covalent bonds. The observed intensity of the resonance due to methyl group protons is unusually low when the sample was equilibrated at room

temperature, Figure 4.5 (a), as compared to the same sample equilibrated at 323K, Figure 4.5 (b). This suggests that higher equilibration temperature can help the probe molecules to be sorbed more uniformly throughout the crystalline particles and individual cavities so that the methyl group protons can be stabilized by the zeolite framework through electrostatic interactions rather than undergoing fast rotation on the NMR time scale. The high RA/TA ratio (~ 55%) observed for the sample with the loading level of 10 TMP/u.c. can be rationalized to be due to the difficulty in optimizing the orientations of probe molecules due to the high population of molecules in the cages and hence constrained mobility and ability to adopt optimum binding configureations. TMP molecules and $TMPH^+$ cations can in some degree block the pathway to some Brønsted acid protons. The binding energy for TMP pointing into the side pocket must be low, due to steric constraints and the difficulty in optimizing interactions with the zeolite framework. In the presence of multiple TMP molecules, it must become impossible for all the $TMPH^+$ molecules to adopt ideal binding interactions with the bare Brønsted acid oxygen atoms, and it is energetically more favorable for the TMP molecules to interact with each other to form $(CH_3)_3PH$---$P(CH_3)_3$ interactions consistent with previous DFT calculations which have shown that unless effective H-bonding between the protonated probe molecule and the framework O sites is possible, H-transfer will not occur[21].

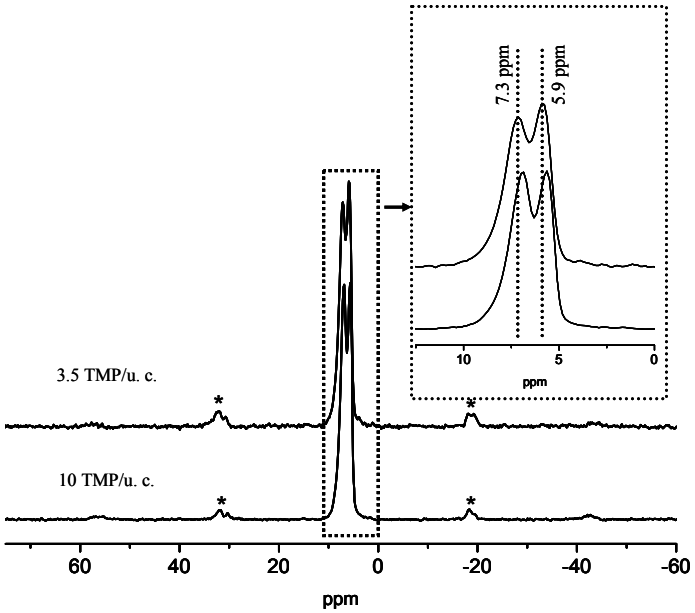

(a)

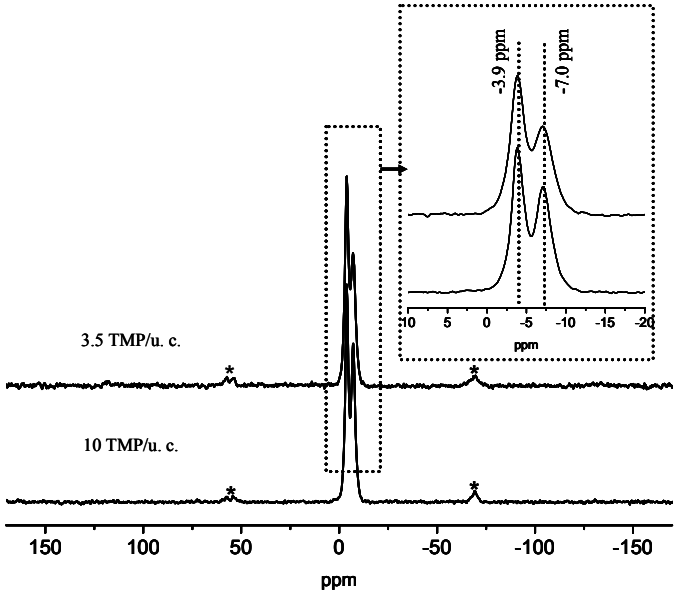

(b)

Figure 4.6 (a) $^{31}P \rightarrow {}^{1}H$ and (b) $^{1}H \rightarrow {}^{31}P$ CP MAS NMR of d_9-TMP loaded H-MOR samples with loading levels of 3.5 and 10 TMP/u. c. at 8.47T, spinning rate 9kHz, spinning sidebands are denoted with *.

Table 4.1 Parameters extracted from the deconvolution of ^{1}H MAS and $^{31}P \rightarrow {}^{1}H$ CP-MAS NMR lineshape.

Experiment	Loading Level (TMP/u.c.)	Equilibrium Temperature (K)	Chemical Shift (ppm)	Line Width (Hz)
^{1}H MAS NMR	2	293	2.0	144
			4.0	287
			6.6	302
	2	323	2.1	186
			4.0	228
			6.8	277
	3.5	323	4.0	556
			6.7	526
	10	323	4.0	547
			5.6	564
			7.0	604
$^{31}P \rightarrow {}^{1}H$ CP MAS NMR	3.5	323	5.9	340
			7.3	422
	10	323	5.6	322
			7.0	468

4.3.7 Correlation of the ^{1}H Chemical Shift Values and the Motion of Probe Molecules.

Close inspection reveals that the resonance associated with the $TMPH^{+}$ protons shifts to a lower frequency upon the increase of TMP loading level. In $^{31}P \rightarrow {}^{1}H$ CP MAS experiments, Figure 4.6 (a), each peak of the doublet shifts by about 0.3 ppm to lower frequency when the loading level increases from 3.5 to 10 TMP/u.c. In Figure 4.5 (a)-(c), the ^{1}H single-pulse resonance singlet shifts from 6.8 ppm (2 TMP/u.c.) to 6.7 ppm (3.5 TMP/u.c.). In Figure 4.5 (d), at the loading level of 10 TMP/u.c., the doublet is now present with two peaks at 7.0 and 5.6 ppm corresponding to an average shift of 6.3 ppm. In contrast, $^{1}H \rightarrow {}^{31}P$ CP MAS NMR did not indicate obvious changes in the ^{31}P chemical shift values. In early studies on TMP loaded zeolites, efforts have been made to establish correlations between acidity and ^{31}P chemical shift/ J_{P-H} coupling values.[23] However no clear correlation based on ^{31}P chemical shift has been successfully established. The trend that the ^{1}H chemical shift values changes from higher to lower frequency upon the increasing loading level of TMP molecules revealed in this study can be correlated with the corresponding change of the dominant component from TMP---H associated with hopping of TMP molecules to the rigid $TMPH^{+}$ cations.

4.3.8 The Locations of Brønsted Acid Sites in Zeolite H-MOR

According to the TMP adsorption experiment with different loading levels, about ~ 20 - 25% of the Brønsted acid sites in zeolite H-MOR are inaccessible to TMP molecules. As discussed earlier this chapter, the acidic sites inaccessible to TMP probe molecules are presumably located on O_9 pointing into the center of the 8-ring channel.

^{1}H MAS NMR on H-MOR sample loaded with 10 d_9-TMP/u.c. shows high RA/TA ratio (~ 55%). This suggests that the large populations of $TMPH^+$ cations and TMP molecules in the main channel at this loading level can block the access to about 20 % acidic sites, which were originally accessible to TMP at lower loading levels. This presumably corresponds to acidic sites located at the intersection of the 12-ring main channel and the side pocket. The oxygen atoms on this 8-ring at the intersection are O_2 and O_5. The acidic hydroxyl group, which is located on O_2, points into the center of the 12-ring channel. However, whether the acidic proton located on O_5 points to the main channel or the side pocket is still under debate. Our results support the point of view that this acidic O-H group slightly points into the side pocket and O_5 is a reasonable location of Brønsted acid site.

4.4 Conclusions

The ^{1}H MAS NMR results of zeolite H-MOR loaded with TMP probe molecules at different adsorption levels illustrated that about 20-25% acidic hydroxyl groups are located in 8-ring channels; 25-30% are located at the intersections of the side pockets and main channels and the rest (45-50%) are located in the 12-ring main channels. By checking the structure, two possible locations for Brønsted acid sites in zeolite H-MOR are suggested based on the results of ^{1}H MAS NMR and $^{1}H \rightarrow {}^{31}P/{}^{31}P \rightarrow {}^{1}H$ CP-MAS NMR of samples adsorbed TMP probe molecules: (a) O_9, pointing into the center of the 8-ring channel and inaccessible to TMP probe molecules; (b) O_5, slightly pointing toward the side pocket.

An observation on the change of ^{1}H chemical shift values upon cooling, which is similar to the result obtained on zeolite HZSM-5, confirms that ^{1}H chemical shift value is a sensitive indicator of the change in framework structure (T-O-T bond angles).

4.5 References

(1) Bowers, C. R.; Storhaug, V.; Webster, C. E.; Bharatam, J.; Cottone, A.; Gianna, R.; Betsey, K.; Gaffney, B. J. *J. Am. Chem. Soc.* **1999**, 121, 9370.

(2) Corma, A. *Chem. Rev.* **1995**, 95, 559.

(3) Derouane, E. G.; Andre, J. M.; Lucas, A. A. *J Catal.* **1988**, 110, 58.

(4) Mortier, W. J.; Pluth, J. J.; Smith, J. V. *Mater. Res. Bull.* **1975**, 10, 1319.

(5) Martucci, A.; Cruciani, G.; Alberti, A.; Ritter, C.; Ciambelli, P.; Rapacciuolo, M. *Micropor. Mesopor. Mater.* **2000**, 35-6, 405.

(6) Bevilacqua, M.; Alejandre, A. G.; Resini, C.; Casagrande, M.; Ramirez, J.; Busca, G. *Phys. Chem. Chem. Phys.* **2002**, 4, 4575.

(7) Bevilacqua, M.; Busca, G. Catal. Comm. **2002**, 3, 497.

(8) Marie, O.; Massiani, P.; Thibault-Starzyk, F. *J. Phys. Chem.B* **2004**, 108, 5073.

(9) Demuth, T.; Hafner, J.; Benco, L.; Toulhoat, H. *J. Phys. Chem.B* **2000**, 104, 4593.

(10) Bucko, T.; Benco, L.; Demuth, T.; Hafner, J. *J. Chem. Phys.* **2002**, 117, 7295.

(11) Dominguez-Soria, V. D.; Calaminici, P.; Goursot, A. *J. Chem. Phys.* **2007**, 127.

(12) Grey, C. P. Nuclear Magnetic Resonance Studies of Zeolites. In *Handbook of Zeolite Science and Technology*; Auerbach, S. M., Carrado, K. A., Dutta, P. K., Eds.; Marcel Dekker, 2003; pp 205.

(13) Klinowski, *J. Anal. Chim. Acta.* **1993**, 283, 929.

(14) Kao, H. M.; Yu, C. Y.; Yeh, M. C. *Micropor. Mesopor. Mater.* **2002**, 53, 1.

(15) Hunger, M.; Horvath, T. Berichte Der Bunsen-Gesellschaft-*Phys. Chem. Chem. Phys.* **1995**, 99, 1316.

(16) Hunger, M. *Solid State Nucl. Magn. Reson.* **1996**, 6, 1.

(17) Hunger, M. *Catal. Rev.*-Science and Engineering **1997**, 39, 345.

(18) Grey, C. P.; Veeman, W. S. *Chem. Phys. Lett.* **1992**, 192, 379.

(19) Spearing, D. R.; Farnan, I.; Stebbins, J. F. *Phys. Chem. Miner.* **1992**, 19, 307.

(20) Huo, H.; Peng, L. M.; Grey, C. P. *J. Phys. Chem.C* **2009**, 113, 8211.

(21) Kao, H. M.; Grey, G. P. *J. Phys. Chem.***1996**, 100, 5105.

(22) Kao, H. M. Probing the Bronsted and Lewis Acid Sites in Zeolite Y with Probe Molecules and Solid-State Double Resonance NMR. *Ph. D. Dissertation*, State University of New York at Stony Brook, 1998.

(23) Lunsford, J. H. *Top. Catal.* **1997**, 4, 91.

Chapter 5

Use of $^{1}H \rightarrow ^{17}O$ and $^{1}H \rightarrow ^{29}Si$ Double Resonance Experiments to Measure Connectivity and Internuclear Distances in Zeolite H-MOR

Abstract

^{17}O-^{1}H and ^{29}Si-^{1}H double resonance NMR spectroscopy was used to study the local structure of zeolite H-MOR. Different contact times were used in cross polarization magic angle spinning (CPMAS) NMR, CP rotational-echo double resonance (CP-REDOR) NMR and heteronuclear correlation (HETCOR) NMR spectroscopy to selectively investigate Brønsted acid sites with different O-H distances. Efforts were made to determine the locations of different Brønsted acid sites in H-Mordenite (H-MOR) and develop correlations between the NMR parameters and the local/long range structure and Brønsted acidity.

5.1 Introduction

With the development of ^{17}O isotopic enrichment methods and high magnetic field NMR instruments with high speed magic angle spinning (MAS) capabilities, high resolution ^{17}O NMR spectra have been collected for a variety of zeolites [1-10]. In our previous work on zeolites HY and HZSM-5, we demonstrated that the ^{17}O signals from the oxygen atoms directly bound to Brønsted acid sites, which are not directly visible in simple one-pulse experiments, can be detected and partially resolved by one-dimensional (1-D) and two-dimensional (2-D) $^{17}O/^{1}H$ double resonance techniques with optimized contact times, such as $^{1}H \rightarrow {}^{17}O$ cross-polarization (CP) NMR, ^{17}O-^{1}H CP rotational echo double resonance (CP-REDOR) NMR and ^{1}H-^{17}O heteronuclear correlation (HETCOR) NMR spectroscopy.

As introduced in Chapter 1, the ^{29}Si chemical shift is sensitive to the coordination number of Si and substitutions of elements in the first and second coordination spheres and the Si-O-Si bond angles and bond lengths. Hence, $^{1}H \rightarrow {}^{29}Si$ CP-MAS NMR can provide structural information about the proximity of specific Si atoms and protons. $^{1}H \rightarrow {}^{29}Si$ CP-MAS NMR has several more advantages over ^{29}Si direct excitation, for instance, enhanced sensitivity, shorter longitudinal relaxation of ^{1}H relative to that of ^{29}Si.

The basic theory about the transfer of polarization between I and S spins during the cross polarization process has been introduced in Chapter 1. The dynamics in CP

experiment, which is directly involved in the studies in this chapter, can be approximately described with Equation 5.1, where M_S^{CP} , T_{IS} and $T_{1\rho}^I$ stand for the magnetization of the S spin, the rate of magnetization build-up between the I and S spins and the T_1 of the I-spin in the rotating frame. Generally speaking, the build-up process of the magnetization of spin S can be quantified using T_{IS}, while the timescale of the decay of the magnetization is determined by $T_{1\rho}^I$. In the results shown in this chapter, the separation of different ^{17}O signals from different hydroxyl groups or ^{29}Si species adjacent to hydroxyl protons, by optimizing the contact times in the cross polarization process, is based on the fact that the CP time constants T_{IS} are governed by dipolar interactions. The dipolar coupling constant D_{IS} is defined in Equation 5.2,

$$M_S^{CP} = M_0^{CP}\left[\frac{e^{-\frac{t}{T_{1\rho}^I}} - e^{-\frac{t}{T_{IS}}}}{1-\frac{T_{IS}}{T_{1\rho}^I}}\right] \tag{5.1}$$

$$D_{IS} = -(\frac{\mu_0}{4\pi})\frac{\gamma_I\gamma_S\hbar}{r_{IS}^3} \tag{5.2}$$

which clearly shows that the dipolar coupling has a $1/r^3$ dependence on the internuclear distance r_{IS} between the source spins I and the target spins S[11]. In this chapter, Brønsted acid sites in H-MOR with different O-H bond lengths (i.e., different acidities) are resolved in ^{17}O double resonance NMR by controlling the contact times. The locations and nature of three types of Brønsted acid sites in zeolite H-MOR are deduced by using this methodology in combination with the results in Chapter 4.

5.2 Experimental Section

5.2.1 Materials Preparation

Zeolite Na-Mordenite (Na-MOR) with framework *n*(Si)/*n*(Al) ratio of 8.8 (HSZ-642NAA) was obtained from Tosoh Corporation. To avoid dealumination upon heat treatment of the hydrated samples, ^{17}O enrichment was carried out on the sodium form of zeolite mordenite. Zeolite Na-MOR was first dehydrated by heating under vacuum (pressure < 10^{-3} torr) from room temperature to 773 K in 4 hours, and then held at this temperature for 12 hours. ^{17}O isotopically enriched Na-MOR was prepared by heating dehydrated zeolite Na-MOR in $^{17}O_2$ gas (50% enriched $^{17}O_2$ from Isotec, Inc.) to 853K and held at this temperature for 12 hours. ^{17}O-enriched zeolite NH_4-MOR was prepared by ion exchange with a 1 M NH_4NO_3 solution at ambient temperature for 12 hours (repeated three times). ^{17}O-enriched H-MOR was prepared by heating ^{17}O-enriched NH_4MOR under vacuum from room temperature to 383 K in 7 h, and then to 673 K in 12 h where the temperature was held at 673 K for a further 12 h. Non-^{17}O-enriched NH_4-MOR and H-MOR samples were prepared following the same procedures described above using non-enriched Na-MOR as starting material instead of the ^{17}O-enriched Na-MOR. The samples were stored and then packed into NMR rotors in the N_2 glove box, prior to the NMR experiments.

5.2.2 Solid-state NMR Spectroscopy

MAS NMR spectra were obtained with Varian Infinityplus 360 and Bruker Avance 750 spectrometers, with 89 mm wide-bore 8.45 and 17.6 T superconducting magnets, respectively, in 4 mm rotors. Rotor caps with o-rings or rotor spacers with screws were used to avoid adsorption of water during the NMR measurements. ^{17}O and ^{29}Si chemical shifts are referenced to external standards, H_2O and Si $(CH_3)_4$ (TMS), respectively; both were set at 0.0 ppm. The Hartmann-Hahn condition for the $^{1}H \rightarrow {}^{17}O$ CP, CPREDOR and 2-D HETCOR NMR experiments were set by using the ^{17}O-enriched zeolite HY sample. *Rf* field strengths of $\omega_1(^{17}O)/2\pi$ =28 kHz and $\omega_1(^{1}H)/2\pi$ =70 kHz were used. ^{1}H decoupling at 70 kHz was applied in both $^{1}H \rightarrow {}^{17}O$ CP and HETCOR experiments. The spectrum width of the ^{1}H dimension in HETCOR was set to 13 kHz. The NMR pulse sequence of the shifted-pulse CP-REDOR experiment is shown in Figure 5.1. NMR lineshape simulations were performed with the Wsolids package developed by Dr. K. Eichele or the SIMPSON package developed by Nielsen and co-workers.[12]

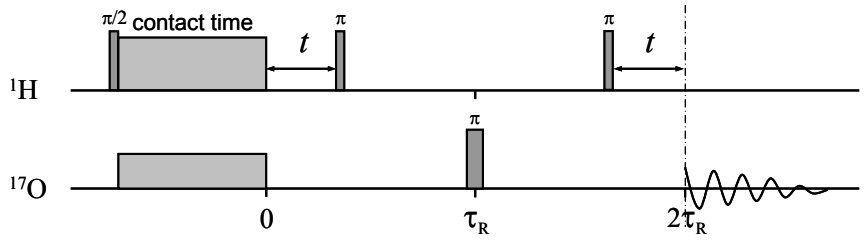

Figure 5.1 NMR pulse sequence: $^{1}H \rightarrow {}^{17}O$-$^{1}H$ CP-REDOR with shifted-pulses.

5.3 Results and Discussion

5.3.1 $^{1}H \rightarrow ^{17}O$ CP MAS NMR

Cross-polarization is a double resonance technique based on the heteronuclear dipolar interaction and hence sensitive to internuclear distance. In our previous study on zeolite HY, a short contact time was applied in the $^{1}H \rightarrow ^{17}O$ CP MAS NMR experiments to selectively detect the ^{1}H- ^{17}O closest contact, i.e., directly bonded OH groups. The lineshape of the ^{17}O signal from the Brønsted acid hydroxyl group in zeolite HY can be fit by a second order quadrupolar lineshape from a single site with a large asymmetric parameter ($\eta \sim 1$)[13]. However the lineshape of the CP resonance obtained from zeolite H-MOR, shown in Figure 5.2 (a), obviously contain more than one site underneath it. This suggests the existence of more than one type of Brønsted acid site. The CP MAS NMR spectra were acquired as a function of contact time. Since the overall lineshape is a sum of multiple resonances, the change of lineshape (the relative intensity of the singularities at -1 and 19 ppm can be taken as a simple indicator) as a function of contact time is due to environments with different O-H distances. The resonance at 35 ppm is enhanced by contact time longer than 400 μs, presumably due to framework oxygen, H-bonded or spatially close to Brønsted acid protons.

The CP intensity was measured and plotted as a function of contact time (Figure 5.2 (b)). Error bars were added to include the possible errors induced by different ways of

defining the integral region. The contact time corresponding to the maximum intensity is 60 μs. Comparing to our previously reported results of 60 μs and 80 μs for zeolite HY and HZSM-5, respectively, this value indicates a O-H bond length that is similar to the acidic hydroxyl group in HY but shorter than that in HZSM-5[13]. Taking into consideration the proton motion in HZSM-5, this shorter contact time at maximum intensity can be explained as due to the more rigid acidic protons in H-MOR.

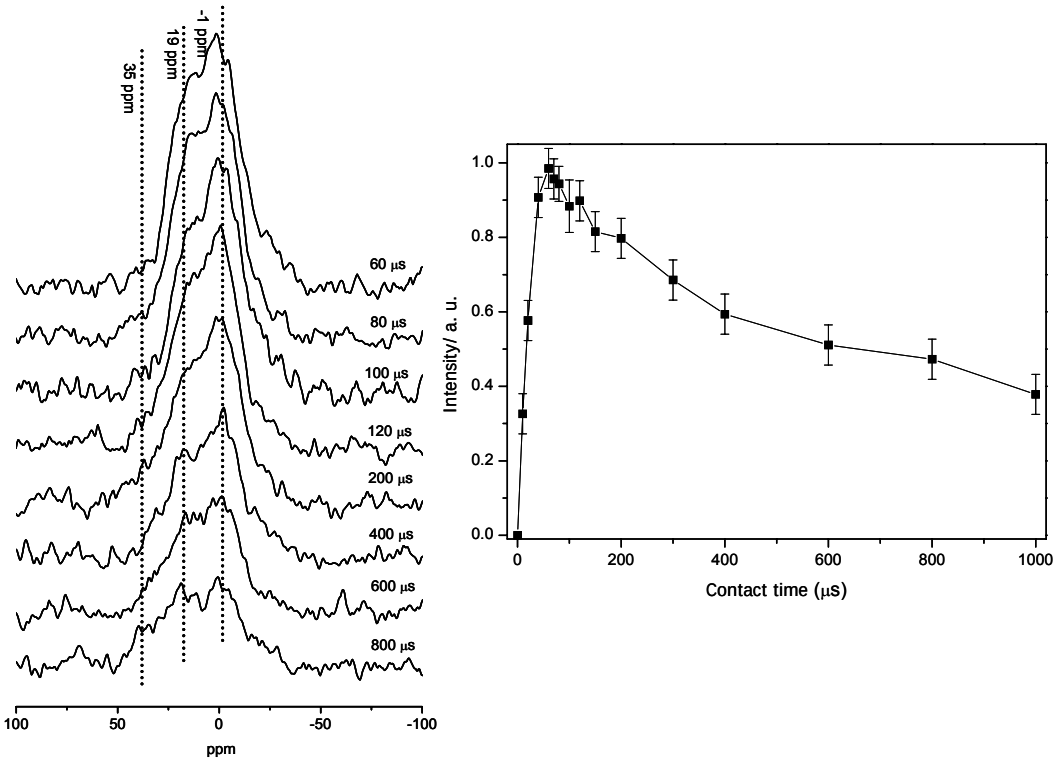

(a) (b)

Figure 5.2 (a) $^{1}H \rightarrow {}^{17}O$ CP MAS NMR spectra and (b) signal intensities of zeolite H-MOR acquired at 17.6 T as a function of contact time.

5.3.2 2D ^{1}H-^{17}O HETCOR NMR

Since one dimensional CP MAS NMR can only give the sum of all the resonances from all the different Brønsted acid sites, 2D ^{1}H-^{17}O HETCOR NMR spectroscopy has been employed to attempt to separate the ^{17}O signals from each distinct site, which are presumably associated with a characteristic O-H bond lengths and hence specific ^{1}H chemical shift values. In order to illustrate the concept that the oxygen resonances from O-H groups with different O-H bond lengths can be favored by optimum choices of contact times, ^{17}O-^{1}H HETCOR spectrum was also taken with a longer contact time of 100 μs (Figure 5.3 (b)) in addition to 70 μs (Figure 5.3 (a)) which corresponds to the maximum CP signal intensity. When a short contact time of 70 μs was applied, only one resonance centered at 3.9 ppm can be observed in the ^{1}H dimension. The simulation result (including quadrupolar and chemical shift parameters) of the slice taken at this position (slice (i), δ_{CS} ^{1}H = 3.9 ppm) is shown in Table 5.1. The value of η of this site is 0.7, corresponding to a lineshape quite different from the projection of sum on the ^{17}O dimension. Slice (ii) was taken at δ_{CS} ^{1}H = 4.8 ppm. The smaller η value of 0.45 indicates the existence of a different type of Brønsted acid sites associated with more positive ^{1}H chemical shift. Figure 5.3 (b) shows the ^{17}O-^{1}H HETCOR spectrum of H-MOR obtained with longer contact time of 100 μs. One noticeable feature of this two dimension spectrum is the projection on ^{1}H dimension with 2 well resolved resonances at 3.8 and 4.8-5.0 ppm. Simulations of the slices taken at these two positions (slice (iii), (iv))

indicate that the oxygen environments associated with these two ^{1}H resonances are similar to those associated with slice (i) and (ii). The poor signal to noise of slice (ii) is directly related with the low intensity of the corresponding resonance in the ^{1}H dimension. The better resolution on ^{1}H dimension compared to the spectrum taken with contact time of 70 μs is presumably due to the enhancement of the oxygen environment connected with the proton at 4.8 ppm by the longer contact time. This confirms that there are multiple acidic hydroxyl groups with different O-H bond lengths in zeolite H-MOR.

Upon exposure to humid atmosphere for long period of time, the H-MOR sample packed in the rotor absorbs trace amount H_2O. Figure 5.3 (c) shows the ^{17}O-^{1}H HETCOR spectrum of the sample contaminated by trace amount of water. A contact time of 120 μs was adopted in order to select the O-H bond presumably elongated by H-bonding to water. On projection of the ^{1}H dimension, a new resonance at 6.2 ppm associated with acidic proton H-bonded to a trace amount of H_2O can be resolved, which is consistent with single pulse ^{1}H MAS NMR result. The absence of the resonance at 4.8 ppm on the ^{1}H dimension suggests that the 4.8 ppm protons tend to form H-bond with water molecules. According to the simulation of the slice taken at δ_{CS} ^{1}H = 6.2 ppm, the local environment around the relevant oxygen atoms has been dramatically changed upon adsorption of water, the quadruple coupling constant (QCC) decreasing from 6.4 to 5.5 MHz, η increasing from 0.45 to 0.8, the ^{17}O isotropic chemical shift changing from 31 ppm to 21 ppm.

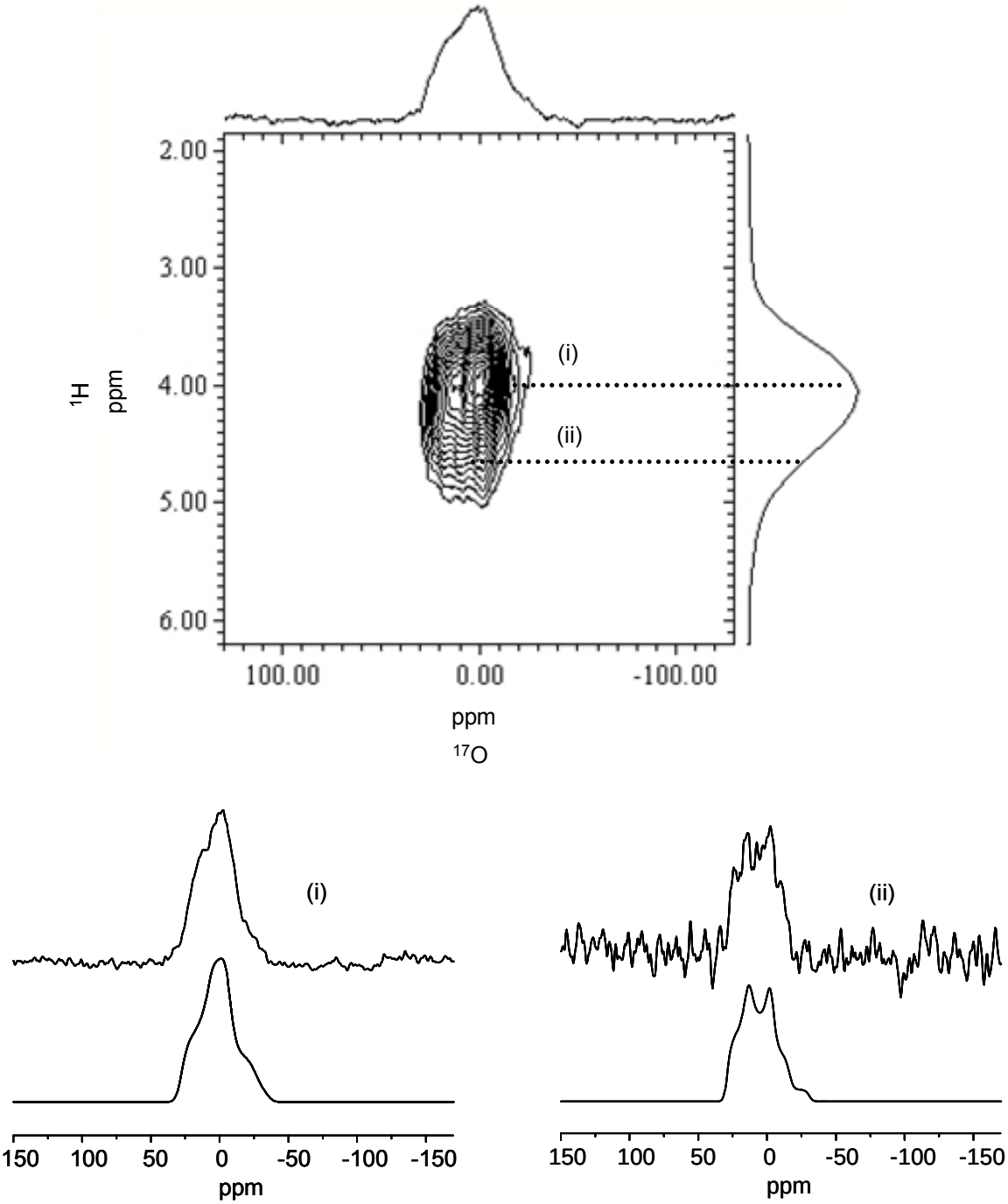
2.00
3.00
4.00
5.00
6.00
^{1}H ppm
(i)
(ii)
100.00
0.00
-100.00
ppm
^{17}O
(i)
(ii)
150 100 50 0 -50 -100 -150
ppm
150 100 50 0 -50 -100 -150
ppm

(a)

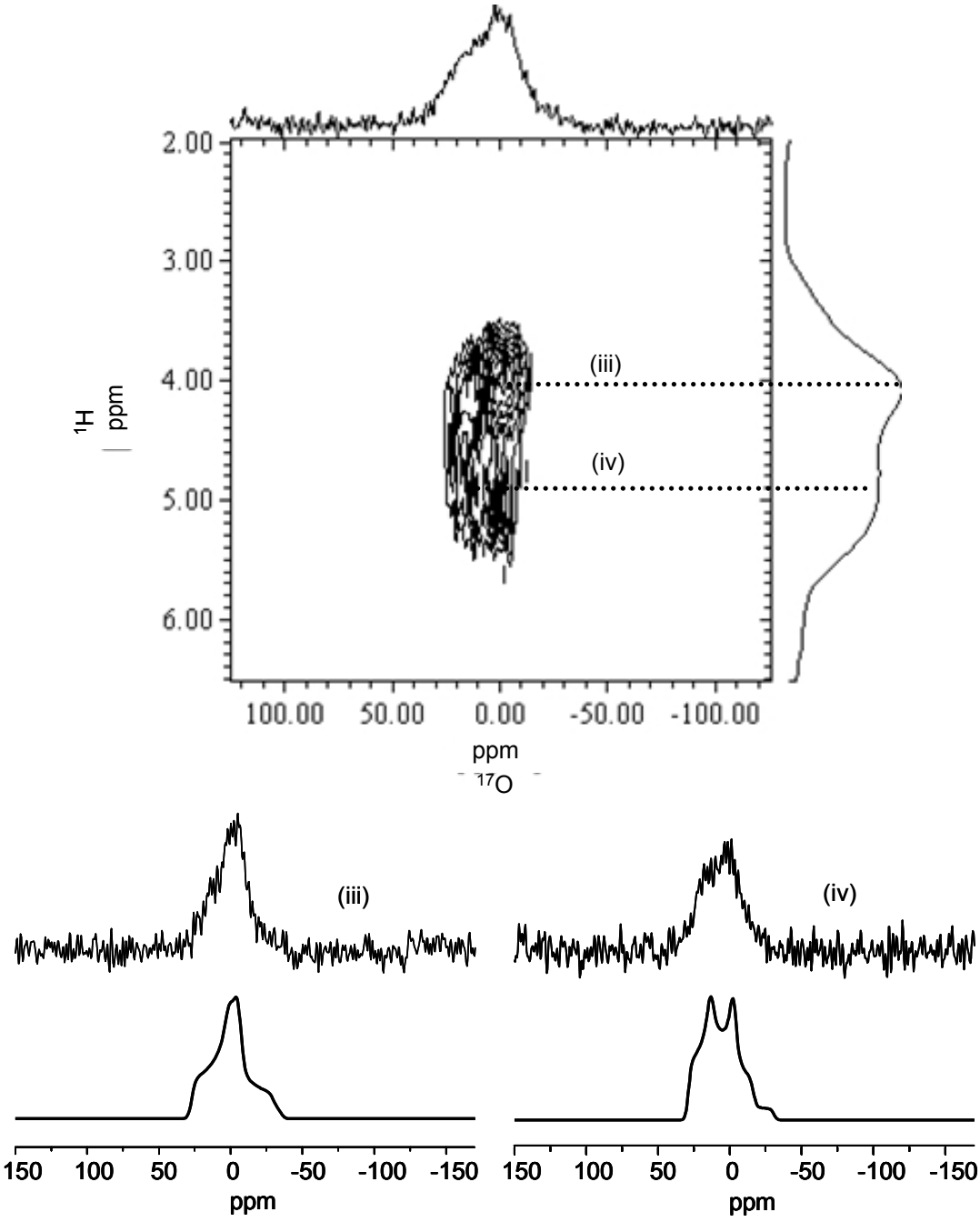
2.00
3.00
4.00
5.00
6.00
^{1}H ppm
(iii)
(iv)
100.00
50.00
0.00
-50.00
-100.00
ppm
^{17}O
(iii)
(iv)
150
100
50
0
-50
-100
-150
ppm
150
100
50
0
-50
-100
-150
ppm

(b)

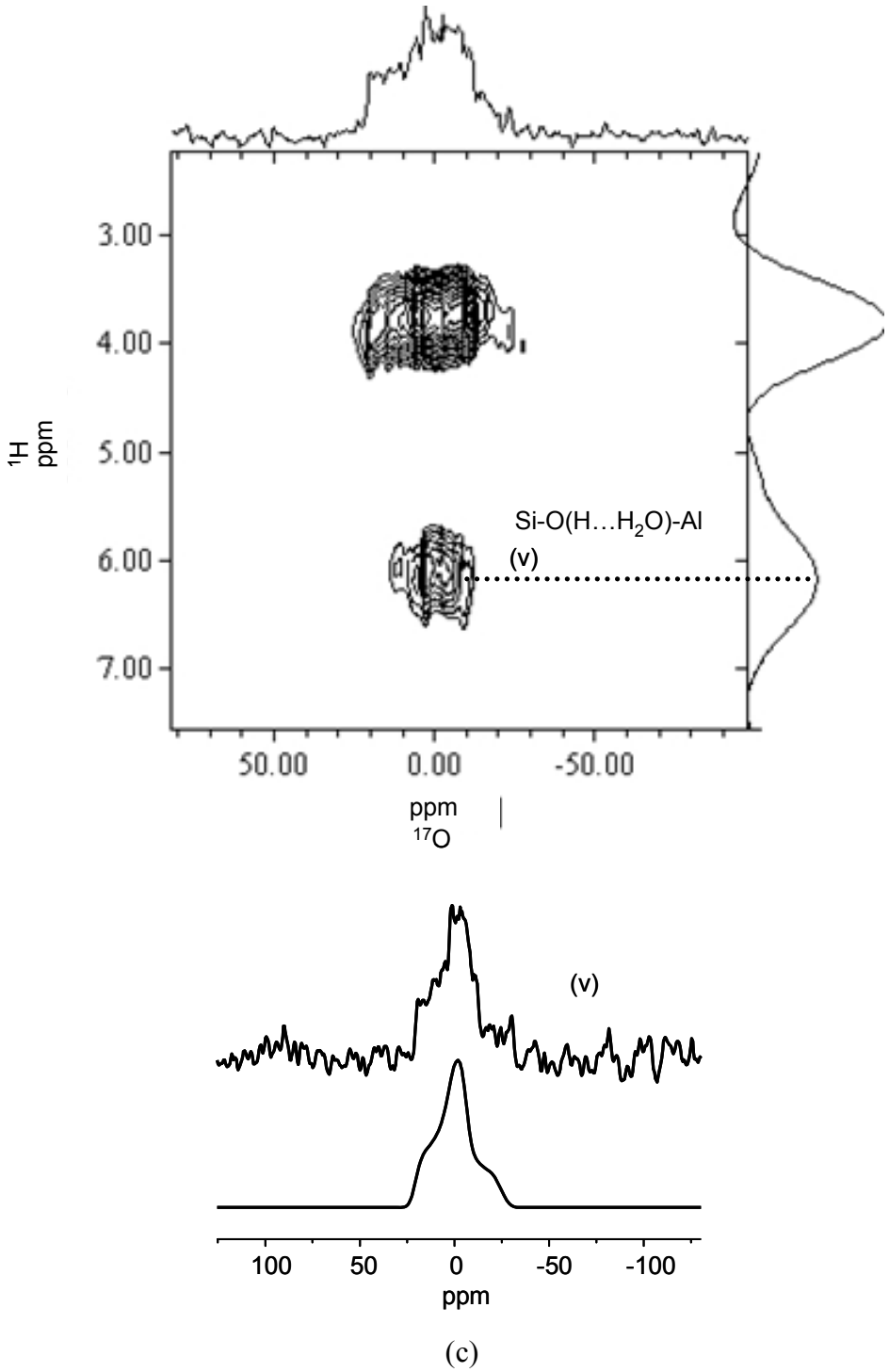

(c)

Figure 5.3 ^{1}H-^{17}O HETCOR NMR at 17.6T of (a) dry H-MOR, contact time: 70μs; (b) dry H-MOR, contact time: 100μs and (c) H-MOR containing trace amount of H_2O, contact time: 120μs.

Table 5.1 NMR parameters of ^{17}O atoms directly bound to Brønsted acid sites obtained from simulations of the HETCOR NMR slices

Slice	δ_{CS} (^{1}H) (ppm)	QCC (MHz)	η	δ_{iso} (ppm)
(i)	3.9	6.3	0.7	28
(ii)	4.8	6.4	0.45	31
(iii)	3.8	6.2	0.8	27
(iv)	4.8	6.4	0.45	31
(v)	6.2	5.5	0.8	21

5.3.3 $^{1}H \rightarrow {}^{17}O\text{-}{}^{1}H$ CP-REDOR

CP-REDOR NMR, developed by Gullion and Schaefer,[14] has become a standard solid-state NMR technique for measuring heteronuclear distances under MAS conditions. In our previous work, $^{1}H \rightarrow {}^{17}O\text{-}{}^{1}H$ CP REDOR has been carried out at both room and low temperatures to probe the O-H distances and H motional processes of the Brønsted acid sites in zeolite HY and HZSM-5[15]. Due to the very large $^{1}H\text{-}{}^{17}O$ dipolar coupling for O-H groups, a 'mirror-symmetric' pulse sequence (Figure 5.1) was used,[16-18] rather than the standard pulse sequence often used for quadrupolar nuclei[14,19].

The REDOR fractions were measured as a function of time 't', which represents the time between the end of the contact time and the ^{1}H π pulse. Data acquired without the two dephasing π pulses on the ^{1}H channel were used as the control experiments. Due to the signal-to-noise limitations of the experiment, the REDOR fractions of zeolite H-MOR were measured by integrating the isotropic resonances only. Two contact times of 80 and 120 μs have been chosen for the cross-polarization to vary the contribution to the spectrum from different O-H distances, and the corresponding CP-REDOR fractions are shown in Figure 5.4. The REDOR fractions increase with increasing value of time 't' and reach a maximum when 't' is approximately 20 and 25 μs, for the data with contact times of 80 and 120 μs, respectively. The slower dephasing and lower REDOR fraction at contact time 120μs indicates that some O-H groups with either longer O-H distance or

more mobile protons have been selected. The nature of this local environment will be discussed in detail later.

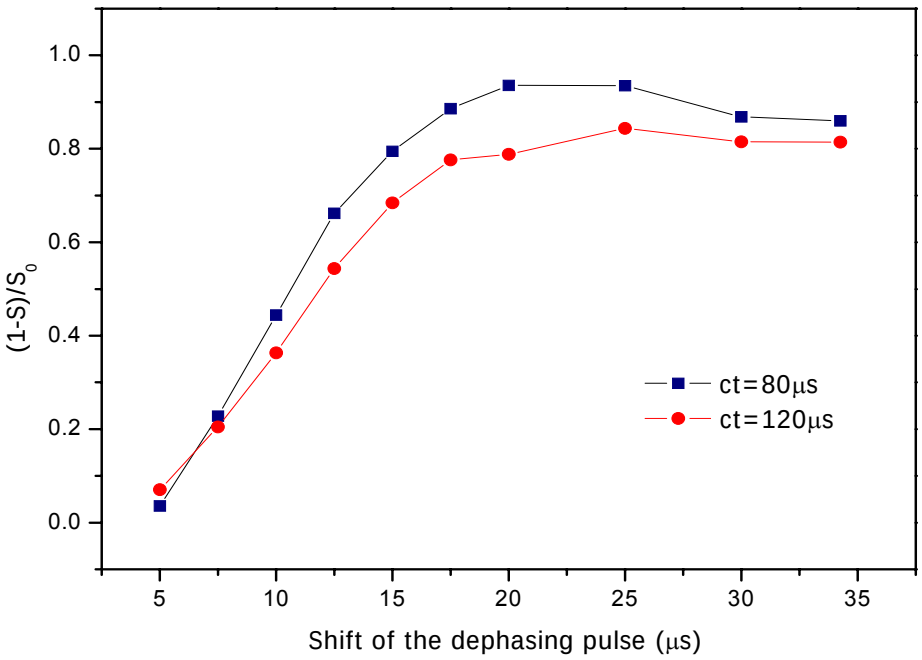

Figure 5.4 $^{1}H \rightarrow {}^{17}O\text{-}{}^{1}H$ CP-REDOR fraction ($1\text{-}S/S_0$) measured as function of the shift of the first dephasing pulse at 17.6 T. Spinning speed: 13 kHz, recycle delay: 1s

The experimental CP-REDOR lineshapes, as a function of the dephasing time, at contact times of 80 and 120 μs are shown in Figure 5.5 (a) and (b), respectively. As discussed in our previous study on zeolite HY, the dephasing behavior is not uniform across the whole second-order quadrupolar lineshape. Two typical quadrupolar lineshapes for two different local environments of oxygen atoms associated with different O-H distances have been successfully resolved in $^{1}H \rightarrow {}^{17}O$ CP and HETCOR experiments of zeolite H-MOR. The simulated lineshapes of these two resolved oxygen sites are adopted in the following analysis of the dephasing behavior of the overall lineshapes observed in the CP-REDOR NMR experiments and hereby noted as "small η" and "large η" sites (Figure 5.6 b and c). The overall lineshape can be considered as a sum of these two types of lineshapes. The ^{17}O resonance with the large η value is from oxygen atoms more tightly bound to the protons and can be enhanced by using shorter contact times. In contrast, the resonance with a small η value corresponds to an oxygen environment with a longer O-H distance and can be selectively enhanced by a longer contact time. As shown in Figure 5.6, the discontinuity at -2 - -3 ppm in the overall lineshape (Figure 5.6 a) resulted from the overlap of the most intense discontinuity of the large η resonance and the most intense lower frequency discontinuity of the small η resonance. The discontinuity at 19 ppm in the overall lineshape is a result of an overlap of the high frequency less intense discontinuity of the larger η resonance and the most intense higher frequency discontinuity of the small η resonance. The general dephasing behavior of a quadrupolar lineshape with a large η value has been discussed in the study of zeolite

HY[13]. The most intense middle frequency discontinuity dephases faster than the less intense higher frequency discontinuity. The intensity of a discontinuity drops and becomes negative at a certain dephasing times, and then becomes positive again. Numerical simulations of the large η site (NMR parameters extracted from the ^{17}O-^{1}H HETCOR spectra) with several chosen dipolar coupling constants using SIMPSON package [12] are shown in Figure 5.7 a-c. The Euler angles used in the simulations defining the relative orientations between the principal axis system (PAS) of the dipolar tensors with respect to the crystal fixed frame are obtained from the *ab inito* calculations on the model compound, zeolite HY.[20] The slight mismatch of the chemical shift between the experimental data and simulations are ascribed to different Brønsted acid oxygen sites in zeolite HMOR while the simulation was performed on a single-site model. The simulations provide a qualitative estimation of the dephasing behaviors. Similar simulations with chosen dipolar coupling constants have been carried out on the small η site using the NMR parameters extracted from ^{17}O-^{1}H CP-HETCOR spectra (Figure 5.7 d-f). In contrast to the large η site, the higher frequency discontinuity at approximately 17 ppm dephases slightly faster than the lower frequency discontinuity at -2 ppm. The intensity of a discontinuity drops to a minimum, and then increases again.

A closer inspection on the experimental dephasing behavior of the overall lineshape suggests the lineshape is dominated by the large η resonance associated with a large dipolar constant (Figure 5.7 a) for a short contact time of 80 μs. The discontinuity at -3 ppm dephases rapidly and the intensity decreases and becomes negative at t = 20 μs,

and then comes back to positive, while the discontinuity at 19 ppm dephases much more slowly and reaches the null point at t = 25~30 μs. At a longer contact time of 120 μs, the contribution from the small η resonance to the overall lineshape cannot be neglected any longer. This small η resonance is more likely associated with a smaller dipolar coupling constant in the range of 16290-19000 Hz, as shown in Figure 5.7 d, e. The discontinuity at -3 ppm does not decrease to negative at the maximum dephasing point of t = 20 μs, which is due to the slow dephasing behavior of the small η resonance. Similar effect can be observed on the discontinuity at 19 ppm. At the maximum dephasing point of t = 25~30 μs, the intensity of this discontinuity does not drop to negative before increases again. One thing that needs to be addressed is the negative intensity of the higher frequency discontinuity at approximately 17-20 ppm observed in the simulation line shape using the small dipolar coupling constant of 16290 Hz (Figure 5.7 c & f). Figure 5.7 (a')-(f') show the corresponding spectra in larger chemical shift scale to include the spinning sidebands. The negative intensity at the center band mentioned above is associated with a compensation of positive intensity in the spinning sidebands. Hence, this should be considered as a characteristic dephasing behavior of the center band in the case of relatively weak dipole-dipole interaction. All these observations support our hypothesis ^{17}O signal associated with a longer O-H distance can be enhanced by a longer contact time.

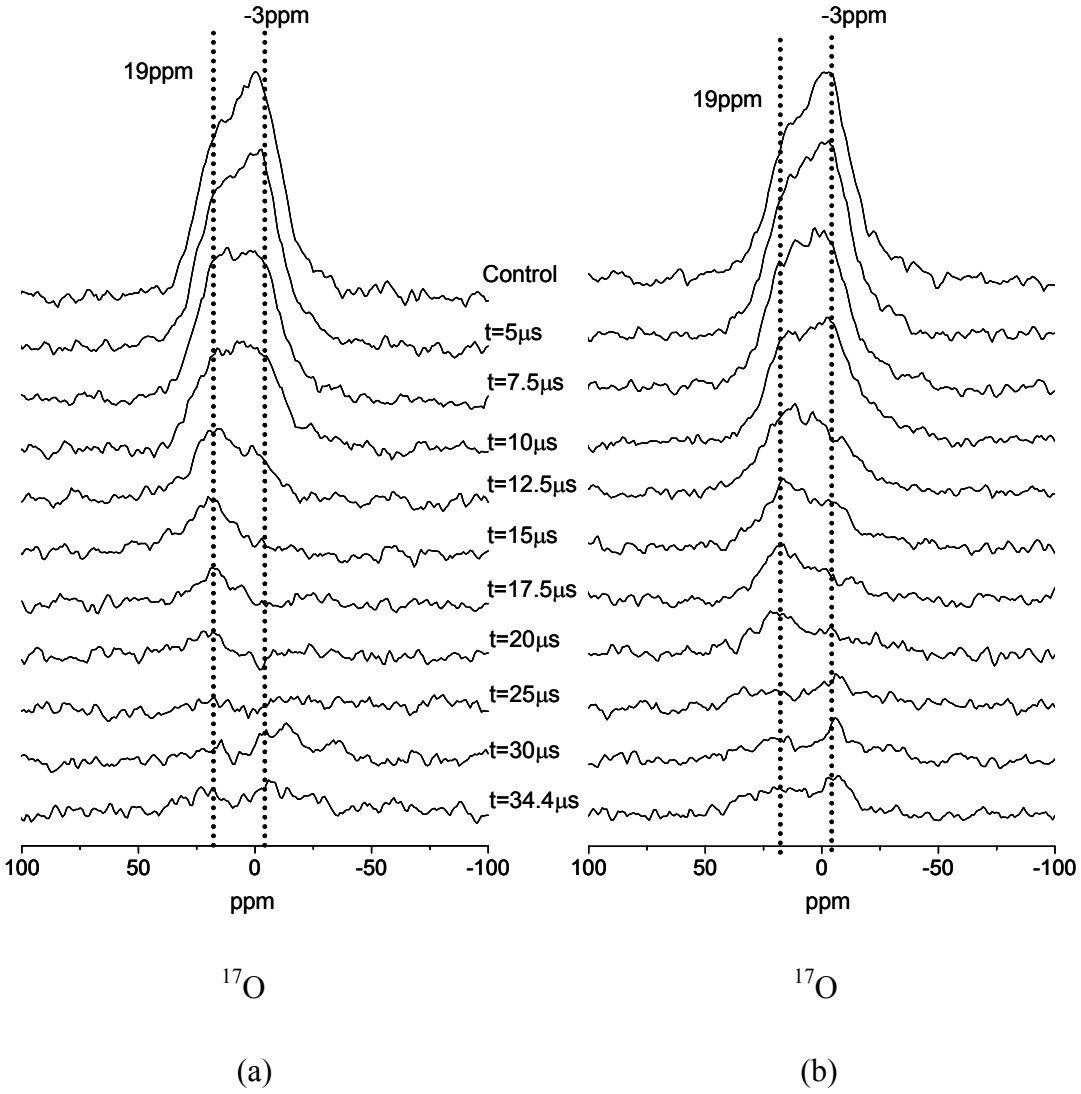

Figure 5.5 The plot of $^{1}H \rightarrow {}^{17}O$-$^{1}H$ CP-REDOR NMR spectra as a function of the shift of the dephasing pulse with contact time of (a) 80 and (b) 120μs, at 17.6 T. Spinning speed: 13 kHz, recycle delay: 1s

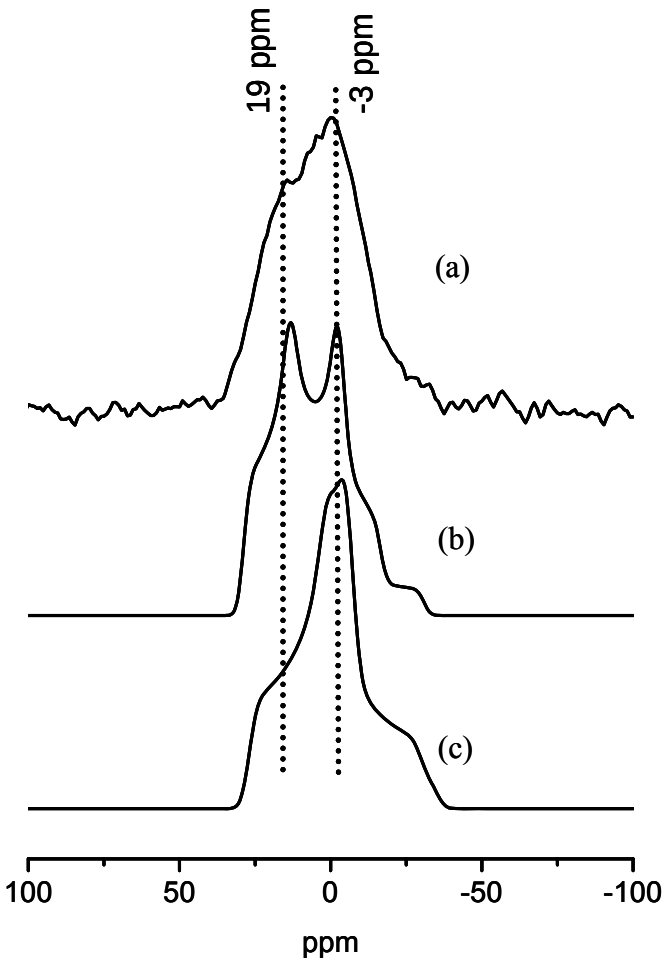

Figure 5.6 Scheme for the lineshape analysis. (a) The experimental spectrum of the control experiment obtained with the contact time of 80 μs and simulations of the (b) small η and (c) large η sites resolved from the 2D ^{17}O-^{1}H HETCOR spectra.

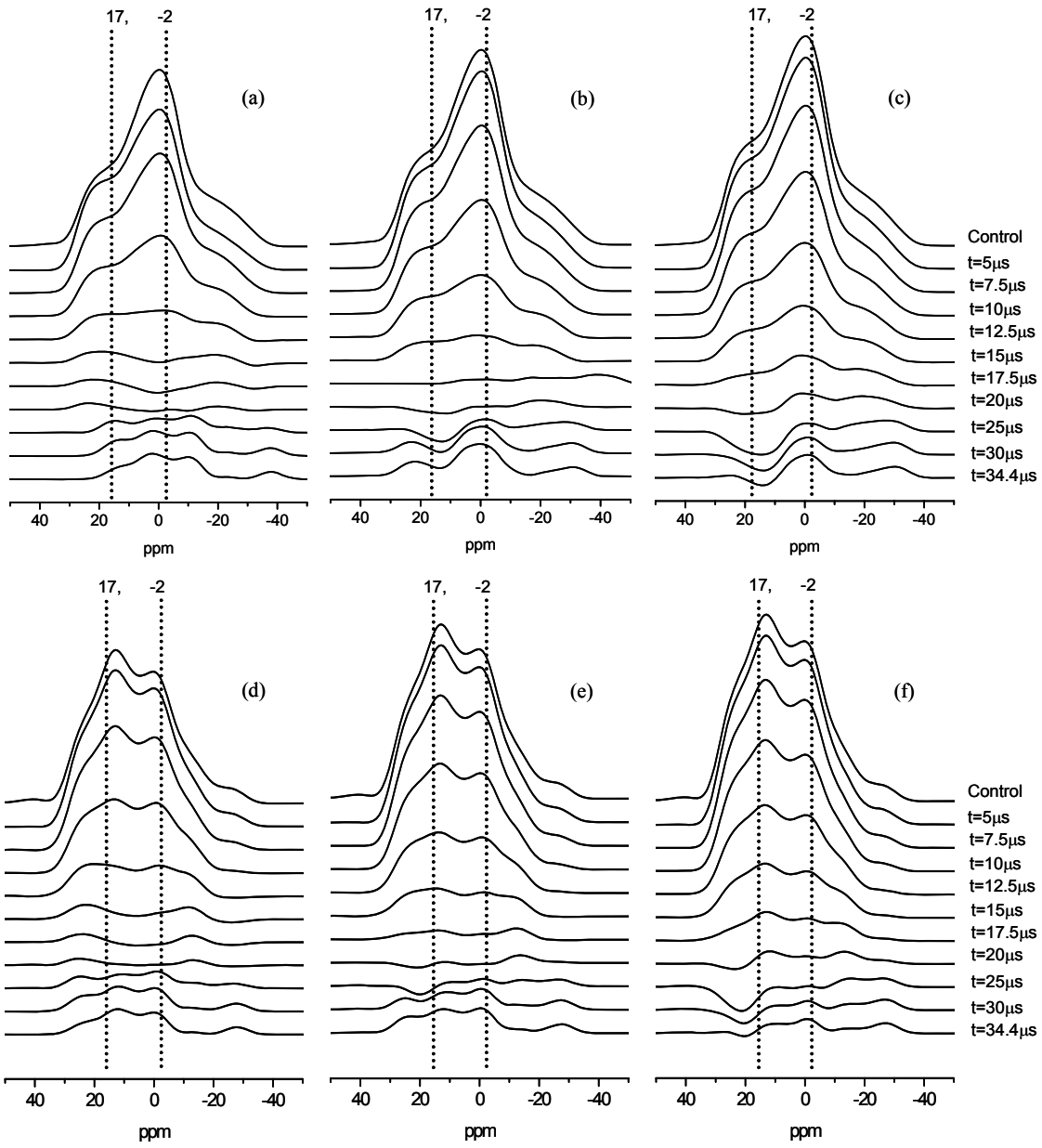
17,
-2
(a)
(b)
(c)
(d)
(e)
(f)
40
20
0
-20
-40
ppm
Control
t=5μs
t=7.5μs
t=10μs
t=12.5μs
t=15μs
t=17.5μs
t=20μs
t=25μs
t=30μs
t=34.4μs

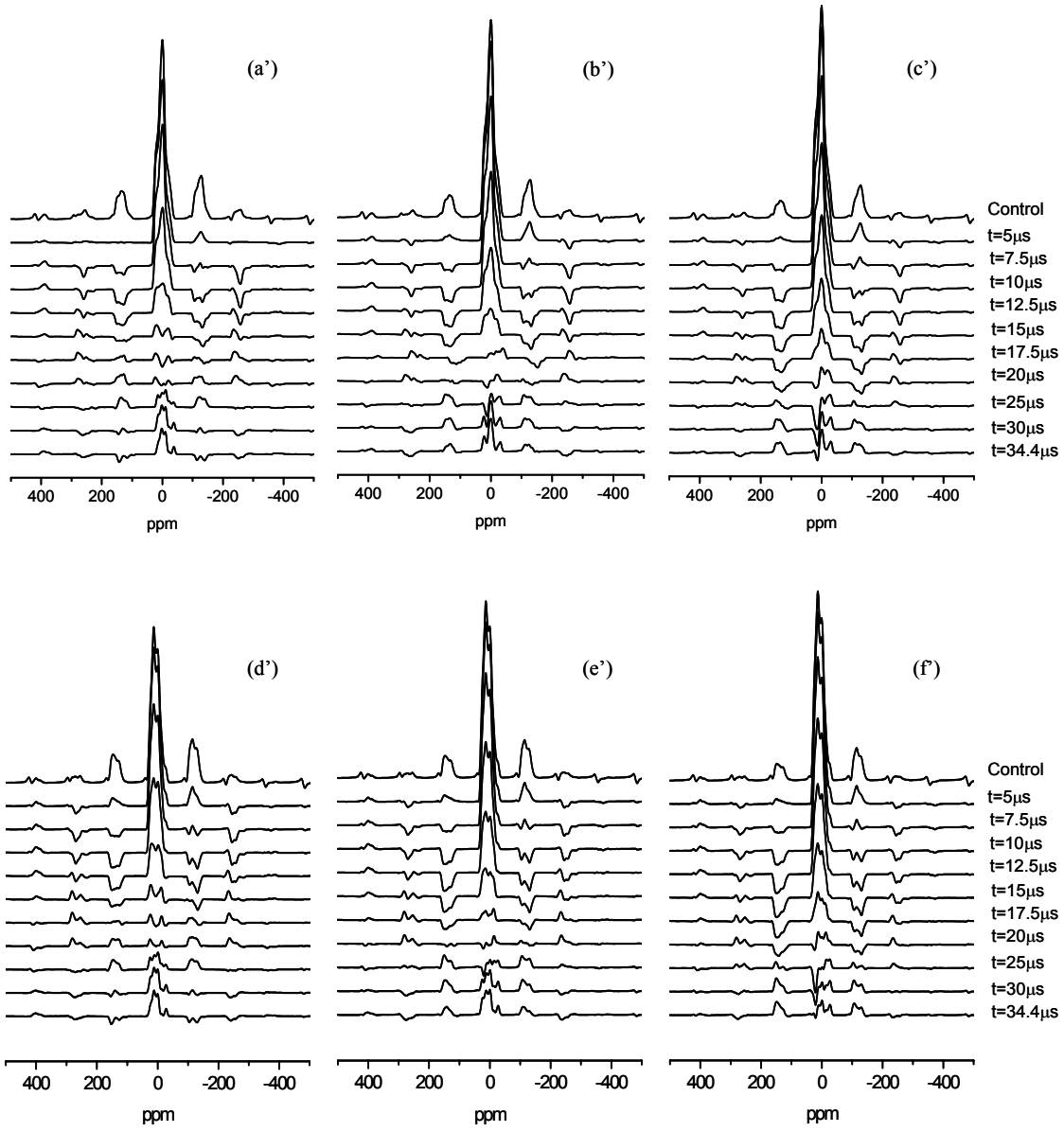

Figure 5.7 NMR line shape simulations performed with the SIMPSON package[12] (a-f) show the center bands, while (a'- f') show the corresponding spectra in larger chemical shift scale to include the spinning sidebands. (a-c) simulations performed with dipolar coupling constants of 22346, 19000 and 16290 Hz, respectively. NMR parameters used in the simulations are δ_{CS} = 27.5, QCC = 6.25 MHz, and η = 0.75 (the average values

taken from the simulation results of the "large η" sites resolved in the ^{17}O-^{1}H HETCOR spectra). (d-f) simulations performed with dipolar coupling constants of 22346, 19000 and 16290 Hz, respectively. NMR parameters used in all simulations are δ_{CS} = 31, QCC = 6.4 MHz, and η = 0.45 (the values taken from the simulation results of the "small η" sites resolved in the ^{17}O-^{1}H HETCOR spectra).

5.3.4 2D ^{1}H-^{29}Si HETCOR NMR

2D ^{1}H-^{29}Si HETCOR NMR spectra are shown in Figure 5.8 with (a) short contact time of 500 μs and (b) long contact time of 10 ms. The observed broad line on the ^{1}H dimension and therefore induced difference of chemical shift values comparing to the ^{1}H MAS NMR are presumably due to less than adequate data points collected on the indirect ^{1}H dimension. The resonances at 5.3 and 6.8 ppm on the ^{1}H dimension are corresponding to the resonances at 4.8 and 6.3 ppm in the ^{1}H MAS NMR. When short contact time is applied, the spectrum is less quantitative since only the Si atoms with the nearest proximity to the protons can be selectively enhanced. As shown in Figure 5.8 (a) with a short contact time of 500 μs, the maximum intensity on the ^{1}H dimension is around 5.3 ppm. The ^{29}Si signal correlated with this ^{1}H resonance covers a wide range of chemical shift values (-92 to -117 ppm). According to Table 5.2, this range of ^{29}Si chemical shift values includes many types of Si environments, from Q_4 (0Al) to Q_2 (2Al)/Q_3, which further confirms the hypothesis that this resonance is associated with Brønsted acid protons forming H-bonding to the framework. In contrast, the ^{1}H resonance

at 3.9 ppm is only correlated to ^{29}Si signal over a narrower range (-99 to -108 ppm), which corresponds to Q_4 (1Al). This is consistent with the assignment of Brønsted acid protons with the most proximity to the Si atoms in the Si-O-Al linkage. When a long contact time of 10 ms is applied, Figure 5.8. (b), all Si atoms can be equally cross polarized and hence the spectrum is more quantitative. The similarity between the projection on the ^{1}H dimension and the ^{1}H MAS NMR spectrum can be taken as evidence that the ^{1}H resonance at 3.9 ppm now is correlated to a wide variety of Si environments.

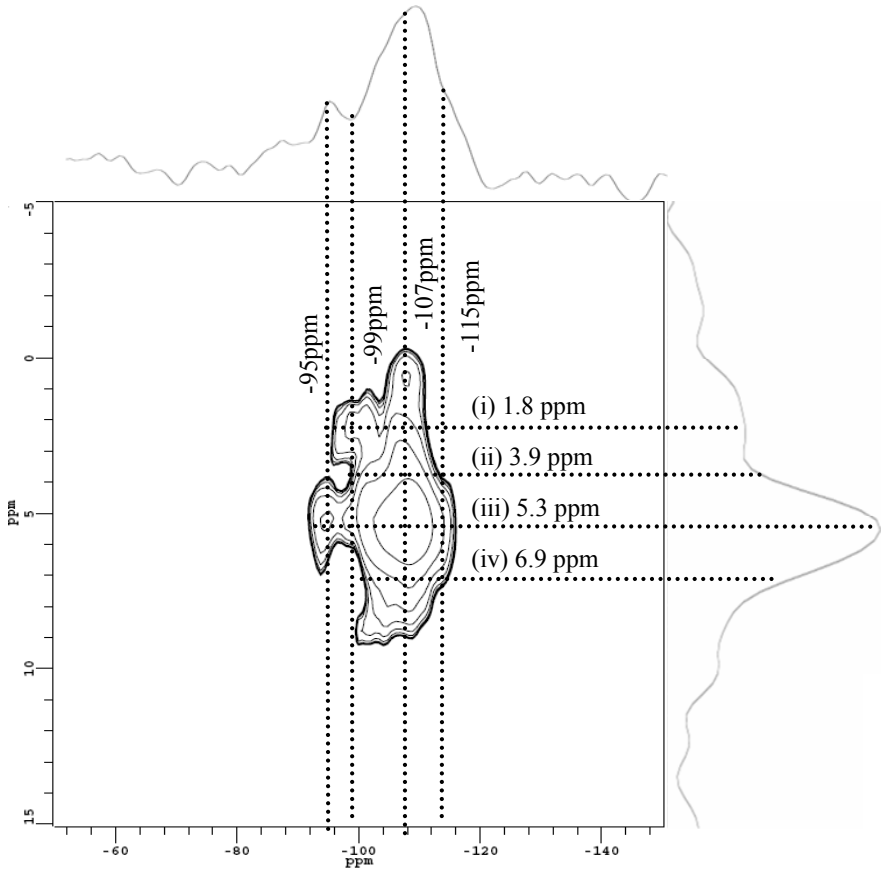
-95ppm
-99ppm
-107ppm
-115ppm
(i) 1.8 ppm
(ii) 3.9 ppm
(iii) 5.3 ppm
(iv) 6.9 ppm
ppm
-5
0
5
10
15
-60
-80
-100
-120
-140
ppm

(a)

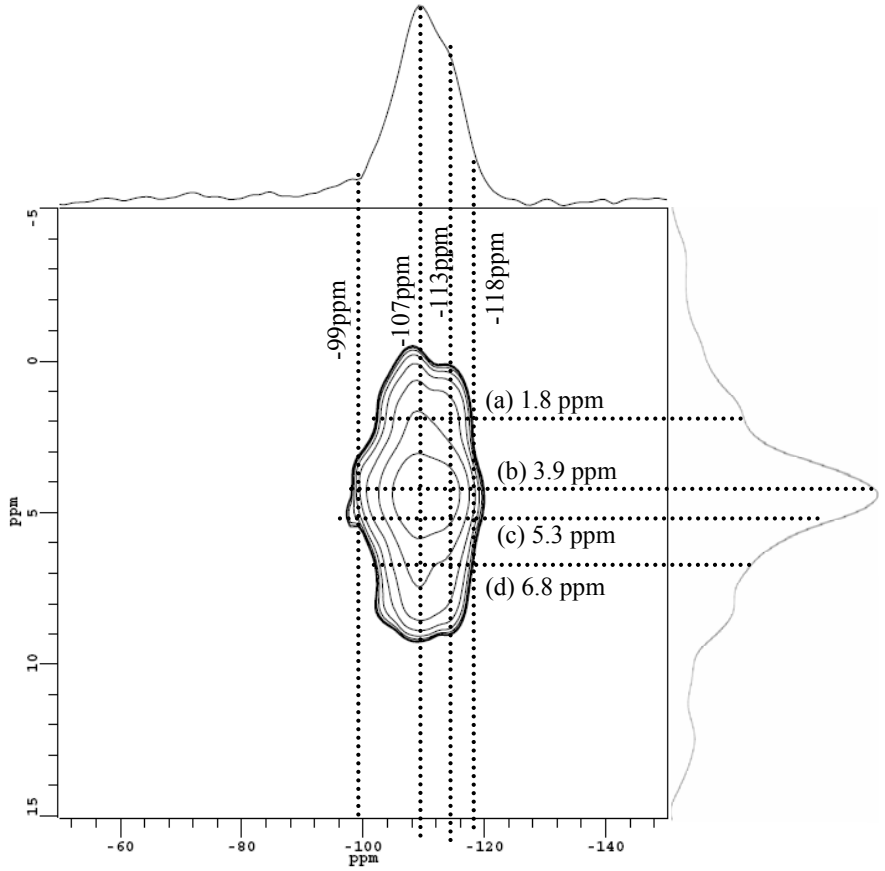

(b)

Figure 5.8 ^{1}H-^{29}Si HETCOR NMR of zeolite H-MOR at 8.45T with contact times of (a) 500μs and (b) 10 ms.

Table 5.2 ^{29}Si chemical shift values of Si atoms with different nearest neighbor atoms in typical aluminosilicates

Coordination type of Si		^{29}Si Chemical Shift (ppm)
Q_4	Q_4(0Al)	-102 to -116
	Q_4(1Al)	-97 to -107
	Q_4(2Al)	-92 to -100
	Q_4(3Al)	-85 to -94
	Q_4(4Al)	-82 to -92
Q_3	[Si-OH]	-83 to -93
Q_2	[Si-$(OH)_2$]	-73 to -85

5.3.5 The Nature of the Brønsted Acid Site at $\delta_{CS}{}^{1}H$ = 4.8 ppm

In the TMP adsorption experiments with different loading levels, the ^{1}H resonance of the residual acid sites inaccessible to TMP probe molecules is centered at 4 ppm. This suggested that the acid site corresponds to the ^{1}H resonance at 4.8 ppm is located in the 12-ring main channel and hence can be easily accessed by TMP probe molecules. The ^{1}H-^{17}O HETCOR experiment of the sample containing trace amount of water further confirms that this $\delta_{CS}{}^{1}H$=4.8 ppm resonance is associated with Brønsted acid sites which were the most easily attacked by the adsorbed water molecules. The ^{17}O signal of the oxygen site connected with this proton site can be favored by a slightly longer contact time in experiments containing cross polarization excitation. Since cross polarization is based on heteronuclear dipolar coupling interaction, which is extremely sensitive to both internuclear distance and motional process, the observed weaker heteronuclear interaction may be due to a longer O-H distance and/or a mobile proton. The smaller asymmetric parameter η compared to the other acidic site oxygen or the result obtained from zeolite HY also confirms that at this specific Brønsted acid site the proton is loosely bound to the oxygen atom. The most reasonable proposal that account for these results would be an acidic hydroxyl group H-bonded to nearby framework oxygen. As indicated by Kobe *et al* in their study on ^{2}H NMR of Brønsted acid site and silanol species in zeolite D-MOR[21], the configuration of the Si-(OD)-Al is not rigid with four coplanar atoms. Instead, the deuteron hops between the two lobes of the sp^3 orbital

of oxygen. This two-site exchange between sites of equal populations can facilitate the formation of H-bonding between adjacent oxygen pairs. The typical oxygen to oxygen distances in moderate-weak H-bonding vary in the range of 2.4 – 2.7 Å[22,23]. A close check of the framework structure identifies the following pairs: O_2_O_5 2.522 Å, O_6_O_1 2.643 Å, O_1_O_9 2.607Å and O_2_O_2 2.677 Å. Among the four choices above, the oxygen pairs of O_2_O_5 and O_2_O_2 fulfill the requirement that both oxygen atoms are located in the 12-ring main channel. The configuration of the O_2_O_2 pair appears the most likely since the sp^3 orbitals of both oxygen atoms point to the same direction, the center of the 12-ring channel.

5.4 Conclusions

In the ^{17}O-^{1}H cross polarization double resonance experiments (CPMAS, CP-REDOR and HETCOR NMR) of zeolite H-MOR, the relative contribution to the spectrum from different Brønsted acid sites associated with different O-H distances can be excited by modulating the experimental parameter in the CP experiment, the contact time. In additional to the normal bridging Si-O(H)-Al group, a second type of acidic hydroxyl group with longer O-H distance has been investigated. The experimental results indicated that this site corresponds to two adjacent O_2 atoms on the wall of 12-ring main channel sharing one proton through H-bonding.

The ^{1}H MAS NMR results of zeolite H-MOR loaded with TMP probe molecules at different adsorption levels illustrated that about 20-25% acidic hydroxyl groups are located in 8-ring channels; 25-30% are located at the intersections of the side pockets and main channels and the rest of 45-50% are located in the 12-ring main channels. By checking the structure, it has been concluded that there are four possible locations for Brønsted acid sites in zeolite H-MOR: (a) O_9, pointing into the center of the 8-ring channel and inaccessible to TMP probe molecules; (b) O_2, adjacent oxygen pair shares one proton through H-bonding; (c) O_5, slightly pointing toward the side pocket; (d) O_7, pointing into the center of the 12-ring.

5.5 References

(1) Amoureux, J. P.; Bauer, F.; Ernst, H.; Fernandez, C.; Freude, D.; Michel, D.; Pingel, U. T. *Chem. Phys. Lett.* **1998**, 285, 10.

(2) Bull, L. M.; Bussemer, B.; Anupold, T.; Reinhold, A.; Samoson, A.; Sauer, J.; Cheetham, A. K.; Dupree, R. *J. Am. Chem. Soc.* **2000**, 122, 4948.

(3) Bull, L. M.; Cheetham, A. K. *Stud. Surf. Sci. Catal.* **1997**, 105, 471.

(4) Bull, L. M.; Cheetham, A. K.; Anupold, T.; Reinhold, A.; Samoson, A.; Sauer, J.; Bussemer, B.; Lee, Y.; Gann, S.; Shore, J.; Pines, A.; Dupree, R. *J. Am. Chem. Soc.* **1998**, 120, 3510.

(5) Freude, D.; Loeser, T.; Michel, D.; Pingel, U.; Prochnow, D. *Solid State Nucl. Magn. Reson.* **2001**, 20, 46.

(6) Loeser, T.; Freude, D.; Mabande, G. T. P.; Schwieger, W. *Chem. Phys. Lett.* **2003**, 370, 32.

(7) Neuhoff, P. S.; Shao, P.; Stebbins, J. F. *Micropor. Mesopor. Mat.* **2002**, 55, 239.

(8) Pingel, U. T.; Amoureux, J. P.; Anupold, T.; Bauer, F.; Ernst, H.; Fernandez, C.; Freude, D.; Samoson, A. *Chem. Phys. Lett.* **1998**, 294, 345.

(9) Readman, J. E.; Kim, N.; Ziliox, M.; Grey, C. P. *Chem. Commun.* **2002**, 2808.

(10) Stebbins, J. F.; Zhao, P. D.; Lee, S. K.; Cheng, X. *Am. Mineral.* **1999**, 84, 1680.

(11) Kolodziejski, W.; Klinowski, J. *Chem. Rev.* **2002**, 102, 613.

(12) Bak, M.; Rasmussen, J. T.; Nielsen, N. C. *J. Magn. Reson.* **2000**, 147, 296.

(13) Peng, L.; Huo, H.; Liu, Y.; Grey, C. P. *J. Am. Chem. Soc.* **2007**, 129, 335

(14) Gullion, T.; Schaefer, J. *J. Magn. Reson.* **1989**, 81, 196.

(15) Huo, H.; Peng, L. M.; Grey, C. P. *J. Phys. Chem.C* **2009**, 113, 8211.

(16) Goetz, J. M.; Wu, J. H.; Yee, H. F.; Schaefer, *J. Solid State Nucl. Magn. Reson.* **1998**, 12, 87.

(17) Gullion, T. *Magn. Reson. Rev.* **1997**, 17, 83.

(18) Wu, J. H.; Xiao, C. D.; Yee, A. F.; Goetz, J. M.; Schaefer, J. *Macromolecules* **2000**, 33, 6849.

(19) Fyfe, C. A.; Mueller, K. T.; Grondey, H.; Wong-Moon, K. C. *J. Phys. Chem.* **1993**, 97, 13484.

(20) Peng, L.; Liu, Y.; Kim, N.; Readman, J. E.; Grey, C. P. *Nature Mater.* **2005**, 4, 216.

(21) Kobe, J. M.; Gluszak, T. J.; Dumesic, J. A.; Root, T. W. *J. Phys. Chem.***1995**, 99, 5485.

(22) Ichikawa, M. *Acta Crystallogr. B* **1978**, 34, 2074.

(23) Ichikawa, M. *J. Mol. Struct.* **2000**, 552, 63.

Chapter 6

^{17}O MQMAS NMR Studies of Zeolites H-MOR

Abstract

High-resolution ^{17}O multiple-quantum MAS (MQMAS) NMR spectra have been obtained for zeolite H-MOR to study its local structure and Brønsted acidity. The ^{17}O NMR signals due to different oxygen environments have been observed in one single two-dimensional experiment, including the readily-resolved signals arising from two types of oxygen atoms at zeolite framework (Si-O-Al and Si-O-Si) and oxygen atoms directly bound to Brønsted acid sites (Si-O(H)-Al). The ^{17}O NMR parameters such as the isotropic chemical shift (δ_{iso}) and quadrupolar coupling parameters (quadrupolar coupling constant, QCC and asymmetry parameter, η) for these oxygen species have been extracted and found to be consistent with the results obtained from the ^{17}O-^{1}H HETCOR NMR measurements as discussed in Chapter 5.

6.1 Introduction

^{17}O MAS NMR spectroscopy is an extremely sensitive probe of the local coordination environment of oxygen in a zeolite framework. The ^{17}O nucleus, as a quadrupolar nucleus, is significantly affected by the electric field gradient (EFG) surrounding the nucleus.[1] The ^{17}O has a large quadrupole moment; hence the single pulse spectra of this nucleus are typically very broad. Taking an aluminum containing zeolite as an example, the single pulse spectra usually consist of a large number of overlapping resonances due to Si-O-Al and Si-O-Si sites in the zeolite framework.[2-7] Dynamic angle spinning (DAS), and multiple-quantum MAS (MQMAS) NMR have been employed to obtain high-resolution ^{17}O spectra, in which the individual resonance due to Si-O-Si or Si-O-Al from different crystalline sites can be readily resolved.[2,6] However, the resonance from the most catalytically relevant oxygen atom, the one that is directly bound to the Brønsted acid sites has been difficult to detect. In our previous ^{17}O MQMAS NMR study on zeolite HY, the ^{17}O NMR signals due to all the different oxygen environments have been observed in one single experiment, including the readily-resolved signals arising from the two types of oxygen atoms of the zeolite framework (Si-O-Al and Si-O-Si), and oxygen atoms directly bound to Brønsted acid sites (Si-O(H)-Al). The ^{17}O NMR parameters δ_{CS}, QCC and η for these oxygen species have been extracted.[8] In this paper, the application of ^{17}O MQMAS NMR spectroscopy has been extended to explore the structural information that can be extracted from zeolite H-MOR.

6.2 Experimental Section

6.2.1 Materials Preparation

Zeolite Na-Mordenite (NaMOR) with framework *n* (Si)/*n* (Al) ratio of 8.8 (HSZ-642NAA) was obtained from Tosoh Corporation. To avoid the dealumination upon heat treatment of the hydrated samples, ^{17}O enrichment was carried out on the sodium form zeolite mordenite. Zeolite NaMOR was first dehydrated by heating under vacuum (pressure < 10^{-3} torr) with a step size of 2 K/ min to 773K, and then held at this temperature for 12 hours. ^{17}O isotopic enriched NaMOR was prepared by heating dehydrated zeolite NaMOR in $^{17}O_2$ gas (50% enriched $^{17}O_2$ from Isotec, Inc.) to 853K and held at this temperature for 12 hours. ^{17}O-enriched zeolite NH_4MOR was prepared by ion exchange with a 1 M NH_4NO_3 solution at ambient temperature for 12 hours (repeated five times). ^{17}O-enriched HMOR was prepared by heating ^{17}O-enriched NH_4MOR under vacuum with a step of 0.2 K/min to 383 K, and then 0.4 K/min to 673 K, after that the temperature was held at 673 K for 12 hours. The samples were stored and packed into NMR rotors in the N_2 glove box, prior to the NMR experiments.

6.2.2 Solid-state NMR Spectroscopy

MAS NMR spectra were obtained with Bruker Avance 600 and 833 spectrometers, with 89 mm wide-bore 14.1 T and 31 mm ultra-narrow-bore 19.4 T superconducting magnets, respectively, in 4 mm rotors. Rotor caps with o-rings were

used to avoid the adsorption of water during the NMR measurements. ^{17}O chemical shifts are referenced to H_2O at 0.0 ppm. A standard triple-quantum MAS pulse sequence with two hard pulses followed by a z-filter was used. In the experiment performed at 14.1 T, two-pulse phase modulated (TPPM)[9] ^{1}H decoupling at 70kHz was applied during t_1-evolution and t_2-acquisition. The optimized parameters for the MQMAS experiments were set by using the ^{17}O-enriched zeolite HY sample described in Chapter 2. NMR line shape simulations were performed with the Wsolids package developed by Dr. K. Eichele.

6.3 Results and Discussion

6.3.1 ^{17}O single pulse MAS NMR

The ^{17}O one-pulse MAS NMR spectrum of zeolite H-MOR sample at the field strength of 17.6 T is shown in Figure 6.1. A broad resonance due to the framework oxygen atoms in the Si-O-Al and Si-O-Si linkages is observed with two singularities at about 31 and 18 ppm. The Si-O-Al and Si-O-Si cannot be readily resolved in one-pulse spectrum, due to the large second-order quadrupole line broadenings[10]. The lineshape is not symmetric. As shown in the previous chapter, the ^{17}O signals arising from the Si-(OH)-Al sites, which can be observed in ^{17}O -^{1}H CP MAS NMR, are probably buried under the small foot of the broad resonance at about -3 ppm. Spectra of quadrupolar nuclei like ^{17}O often contain shoulders and discontinuities that arise from the second-order quadruple line broadenings. To resolve the resonances arising from different environments, ^{17}O MQMAS NMR experiments have been performed.

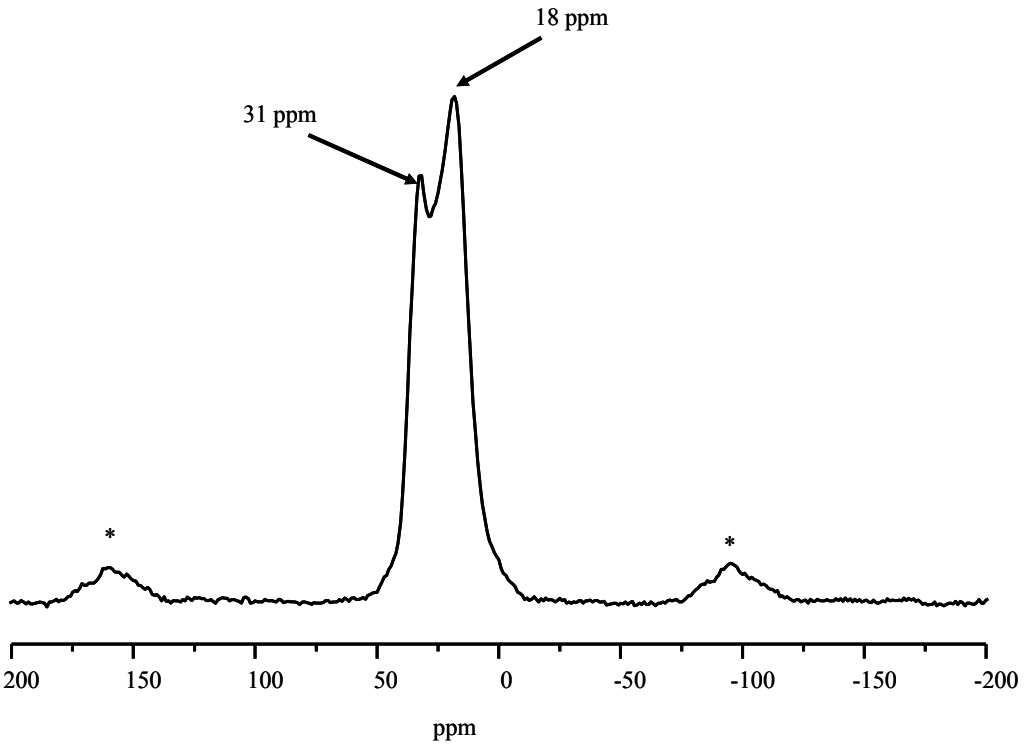

Figure 6.1 ^{17}O single pulse MAS NMR of zeolite H-MOR obtained at 17.6 T, spinning speed 13kHz. Spinning sidebands are denoted by " * ".

6.3.2 2-D MQMAS Spectrum Obtained at A 14.1 T Magnet

The two-dimensional (2-D) ^{17}O MQMAS NMR (with ^{1}H decoupling) spectrum of zeolite H-MOR and its F_1/ F_2 projection acquired at a magnetic strength of 14.1 T are shown in Figure 6.2 (a). Similar to the single pulse spectrum, the anisotropic projection of the MQMAS spectrum shows one broad resonance (δ_2 = 45 to –40) with two maxima at δ_2 =20 and 3 ppm and a small foot centered at δ_2 = –15 ppm, where δ_2 is the center of gravity of the resonance in the anisotropic (F_2) dimension, respectively. The isotropic (F_1) projection, however, shows at least three resonances with centers of gravity, δ_1 of 31.5, 47.0 and 54.5 ppm. The resonances centered at 31.5 and 54.5 ppm on the F_1 dimension can be assigned to framework oxygen sites in Si-O-Al and Si-O-Si linkages, respectively. The NMR parameters for the Si-O-Si and Si-O-Al linkages were therefore extracted by simulating the slices of the F_2 dimension (Figure 6.2. (b)- (d)) and the parameters (quadrupolar coupling constants, QCC, asymmetry parameter, η, and isotropic chemical shift, δ_{iso}) are listed in Table 6.1. The shifts δ_1 and δ_2 can be used to extract the values for isotropic chemical shift, δ_{iso}, and quadrupolar product, P_Q, directly, without simulating the F_2 dimension. For a spin I = 5/2 nucleus these parameters are given by:

$$\delta_{iso} = \frac{17}{27}\delta_1 + \frac{10}{27}\delta_2 \qquad (6.1)$$

$$P_Q = \frac{\nu_0}{25}\sqrt{\frac{85(\delta_1 - \delta_2)}{1296}} \qquad (6.2)$$

$$P_Q = QCC\sqrt{1+\frac{\eta^2}{3}} \qquad (6.3)$$

where ν_0, QCC and η are the carrier frequency, the quadrupolar coupling constant and the asymmetry parameter, respectively. The predicted δ_{iso} and P_Q (Table 6.1) have been used to examine the results of lineshape simulation. Conversely, the values of δ_1 and δ_2 can be predicted, if δ_{iso} and P_Q are known.

The ^{17}O signal due to oxygen directly bound to acidic proton is not clearly seen in the MQMAS spectrum. As mentioned above, the center of gravity (values of δ_1 and δ_2) of an unknown site can be predicted, if δ_{iso} and P_Q are known. The δ_{iso} and P_Q values of the oxygen atoms at Brønsted acid sites have been calculated by applying the NMR parameters extracted from ^1H-^{17}O HETCOR experiment (Chapter 5) to Equations (1) and (3) and are listed in Table 6.2. The predicted centers of gravities of the corresponding ^{17}O signals are in the range of δ_2= -8 - -16 and δ_1= 52-54 ppm, which partially overlap with the signal arising from the Si-O-Si groups. In Figure 6.2 (d) the left spectrum shows the simulated lineshape with on Si-O-Si site. The intensity of the lower frequency, most intense singularity in the simulated line is obviously lower than the experimental lineshape. A two-site simulation is shown in the right spectrum of Figure 6.2 (d) by adding a Si-(OH)-Al site with the NMR parameters extracted from the lineshape simulation of ^{17}O-^1H HETCOR experiment. This two-site simulation provides a good fit to the experimental lineshape, which is consistent with the predicted centers of gravities of the ^{17}O signals arising from the Brønsted acid oxygen atoms.

Slice (ii) taken at δ_1= 47 ppm has been labeled as an "unknown" site. The lineshape simulation gives a result of QCC= 5.5 MHz, η= 0.7 and δ_{iso}= 21 ppm. This result is quite similar to the Brønsted acid site contaminated with trace amount of water resolved in the ^{17}O-^{1}H HETCOR experiment.

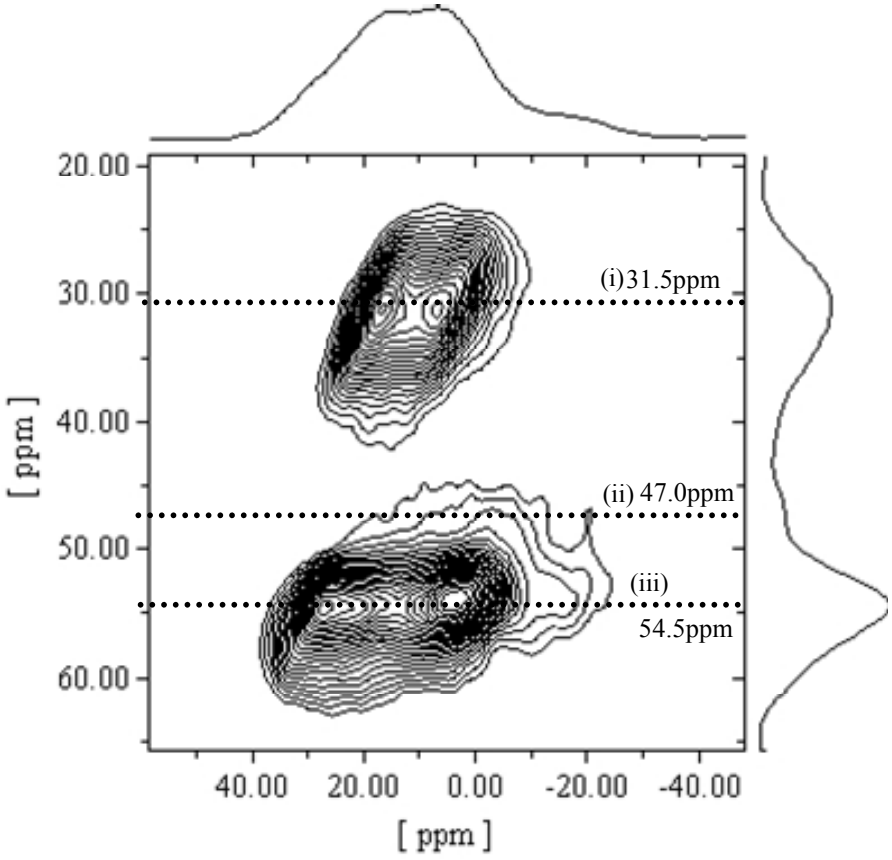

(a)

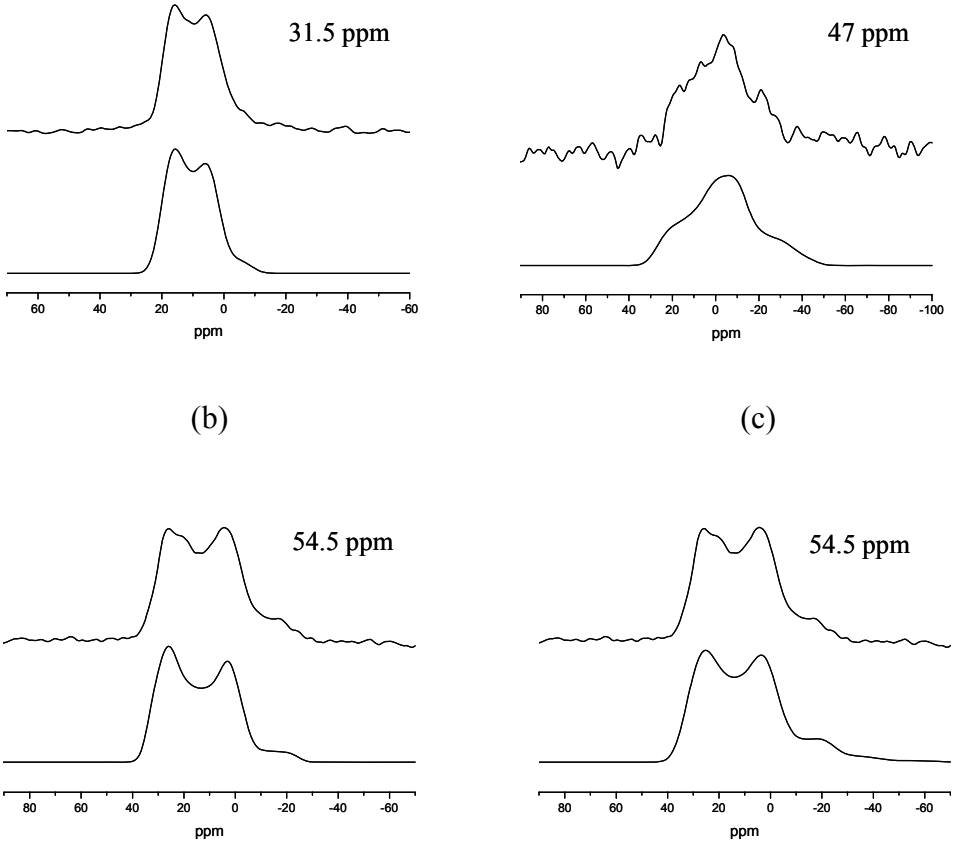

Figure 6.2 (a) 2-D-^{17}O MQMAS NMR spectrum of ^{17}O-enriched H-MOR acquired at 14.1 T, with a spinning speed of 13 kHz and recycle delay of 1 s. The projections (sum) of F_2 and F_1 dimension are shown on the above and right side of the 2D-spectrum, respectively. (b), (c) and (d): slices of anisotropic dimension at 31.5, 47.0 and 54.5 ppm, respectively, in isotropic dimension (top), in comparison with simulations performed with WSolids NMR package (bottom). Simulation parameters are shown in Table 6.1a. The dotted lines in the 2-D spectrum show where the slices are taken. Note: (d) left and right figures show one Si-O-Si site and Si-O-Si + Si-(OH)-Al two sites simulations of the slice taken at 54.5 ppm in isotropic dimension.

Table 6.1 δ_2s and δ_1s are the observed center of gravities of the resonances in the anisotropic (F_2) and isotropic (F_1) dimension for oxygen atoms at 14.1 T in zeolite H-MOR, respectively. The predicted values of P_Q and δ_{iso} were calculated from the observed shifts of center of gravity of the resonances, using Eq. 6.1 and 6.2. The simulation data values of QCC, η and δ_{iso} were obtained from the Wsolid simulation result of each slice. The value of P_Q can also be calculated with Eq. 6.3 using the simulation data. The predicted δ_{iso} and P_Q have been used to examine the results of lineshape simulation.

Site	Slice	δ_1 (ppm)	δ_2 (ppm)	Predicted values		Simulation data			
				δ_{iso} (ppm)	P_Q	QCC (MHz)	η	δ_{iso} (ppm)	P_Q
Si-O-Al	(i)	31.5	11	23.9	3.8	3.78	0.23	23.4	3.81
Unknown	(ii)	47	-3.5	28.3	5.96	5.5	0.70	21	5.93
Si-O-Si	(iii)	54.5	14	39.5	5.34	5.30	0.22	39.5	5.34

Table 6.2 Predicted centers of gravities of the Brønsted acid sites in the ^{17}O MQMAS spectrum obtained at 14.1T. ^{17}O NMR parameters (QCC, η and δ_{iso}) and corresponding coupled nearby ^{1}H sites were obtained in ^{1}H-^{17}O HETCOR NMR studies. The predicted centers of gravities (δ_1, δ_2) were calculated with Equation 6.1, 6.2 and 6.3.

$\delta_{CS}{}^{1}H$ (ppm)	QCC (MHz)	η	δ_{iso} (ppm)	δ_1 (ppm)	δ_2 (ppm)
3.8	6.3	0.8	27	52.4	-16.1
4.8	6.4	0.45	31	54	-8.16
6.2	5.5	0.8	21	40.3	-11.9

6.3.3 2-D MQMAS Spectrum Obtained at a 19.4 T Magnet

The two-dimensional (2-D) ^{17}O MQMAS NMR spectrum of zeolite H-MOR and its F_1/F_2 projection acquired at a magnetic field strength of 19.4T are shown in Figure 6.3 (a). In contrast to the 2-D MQMAS spectrum obtained at 14.1 T, the high field strength of 19.4 T leads to a larger distribution of isotropic chemical shift values and hence a better resolution in the isotropic dimension. The isotropic (F_1) projection shows five resonances with centers of gravity δ_1 of 18.5, 24, 28, 41 and 44.5 ppm, which can be assigned to framework oxygen sites in Si-O-Al (18.5, 24 and 28 ppm, green circle area) and Si-O-Si (41 and 44.5 ppm, blue circle area) linkages. The NMR parameters for the Si-O-Si and Si-O-Al linkages were extracted by simulating the slices of the F_2 dimension. The NMR parameters (quadrupolar coupling constants, QCC, asymmetry parameter, η, and chemical shift, δ_{iso}) are listed in Table 6.3. Similar to the procedure dealing with the data set obtained at 14.1 T, the shifts δ_1 and δ_2 can be used to extract the values for isotropic chemical shift, δ_{iso}, and quadrupolar product, P_Q, directly, without simulating the F_2 dimension. The predicted δ_{CS} and P_Q have been used to examine the results of lineshape simulation. Conversely, the values of δ_1 and δ_2 can be predicted, if δ_{CS} and P_Q are known.

The slice (iv) taken at δ_1= 34.5 ppm corresponds to the unassigned site. The lineshape simulation gives a result of QCC= 5.3 MHz, η= 0.7 and δ_{iso}= -26.2 ppm. This result is similar to the Brønsted acid site contaminated with trace amount of water

resolved in the ^{17}O-^{1}H HETCOR experiment. The slight discrepancy in the values of the NMR parameters obtained between the ^{17}O-^{1}H HETCOR and ^{17}O MQMAS data in some degree lies in the poor S/N of the slice taken from the 2-D spectrum.

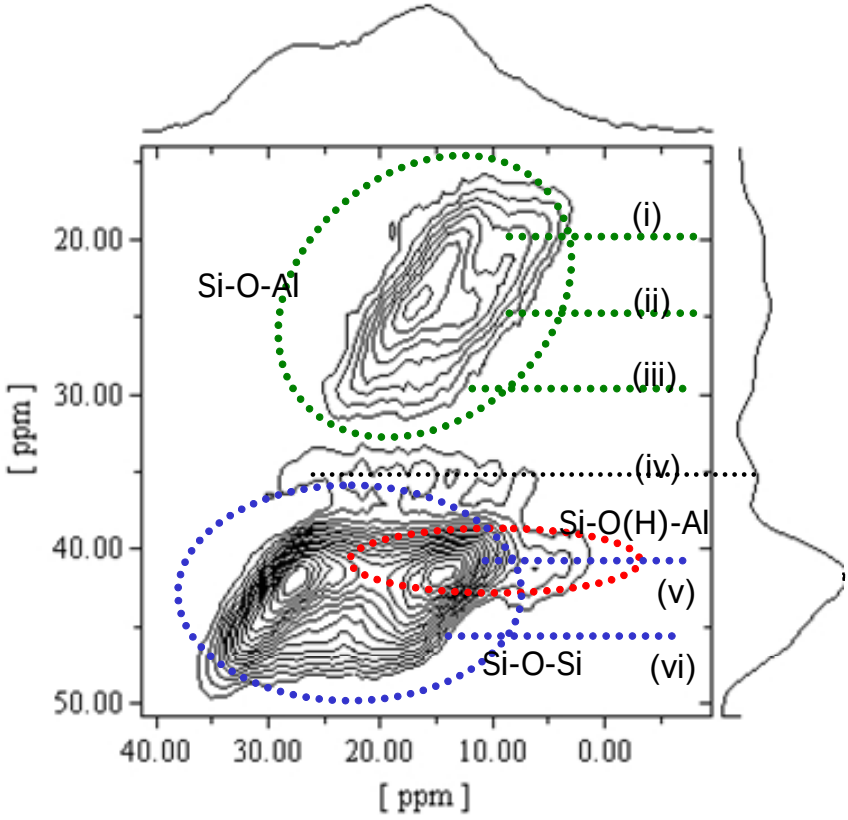

(a)

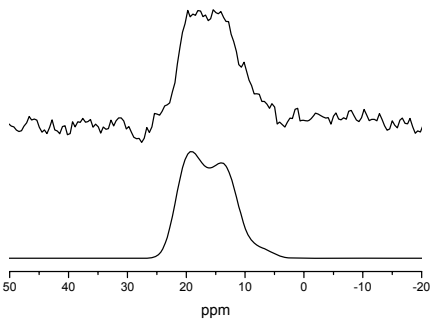
50 40 30 20 10 0 -10 -20
ppm

(b)

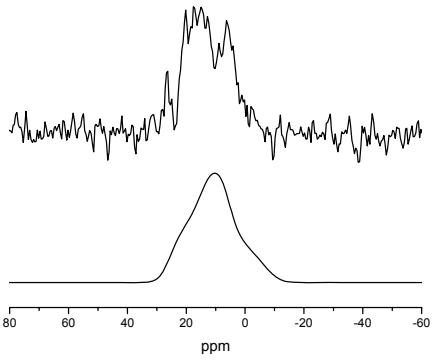
80 60 40 20 0 -20 -40 -60
ppm

(c)

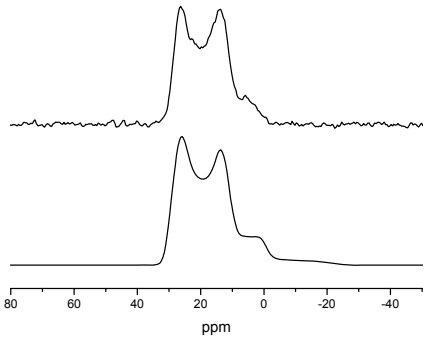
80 60 40 20 0 -20 -40
ppm

(d)

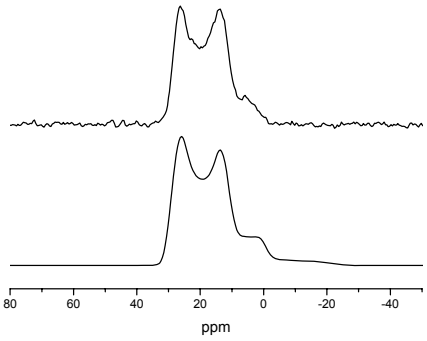
80 60 40 20 0 -20 -40
ppm

(e)

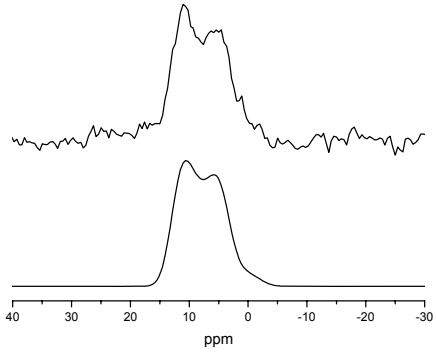
40 30 20 10 0 -10 -20 -30
ppm

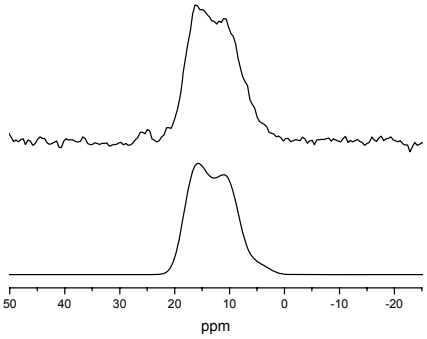
50 40 30 20 10 0 -10 -20
ppm

(f)

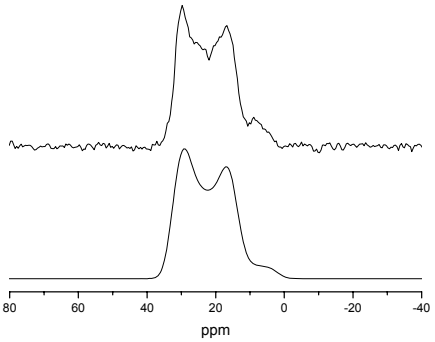

(g)

Figure 6.3 (a) 2-D-^{17}O MQMAS NMR spectrum of ^{17}O-enriched H-MOR acquired at 19.4 T, with a spinning speed of 10 kHz and recycle delay of 0.5 s. The projections (sum) of F_2 and F_1 dimension are shown on the above and right side of the 2D-spectrum, respectively. (b), (c), (d), (e), (f) and (g): slices of anisotropic dimension at 18.5, 24.0, 28.0, 34.5, 41.0 and 44.5 ppm in the isotropic dimension (top), in comparison with simulations performed with WSolids NMR package (bottom). Simulation parameters are shown in Table 6.1b. The dotted lines in 2-D spectra show where the slices are taken. Note: (f) left and right figures show one Si-O-Si site and Si-O-Si + Si-O(H)-Al two sites simulations of the slice taken at 41.0 ppm in the isotropic dimension.

Table 6.3 δ_2s and δ_1s are the observed center of gravities of the resonances in the anisotropic (F_2) and isotropic (F_1) dimension for oxygen atoms at 19.4 T in zeolite H-MOR, respectively. The predicted values of P_Q and δ_{iso} were calculated from the observed shifts of center of gravity of the resonances, using Eq. 6.1 and 6.2. The simulation data values of QCC, η and δ_{iso} were obtained from the Wsolid simulation result of each slice. The values of P_Q calculated with Eq. 6.3 using the simulation data in comparison to the predicted values of P_Q from the observed center of gravities can be taken as an examination of the reliability of the simulation.

Site	Slice	δ_1 (ppm)	δ_2 (ppm)	Predicted values		Simulation data			
				δ_{iso} (ppm)	P_Q	QCC (MHz)	η	δ_{iso} (ppm)	P_Q
Si-O-Al	(i)	18.5	8	14.6	3.73	3.75	0.2	14.6	3.77
	(ii)	24	13	19.9	3.82	3.80	0.25	20	3.84
	(iii)	28	16	23.6	3.99	3.95	0.25	23.6	3.99
Unknown	(iv)	34.5	14	26.0	5.21	5.3	0.7	26.2	5.71
Si-O-Si	(v)	41	18.5	32.7	5.46	5.40	0.2	33	5.44
	(vi)	44.5	22.5	36.4	5.4	5.38	0.2	36.4	5.42

Table 6.4 Predicted centers of gravities of the Brønsted acid sites in the ^{17}O MQMAS spectrum obtained at 19.4 T. ^{17}O NMR parameters (QCC, η and δ_{iso}) and corresponding coupled nearby ^{1}H sites were obtained in ^{1}H-^{17}O HETCOR NMR studies. The predicted centers of gravities (δ_1, δ_2) were calculated with Equation 6.1, 6.2 and 6.3.

δ_{CS} ^{1}H (ppm)	QCC (MHz)	η	δ_{iso} (ppm)	δ_1 (ppm)	δ_2 (ppm)
3.8	6.3	0.8	27	40.4	4.14
4.8	6.4	0.45	31	43.2	10.2
6.2	5.5	0.8	21	31.2	3.58

Table 6.5 Structural parameters for the Brønsted acid sites of zeolites D(H)-MOR, H-Y and H-ZSM-5 reported in the literature**.**

Zeolite	Site	T-O distance (Å)	T-O-T angle (°)	O-D(H) distance (Å)
D-MOR[11]	O_2	1.63 (T_4-O_2)	146	0.975(O-H)
	O_2	1.58(T_2-O_2)	146	
	O_7	1.61	139	0.977(O-H)
	O_9	1.63	160	1.00
	O_{10}	1.62	152	1.00
	O_5	1.65	139	1.01
	O_6	1.63	165	1.01
H-Y[12]	O_1	1.677	135.7	0.83
	O_2	1.632	144.6	1.02
	O_3	1.654	139.8	0.98
H-ZSM-5[13]	O	1.57-1.60	153-169	

Previous MQMAS[5] and double rotation (DOR)[6] NMR results indicate there is a linear correlation with a negative linear coefficient between the ^{17}O isotropic chemical shift and the Si-O-Al bond angles (δ/ppm = -0.65α/° + 134) or (δ/ppm = -0.71α/° + 143.7), obtained in zeolites with high Al contents[5,6]. Based on this correlation, the resonances arising from the Si-O-Al sites at δ_{iso} = 14.6, 20 and 23.6 ppm correspond to Si-O-Al bond angles of 180, 174 and 169°, respectively. According to crystallographic studies on zeolite H-MOR[14] or deuterated form D-MOR[11], while the T-O-T band angles are distributed over in a wide range of 140-180°, only the T-O-T band angles at O_4, O_6 and O_8 are larger than 165°. Two possible explanations to this discrepancy can be proposed. First, the correlation between Si-O-Al bond angles and the isotropic chemical shifts may vary from sample to sample[15]. The equations we adopt here were developed from high Al-containing zeolites[5,6] where the oxygen atoms in Si-O-Al environments are nearby cations, which may be not suitable for the high siliceous zeolite H-MOR sample (Si/Al ~ 8.8) used in this study. MOR bond angles dominated by Si-O-Si angles, hence the Si-O-Al may be quite different. A comparison of the distributions of T-O-T band angles among the three types of zeolites H (D)-MOR, HY and HZSM-5 is listed in Table 6.5. The T-O-T angles in zeolite HY are distributed in a much narrower range with smaller values of 135.7-144.6° in contrast to zeolite H (D)-MOR. In our previous ^{17}O MQMAS study on zeolite HY[16] at the same strength of field, the isotropic shift values associated with the Si-O-Al groups are correspondingly distributed within a narrower range with larger values of δ_{iso}=27.5-33.3 ppm. This suggested that the linear correlation

of δ/ppm = kα/° + β may still hold in zeolites HY and H-MOR. However, the specific values of the coefficients k and β need to be modified. The second possibility is that the Si-O-Al sites in zeolite H-MOR are preferentially located at O_4, O_6 and O_8, since these Si-$O_{4,6,8}$-Al bond angles are larger. At this point, all the other oxygen atoms sharing the same T atom with any of these three oxygen atoms can be a candidate for the possible location of Brønsted acid site.

Similar to the results obtained at 14.1 T, the ^{17}O signal due to oxygen directly bound to acidic proton is not clearly shown in the MQMAS spectrum. As mentioned above, the center of gravity (values of δ_1 and δ_2) of an unknown site can be predicted, if δ_{iso} and P_Q are known. The δ_{iso} and P_Q values of the oxygen atoms at Brønsted acid sites have been calculated by applying the NMR parameters extracted from ^{1}H-^{17}O HETCOR experiment to Eq. 6.1 and 6.3 and listed in Table 6.4. The predicted area of the corresponding ^{17}O signal has been shown with a red dashed line circle on Figure 6.3 (a), and partially overlaps with the signal arising from the Si-O-Si groups.

To confirm the overlap of the ^{17}O resonances arising from the Si-O-Si and Si-(OH)-Al sites, a closer inspection of slice (v) and (vi) was performed. Slice (v) is taken from the overlapping area with F_1 = 41 ppm, while slice (vi) taken at F_1 = 44.5 ppm should be a Si-O-Si site only. The lineshape simulations are shown in Figure 6.3 (b)-(g). Slice (vi) can be simulated by using only a single Si-O-Si site (Figure 6.3 (g)), where NMR parameters are listed in Table 3. In slice (v), the discontinuity at 14 ppm and the foot at lower frequency are more intense compared to the classic second order

quadrupolar lineshape of a normal Si-O-Si site (left spectrum of Figure 6.3 (f)). Adding another site with the NMR parameters extracted from ^{1}H-^{17}O HETCOR experiment at $\delta_{CS}{}^{1}H$ = 3.8 ppm can make the overall lineshape a better fit to the experimental result (right spectrum of Figure 6.3 (f)). This confirms the overlap of the ^{17}O resonances arising from Si-O-Si and Si-(OH)-Al sites. As discussed in our previous studies,[16] in MQMAS experiments, inadequate or no decoupling on the ^{1}H channel may lead to a loss of intensity of the ^{17}O signal arising from the Brønsted acid site, in which the O atom is strongly dipolar coupled to the proton. Since this experiment was performed with a single resonance probe, no decoupling was applied on the ^{1}H channel due to instrumental limitation.

6.4 Conclusions

Signals arising from Si-O-Al, Si-O-Si, Si-OH-Al and Si-OH (H_2O)-Al sites can be detected simultaneously in ^{17}O MQMAS NMR spectrum of zeolite H-MOR. Due to very distinct NMR parameters possessed by the three different oxygen species, these signals can be well resolved in MQMAS spectrum. The QCCs and ηs of Si-OH-Al sites are significantly larger than those of the Si-O-Al and Si-O-Si sites, which, in combination with the effects due to the larger ^{1}H-^{17}O dipolar coupling, result in inefficient excitation of the signals of the Brønsted acid sites in comparison to the framework sites.

The ^{17}O signals from a wide range of Si-O-Al and Si-O-Si linkages can be distinguished in the MQMAS spectra, especially in the spectrum obtained at high field.

The resonances from oxygen sites in the Si-OH (H_2O) and Si-OH-Al linkages can also be separated. The two sets of NMR parameters extracted for the Brønsted acid sites are consistent with our results obtained in the ^{1}H-^{17}O HETCOR NMR experiments.

The results presented in this study show that ^{17}O MQMAS NMR spectroscopy can probe both framework and Brønsted acid oxygen sites in zeolite catalysts at the same time allowing the various NMR parameters to be extracted. Since oxygen atoms are intimately involved in gas sorption, ^{17}O MQMAS NMR spectroscopy provides a powerful probe with which to investigate sorption and catalysis processes and to develop structure-function relationships of catalysts.

6.5 References

(1) Grey, C. P. Nuclear Magnetic Resonance Studies of Zeolites. In *Handbook of Zeolite Science and Technology*; Auerbach, S. M., Carrado, K. A., Dutta, P. K., Eds.; Marcel Dekker, 2003; pp 205.

(2) Amoureux, J. P.; Bauer, F.; Ernst, H.; Fernandez, C.; Freude, D.; Michel, D.; Pingel, U. T. *Chem. Phys. Lett.* **1998**, *285*, 10.

(3) Bull, L. M.; Bussemer, B.; Anupold, T.; Reinhold, A.; Samoson, A.; Sauer, J.; Cheetham, A. K.; Dupree, R. *J. Am. Chem. Soc.* **2000**, *122*, 4948.

(4) Bull, L. M.; Cheetham, A. K.; Anupold, T.; Reinhold, A.; Samoson, A.; Sauer, J.; Bussemer, B.; Lee, Y.; Gann, S.; Shore, J.; Pines, A.; Dupree, R. *J. Am. Chem. Soc.* **1998**, *120*, 3510.

(5) Freude, D.; Loeser, T.; Michel, D.; Pingel, U.; Prochnow, D. *Solid State Nucl. Magn. Reson.* **2001**, *20*, 46.

(6) Pingel, U. T.; Amoureux, J. P.; Anupold, T.; Bauer, F.; Ernst, H.; Fernandez, C.; Freude, D.; Samoson, A. *Chem. Phys. Lett.* **1998**, *294*, 345.

(7) Readman, J. E.; Kim, N.; Ziliox, M.; Grey, C. P. *Chem. Commun.* **2002**, 2808.

(8) Peng, L.; Huo, H.; Liu, Y.; Grey, C. P. *J. Am. Chem. Soc.* **2007**, *129*, 335

(9) Bennett, A. E.; Rienstra, C. M.; Auger, M.; Lakshmi, K. V.; Griffin, R. G. *J. Chem. Phys.* **1995**, *103*, 6951.

(10) Neuhoff, P. S.; Shao, P.; Stebbins, J. F. *Micropor. Mesopor. Mat.* **2002**, *55*, 239.

(11) Martucci, A.; Cruciani, G.; Alberti, A.; Ritter, C.; Ciambelli, P.; Rapacciuolo, M. *Micropor. Mesopor. Mater.* **2000**, *35-6*, 405.

(12) Czjzek, M.; Jobic, H.; Fitch, A. N.; Vogt, T. *J. Phys. Chem.* **1992**, *96*, 1535.

(13) Vankoningsveld, H.; Jansen, J. C.; Vanbekkum, H. *Zeolites* **1990**, *10*, 235.

(14) Mortier, W. J.; Pluth, J. J.; Smith, J. V. *Mater. Res. Bull.* **1975**, *10*, 1319.

(15) Loeser, T.; Freude, D.; Mabande, G. T. P.; Schwieger, W. *Chem. Phys. Lett.* **2003**, *370*, 32.

(16) Peng, L.; Huo, H.; Gan, Z.; Grey, C. P. *Micropor. Mesopor. Mater.* **2008**, *109*, 156.

Chapter 7

Conclusions

In this chapter, some comments and speculations about the general trends of the Brønsted acidity measurement and acidity-structure correlation will be given by crosschecking the experimental results obtained on all the three zeolites (HY, HMOR and HZSM-5) involved in this PhD study.

In term of constructing a measurement system of the strength of Brønsted acid sites, the O-H distance is a promising parameter to be correlated with the acidity. However, the measurement of an O-H distance by quantitatively extracting the O-H dipolar coupling information from $^{1}H \rightarrow {}^{17}O\text{-}^{1}H$ CP-REDOR NMR spectroscopy is based on the assumption that the O-H group is rigid. This requirement can only be fulfilled under low temperature. Low temperature $^{1}H \rightarrow {}^{17}O\text{-}^{1}H$ CP-REDOR NMR results on zeolites HY (0.975 ± 0.025Å) and HZSM-5 (0.976 Å) revealed similar O-H distances in both compounds. The O-H bond can not be treated as fully rigid at room temperature, especially in zeolite HZSM-5 in which the proton motional process associated with the residual H_2O can significantly reduce the apparent dipolar coupling. Furthermore, the traditional sample preparation method cannot totally remove the residual H_2O in zeolite HZSM-5 due to the 1-D framework structure and the small pentasil units. The low

activation energy of proton motion or the strong acidity in zeolite HZSM-5 reported in the literature is mainly due to the motional process involving both the Brønsted protons and the residual H_2O.

Zeolite H-MOR samples tend to adsorb trace amounts of water, or in some case, tiny amount of residual water may exist in zeolite H-MOR. Some hint about the relative rigidity of the O-H groups in zeolite H-MOR and HZSM-5 can be speculated by comparing the ^{1}H MAS NMR of the "wet" samples. In contrast to zeolite HZSM-5, no obvious protonic motional process is observed even with the presence of a trace amount of water in zeolite H-MOR. In the 2-D ^{17}O-^{1}H HETCOR NMR, an oxygen site associated with a Si-O (H$\cdots H_2O$)-Al structure is observed, which indicates that instead of helping the proton to move around, the H_2O molecules can be localized and H-bonded to the Brønsted acid protons in zeolite H-MOR. In the $^{1}H/^{27}Al$ TRAPDOR NMR, the resolution of two resonances associated with two proton species (center H in the O-H$\cdots OH_2$ structure and the protons in the $\cdots OH_2$) at 6.2 and 6.4 ppm with different TRAPDOR effects further confirms that the Brønsted acid O-H bonds in zeolite H-MOR remain rigid upon the loading of a trace amount of water. Based on the analysis above, a general trend of the strength of the Brønsted acidity among HY, HMOR and HZSM-5 can be concluded: HY$\leq$ H-MOR < HZSM-5.

Slight changes of the framework structures take place at low temperature. The T-O-T linkages in the frameworks of zeolites presumably undergo vibrational motion at room temperature. This motional process can be frozen out upon cooling and lead to a

more rigid framework. The QCC value of the oxygen atom directly involved in the Si-O(H)-Al group changes from 6.0 MHz at room temperature to 6.2 MHz at 183K. The ^{1}H chemical shift of the resonance due to the Brønsted acidic protons changes from lower frequency to higher frequency in both zeolites H-MOR and HZSM-5. The results of the Rietveld refinement of the HZSM-5 structure with the XRD patterns obtained at both 290 and 200K indicates that this change does not affect the space group. We speculate that this change is mainly related with more constrained and distorted T-O-T angles at lower temperatures.

References

Amoureux JP, Bauer F, Ernst H, Fernandez C, Freude D, et al. 1998. 17O multiple-quantum and 1H MAS NMR studies of zeolite ZSM-5. *Chem. Phys. Lett.* 285:10-4

Amoureux JP, Fernandez C. 1998. Triple, quintuple and higher order multiple quantum MAS NMR of quadrupolar nuclei. *Solid State Nucl. Magn. Reson.* 10:211-23

Amoureux JP, Fernandez C, Steuernagel S. 1996. Z filtering in MQMAS NMR. *J. Magn. Reson. A* 123:116-8

Andrew ER, Bradbury A, Eades RG. 1958. Nuclear Magnetic Resonance Spectra from a Crystal Rotated at High Speed. *Nature* 182:1659-

Baba T, Inoue Y, Shoji H, Uematsu T, Ono Y. 1995. Temperature-Dependent Lineshape of H-1 Magic-Angle-Spinning Nuclear-Magnetic-Resonance Spectra of Acidic Hydroxyl-Groups in Zeolites. *Microporous Mater.* 3:647-55

Baba T, Kumasito N, Ono Y. 1998a. Mobility of acidic protons in H-ZSM-5 as studied by variable temperature 1H MAS NMR. *J. Phys. Chem. B*:804-8

Baba T, Kumasito N, Ono Y, Sugisawa H, Takahashi T. 1998b. Nature of acidic protons in H-Mordenite and H-MCM-22 as studied by variable temperature1H MAS NMR. *Micropor. Mesopor. Mater.* 22:203-10

Baba T, Ono Y. 1999. Dynamic properties of protons in solid acids as studied by variable temperature H-1 MAS NMR. *Applied Catalysis a-General* 181:227-38

Bak M, Rasmussen JT, Nielsen NC. 2000. SIMPSON: A general simulation program for solid-state NMR spectroscopy. *J. Magn. Reson.* 147:296-330

Batamack P, Doremieuxmorin C, Fraissard J, Freude D. 1991. Broad-Line and High-Resolution Nmr-Studies Concerning the Hydroxonium Ion in Hzsm-5 Zeolites. *J. Phys. Chem.*95:3790-6

Beck LW, White JL, Haw JF. 1994. H-1(Al-27) Double-Resonance Experiments in Solids - an Unexpected Observation in the H-1 Mas Spectrum of Zeolite Hzsm-5. *J. Am. Chem. Soc.* 116:9657-61

Bennett AE, Rienstra CM, Auger M, Lakshmi KV, Griffin RG. 1995. Heteronuclear Decoupling in Rotating Solids. *J. Chem. Phys.* 103:6951-8

Bevilacqua M, Alejandre AG, Resini C, Casagrande M, Ramirez J, Busca G. 2002. An FTIR study of the accessibility of the protonic sites of H-mordenites. *Phys. Chem. Chem. Phys.* 4:4575-83

Bevilacqua M, Busca G. 2002. A study of the localization and accessibility of Bronsted and Lewis acid sites of H-mordenite through the FT-IR spectroscopy of adsorbed branched nitriles. *Catal. Comm.* 3:497-502

Bowers CR, Storhaug V, Webster CE, Bharatam J, Cottone A, et al. 1999. Exploring surfaces and cavities in lipoxygenase and other proteins by hyperpolarized xenon-129 NMR. *J. Am. Chem. Soc.* 121:9370-7

Breck DW. 1974a. *Zeolite Molecular Sieves: Structure, Chemistry, and Use.* . New York, N.Y.: Wiley-Interscience. 752 pp.

Breck DW. 1974b. *Zeolite Molecular Sieves: Structure, Chemistry, and Use*: John Wiley & Sons, Inc.

Brunner E. 1990. Limitations of Resolution in the H-1 Magic-Angle-Spinning Nuclear-Magnetic-Resonance Spectroscopy of Zeolites. *J. Chem. Soc. Faraday T.* 86:3957-60

Brunner E, Beck K, Koch M, Heeribout L, Karge HG. 1995. Verification and Quantitative-Determination of a New-Type of Bronsted Acid Sites in H-Zsm-5 by H-1 Magic-Angle-Spinning Nuclear-Magnetic-Resonance Spectroscopy. *Microporous Mater.* 3:395-9

Bucko T, Benco L, Demuth T, Hafner J. 2002. Ab initio density functional investigation of the (001) surface of mordenite. *J. Chem. Phys.* 117:7295-305

Bull LM, Bussemer B, Anupold T, Reinhold A, Samoson A, et al. 2000. A high-resolution 17O and 29Si NMR study of zeolite siliceous ferrierite and ab initio calculations of NMR parameters. *J. Am. Chem. Soc.* 122:4948-58

Bull LM, Cheetham AK. 1997. O-17 NMR studies of siliceous faujasite. *Stud. Surf. Sci. Catal.* 105:471-7

Bull LM, Cheetham AK, Anupold T, Reinhold A, Samoson A, et al. 1998. A high-resolution 17O NMR study of siliceous zeolite faujasite. *J. Am. Chem. Soc.* 120:3510-1

Chan JCC, Eckert H. 2000. Dipolar coupling information in multispin systems: Application of a compensated REDOR NMR approach to inorganic phosphates. *J. Magn.c Reson.* 147:170-8

Chaudhuri S. 2003. *Solid State NMR and Atomistic Molecular Dynamics Simulation Study of Ionic Conductors, Catalysts and Perovskites*. Ph. D. Dissertation. State University of New York at Stony Brook, Stony Brook

Chuang IS, Maciel GE. 1997. A detailed model of local structure and silanol hydrogen banding of silica gel surfaces. *J. Phys. Chem.B* 101:3052-64

Corma A. 1995a. Inorganic solid acids and their use in acid-catalyzed hydrocarbon Reactions. *Chem. Rev.* 95:559-614

Corma A. 1995b. Inorganic Solid Acids and Their Use in Acid-Catalyzed Hydrocarbon Reactions. *Chem. Rev.* 95:559-614

Corma A, Rey F, Rius J, Sabater MJ, Valencia S. 2004. Supramolecular self-assembled molecules as organic directing agent for synthesis of zeolites. *Nature* 431:287-90

Czjzek M, Jobic H, Fitch AN, Vogt T. 1992. Direct determination of proton positions in D-Y and H-Y zeolite samples by neutron powder diffraction. *J. Phys. Chem.* 96:1535-40

Demuth T, Hafner J, Benco L, Toulhoat H. 2000. Structural and acidic properties of mordenite. An ab initio density-functional study. *J. Phys. Chem.B* 104:4593-607

Deng F, Du YR, Ye CH, Wang JZ, Ding TT, Li HX. 1995. Acid Sites and Hydration Behavior of Dealuminated Zeolite Hzsm-5 - a High-Resolution Solid-State Nmr-Study. *J. Phys. Chem.*99:15208-14

Derouane EG, Andre JM, Lucas AA. 1988. Surface Curvature Effects in Physisorption and Catalysis by Microporous Solids and Molecular-Sieves. *J Catal.* 110:58-73

Dominguez-Soria VD, Calaminici P, Goursot A. 2007. Theoretical study of the structure and properties of Na-MOR and H-MOR zeolite models. *J. Chem. Phys.* 127:-

Du LS. 2000. *Application and Theoretical Study of Solid-State NMR to Inorganic Fluorides and Oxyfluorides*. Ph. D. Dissertation. State University of New York at Stony Brook, Stony Brook

Duer MJ. 2004. *Introduction to Solid-State NMR Spectroscopy*. Oxford: Blackwell Publishing Ltd

Ernst RR, Bodenhausen G, Wokaun A. 1987. *Principles of Nuclear Magnetic Resonance in One and Two Dimensions*. Oxford: Oxford University Press

Farcasiu D, Leu R, Corma A. 2002. Evaluation of accessible acid sites on solids by N-15 NMR spectroscopy with di-tert-butylpyridine as base. *J. Phys. Chem.B* 106:928-32

Farneth WE, Gorte RJ. 1995. Methods for Characterizing Zeolite Acidity. *Chem. Rev.* 95:615-35

Fois E, Gamba A, Tabacchi G. 1998. Structure and dynamics of a Bronsted acid site in a zeolite: An ab initio study of hydrogen sodalite. *J. Phys. Chem. B* 102:3974-9

Franke ME, Simon U. 1999. Proton mobility in H-ZSM5 studied by impedance spectroscopy. *Solid State Ionics* 118:311-6

Franke ME, Simon U. 2000. Characteristics of proton hopping in zeolite H-ZSM5. *Phys. Status Solidi B* 218:287-90

Freude D. 1995. Enhanced Resolution in the H-1-Nmr Spectra of Zeolite H-Zsm-5 by Heteronuclear Dipolar-Dephasing Spin-Echo Mas. *Chem. Phys. Lett.* 235:69-75

Freude D, Ernst H, Wolf I. 1994. Solid-state nuclear magnetic resonance studies of acid sites in zeolites. *Solid State Nucl. Magn. Reson.* 3:271-86

Freude D, Hunger M, Pfeifer H, Schwieger W. 1986. 1H MAS NMR studies on the acidity of zeolites. *Chem. Phys. Lett.* 128:62-6

Freude D, Klinowski J. 1988. Solid-State H-1-Nmr Studies of the Structure of the Active-Site in Zeolite H-Zsm-5. *J. Chem. Soc. Chem. Comm.*:1411-3

Freude D, Loeser T, Michel D, Pingel U, Prochnow D. 2001. 17O NMR studies of low silicate zeolites. *Solid State Nucl. Magn. Reson.* 20:46-60

Frydman L, Harwood JS. 1995. Isotropic Spectra of Half-Integer Quadrupolar Spins from Bidimensional Magic-Angle-Spinning Nmr. *J. Am. Chem. Soc.* 117:5367-8

Fyfe CA, Feng Y, Grondey H, Kokotailo GT, Gies H. 1991. One-Dimensional and 2-Dimensional High-Resolution Solid-State Nmr-Studies of Zeolite Lattice Structures. *Chem. Rev.* 91:1525-43

Fyfe CA, Mueller KT, Grondey H, Wong-Moon KC. 1993. Solid-State Double-Resonance NMR Experiments Involving Quadrupolar and Spin 1/2 Nuclei. *J. Phys. Chem.* 97:13484-95

Gan ZH. 2000. Isotropic NMR spectra of half-integer quadrupolar nuclei using satellite transitions and magic-angle spinning. *J. Am. Chem. Soc.* 122:3242-3

Goetz JM, Wu JH, Yee HF, Schaefer J. 1998. Two-dimensional transferred-echo double resonance study of molecular motion in a fluorinated polycarbonate. *Solid State Nucl. Magn. Reson.* 12:87-95

Grandinetti PJ, Baltisberger JH, Farnan I, Stebbins JF, Werner U, Pines A. 1995. Solid-State O-17 Magic-Angle and Dynamic-Angle Spinning Nmr-Study of the SiO2 Polymorph Coesite. *J. Phys. Chem.* 99:12341-8

Greaves GN, Meneau F, Majerus O, Jones DG, Taylor J. 2005. Identifying vibrations that destabilize crystals and characterize the glassy state. *Science* 308:1299-302

Grey CP. 2003. Nuclear Magnetic Resonance Studies of Zeolites. In *Handbook of Zeolite Science and Technology*, ed. SM Auerbach, KA Carrado, PK Dutta, pp. 205-55: Marcel Dekker

Grey CP, Veeman WS. 1992a. The Detection of Weak Heteronuclear Coupling between Spin-1 and Spin-1/2 Nuclei in Mas Nmr - N-14/C-13/H-1 Triple Resonance Experiments. *Chem Phys Lett* 192:379-85

Grey CP, Veeman WS. 1992b. The Detection of Weak Heteronuclear Coupling between Spin-1 and Spin-1/2 Nuclei in Mas Nmr - N-14/C-13/H-1 Triple Resonance Experiments. *Chem. Phys. Lett.* 192:379-85

Grey CP, Vega AJ. 1995. Determination of the quadrupole coupling constant of the invisible aluminum spins in zeolite HY with 1H/27Al TRAPDOR NMR. *J. Am. Chem. Soc.* 117:8232-42

Gullion T. 1997. Measurement of Heteronuclear Dipolar Interactions by Rotational-Echo, Double-Resonance Nuclear Magnetic Resonance. *Magn. Reson. Rev.* 17:83-131

Gullion T, Schaefer J. 1989. Rotational-echo double-resonance NMR. *J. Magn. Reson.* 81:196-200

Hartmann SR, Hahn EL. 1962. Nuclear Double Resonance in Rotating Frame. *Phys. Rev.* 128:2042-&

Heeribout L, Semmer V, Batamack P, Doremieuxmorin C, Fraissard J, Antos G. 1995. Solid-State H-1-Nmr Studies of the Acidity of Mordenites. *J. Chem. Soc. Faraday T.* 91:3933-9

Hunger M. 1991. *Habilitation Thesis*. University of Leipzig

Hunger M. 1996. Multinuclear solid-state NMR studies of acidic and non-acidic hydroxyl protons in zeolites. *Solid State Nucl. Magn. Reson.* 6:1-29

Hunger M. 1997. Bronsted acid sites in zeolites characterized by multinuclear solid-state NMR spectroscopy. *Catalysis Reviews-Science and Engineering* 39:345-93

Hunger M, Freude D, Frohlich T, Pfeifer H, Schwieger W. 1987. H-1-Mas Nmr-Studies of Zsm-5 Type Zeolites. *Zeolites* 7:108-10

Hunger M, Freude D, Pfeifer H. 1988. ^{1}H MAS Studies of Acid Sites in ZSM-5 Type Zeolites. *Catal. Today* 3:507-12

Hunger M, Freude D, Pfeifer H. 1991. Magic Angle Spinning Nuclear Magnetic Resonance Studies of Water-Molecules Adsorbed on Brønsted-Acid and Lewis-Acid Sites in Zeolites and Amorphous Silica-Aluminas. *J. Chem. Soc. Faraday T.* 87:657-62

Hunger M, Freude D, Pfeifer H, Schwieger W. 1990. Mas Nmr-Studies of Silanol Groups in Zeolites Zsm-5 Synthesized with an Ionic Template. *Chem. Phys. Lett.* 167:21-6

Hunger M, Horvath T. 1995. Multinuclear Solid-State Nmr-Study of the Local-Structure of Siohal Groups and Their Interaction with Probe-Molecules in Dehydrated Faujasite, Mordenite and Zeolite Zsm-5. *Berichte Der Bunsen-Gesellschaft-Phys. Chem. Chem. Phys.* 99:1316-20

Huo H, Peng LM, Grey CP. 2009. Low Temperature H-1 MAS NMR Spectroscopy Studies of Proton Motion in Zeolite HZSM-5. *J. Phys. Chem.C* 113:8211-9

Ichikawa M. 1978. O-H Vs O ... O Distance Correlation, Geometric Isotope Effect in Oho Bonds, and Its Application to Symmetric Bonds. *Acta Crystallogr. B* 34:2074-80

Ichikawa M. 2000. Hydrogen-bond geometry and its isotope effect in crystals with OHO bonds - revisited. *J. Mol. Struct.* 552:63-70

Iuga D, Morais C, Gan ZH, Neuville DR, Cormier L, Massiot D. 2005. NMR heteronuclear correlation between quadrupolar nuclei in solids. *Journal of the American Chemical Soceity* 127:11540-1

Jobic H, Tuel A, Krossner M, Sauer J. 1996. Water in interaction with acid sites in H-ZSM-5 zeolite does not form hydroxonium ions. A comparison between neutron scattering results and ab initio calculations. *J. Phys. Chem.*100:19545-50

Juamain D, Su BL. 2002. Monitoring the Bronsted acidity of zeolites by means of in situ FT-IR and catalytic testing using chloromethane as probe molecule. *Catal. Today* 73:187-96

Kalwei M, Koller H. 2002. Quantitative comparison of REAPDOR and TRAPDOR experiments by numerical simulations and determination of H-Al distances in zeolites. *Solid State Nucl. Magn. Reson.* 21:145-57

Kanellopoulos J, Gottert C, Schneider D, Knorr B, Prager D, et al. 2008. NMR investigation of proton mobility in zeolites. *J Catal.* 255:68-78

Kao HM. 1998. *Probing the Bronsted and Lewis Acid Sites in Zeolite Y with Probe Molecules and Solid-State Double Resonance NMR*. Ph. D. Dissertation. State University of New York at Stony Brook, Stony Brook

Kao HM, Grey GP. 1996. Probing the Bronsted and Lewis acidity of zeolite HY: A H-1/Al-27 and N-15/Al-27 TRAPDOR NMR study of monomethylamine adsorbed on HY. *J. Phys. Chem.*100:5105-17

Kao HM, Yu CY, Yeh MC. 2002. Detection of the inhomogeneity of Bronsted acidity in H-mordenite and H-P zeolites: a comparative NMR study using trimethylphosphine and trimethylphosphine oxide as P-31 NMR probes. *Micropor. Mesopor. Mater.* 53:1-12

Karge HG, Hunger M, Beyer HK. 1999. Characterization of zeolites - infrared and nuclear magnetic resonance spectroscopy and X-ray diffraction. In *Catalysis and Zeolites: Fundamentals and Applications*, ed. J Weitkamp, L Puppe, pp. 198-326. New York: Springer

Kentgens APM, Iuga D, Kalwei M, Koller H. 2001. Direct observation of Bronsted acidic sites in dehydrated zeolite H-ZSM5 using DFS-enhanced Al-27 MQMAS NMR spectroscopy. *J. Am. Chem. Soc.* 123:2925-6

Klinowski J. 1993. Applications of solid-state NMR for the study of molecular-sieves. *Anal. Chim. Acta.* 283:929-65

Kobe JM, Gluszak TJ, Dumesic JA, Root TW. 1995. Deuterium Nmr Characterization of Bronsted Acid Sites and Silanol Species in Zeolites. *J. Phys. Chem.*99:5485-91

Kokotailo GT, Lawton SL, Olson DH, Olson DH, Meier WM. 1978. Structure of Synthetic Zeolite Zsm-5. *Nature* 272:437-8

Kolodziejski W, Klinowski J. 2002. Kinetics of cross-polarization in solid-state NMR: A guide for chemists. *Chem. Rev.* 102:613-28

Kreuer KD. 1996. Proton conductivity: Materials and applications. *Chem. Mater.* 8:610-41

Kreuer KD, Rabenau A, Weppner W. 1982. Vehicle Mechanism, a New Model for the Interpretation of the Conductivity of Fast Proton Conductors. *Angew Chem Int. Edit.* 21:208-9

Krossner M, Sauer J. 1996. Interaction of water with Bronsted acidic sites of zeolite catalysts. Ab initio study of 1:1 and 2:1 surface complexes. *J. Phys. Chem.*100:6199-211

Larin AV, Vercauteren DP. 2001. Lower order atomic multipole moments of the oxygen atoms of "small size" H-form aluminosilicate frameworks. *J. Mol. Catal. A-Chem.* 168:123-38

Larson AC, VonDreele RB. 1985. General Structure Analysis System, Los Alamos National Laboratory, Los Alamos, NM

Levitt MH. 2001. *Spin Dynamics: Basics of Nuclear Magnetic Resonance*. Chichester: John Wiley & Sons, Ltd

Lippmaa E, Magi M, Samoson A, Engelhardt G, Grimmer AR. 1980. Structural Studies of Silicates by Solid-State High-Resolution Si-29 Nmr. *J. Am. Chem. Soc.* 102:4889-93

Lippmaa E, Magi M, Samoson A, Tarmak M, Engelhardt G. 1981. Investigation of the Structure of Zeolites by Solid-State High-Resolution Si-29 Nmr-Spectroscopy. *J. Am. Chem. Soc.* 103:4992-6

Liu HM. 2001. *Structural and Functional Characterization of Inorganic Materials by Solid-State NMR and Diffraction Techniques*. Ph. D. Dissertation. State University of New York at Stony Brook, Stony Brook

Loeser T, Freude D, Mabande GTP, Schwieger W. 2003. 17O NMR studies of sodalites. *Chem. Phys. Lett.* 370:32-8

Loewenstein W. 1954. The Distribution of Aluminum in the Tetrahedra of Silicates and Aluminates. *Am. Mineral.* 39:92-6

Lunsford JH. 1997. Characterization of acidity in zeolites and related oxides using trimethylphosphine as a probe. *Top. Catal.* 4:91-8

Luz Z, Vega AJ. 1987. Interaction of H-Rho Zeolite with Water and Methanol Studied by Multinuclear Nmr-Spectroscopy. *J. Phys. Chem.*91:374-82

Man PP. 1996. Quadrupolar Interactions. In *Encyclopedia of Nuclear Magnetic Resonance*, ed. DM Grant, RK Harris, pp. 3838-48. Chichester: Wiley

Marchese L, Chen JS, Wright PA, Thomas JM. 1993. Formation of H3o+ at the Bronsted Site in Sapo-34 Catalysts. *J. Phys. Chem.*97:8109-12

Marie O, Massiani P, Thibault-Starzyk F. 2004. Infrared evidence of a third bronsted site in mordenites. *J. Phys. Chem.B* 108:5073-81

Martucci A, Cruciani G, Alberti A, Ritter C, Ciambelli P, Rapacciuolo M. 2000. Location of Bronsted sites in D-mordenites by neutron powder diffraction. *Micropor. Mesopor. Mater.* 35-6:405-12

Mehring M. 1983. *Principles of High Resolution NMR in Solids*. Berlin Heidelberg New York: Springer-Verlag

Mortier WJ, Pluth JJ, Smith JV. 1975. Positions of Cations and Molecules in Zeolites with Mordenite-Type Framework .2. Dehydrated Hydrogen-Ptilolite. *Mater. Res. Bull.* 10:1319-25

Mueller KT, Sun BQ, Chingas GC, Zwanziger JW, Terao T, Pines A. 1990. Dynamic-Angle Spinning of Quadrupolar Nuclei. *J. Magn.c Reson.* 86:470-87

Mueller KT, Wu Y, Chmelka BF, Stebbins J, Pines A. 1991. High-Resolution O-17 Nmr of Solid Silicates. *J. Am. Chem. Soc.* 113:32-8

Neuhoff PS, Shao P, Stebbins JF. 2002. Effect of extraframework species on 17O NMR chemical shifts in zeolite A. *Micropor. Mesopor. Mat.* 55:239-51

Olson DH. 2001. *Atlas of Zeolite Framework Types*: Elsevier

Olson DH, Reischman PT. 1996. Structure-related paraffin sorption in ZSM-5. *Zeolites* 17:434-6

Paillaud JL, Harbuzaru B, Patarin J, Bats N. 2004. Extra-large-pore zeolites with two-dimensional channels formed by 14 and 12 rings. *Science* 304:990-2

Peng L, Huo H, Gan Z, Grey CP. 2008. O-17 MQMAS NMR studies of zeolite HY. *Micropor. Mesopor. Mater.* 109:156-62

Peng L, Huo H, Grey CP. 17O MAS NMR Studies of Brønsted Acid Sites in Zeolite HY and HZSM-5. *In preparation*

Peng L, Huo H, Liu Y, Grey CP. 2007. 17O Magic Angle Spinning NMR Studies of Brnsted Acid Sites in Zeolites HY and HZSM-5. *J. Am. Chem. Soc.* 129:335 - 46

Peng L, Liu Y, Kim N, Readman JE, Grey CP. 2005a. Detection of Bronsted acid sites in zeolite HY with high-field O-17-MAS-NMR techniques. *Nature Mater.* 4:216-9

Peng LM, Liu Y, Kim NJ, Readman JE, Grey CP. 2005b. Detection of Bronsted acid sites in zeolite HY with high-field O-17-MAS-NMR techniques. *Nat. Mater.*4:216-9

Pines A, Gibby MG, Waugh JS. 1973. Proton-enhanced NMR of dilute spins in solids. *J. Chem. Phys.* 59:569-90

Pingel UT, Amoureux JP, Anupold T, Bauer F, Ernst H, et al. 1998. High-field 17O NMR studies of the SiOAl bond in solids. *Chem. Phys. Lett.* 294:345-50

Readman JE, Kim N, Ziliox M, Grey CP. 2002. 17O MQMAS NMR studies of Na-A and Ca-A. *Chem. Commun.*:2808-9

Redondo A, Hay PJ. 1993. Quantum chemical studies of acid sites in zeolite ZSM-5. *J. Phys. Chem.* 97:11754-61

Samoson A, Lippmaa E, Pines A. 1988. High-Resolution Solid-State Nmr Averaging of 2nd-Order Effects by Means of a Double-Rotor. *Molecular Physics* 65:1013-8

Sarv P, Tuherm T, Lippmaa E, Keskinen K, Root A. 1995. Mobility of the Acidic Proton in Bronsted Sites of H-Y, H-Mordenite, and H-Zsm-5 Zeolites, Studied by High-Temperature H-1 Mas Nmr. *J. Phys. Chem.* 99:13763-8

Sauer J. 1996. Probing catalysts with water. *Science* 271:774-5

Simperler A, Bell RG, Foster MD, Gray AE, Lewis DW, Anderson MW. 2004. Probing the acid strength of Bronsted acidic zeolites with acetonitrile: An atomistic and quantum chemical study. *J. Phys. Chem.B* 108:7152-61

Smith JV, Blackwell CS. 1983. Nuclear Magnetic-Resonance of Silica Polymorphs. *Nature* 303:223-5

Smith JV, Blackwell CS, Hovis GL. 1984. Nmr of Albite Microcline Series. *Nature* 309:140-2

Smith L, Cheetham AK, Morris RE, Marchese L, Thomas JM, et al. 1996. On the nature of water bound to a solid acid catalyst. *Science* 271:799-802

Spearing DR, Farnan I, Stebbins JF. 1992. Dynamics of the Alpha-Beta Phase-Transitions in Quartz and Cristobalite as Observed by Insitu High-Temperature Si-29 Nmr and O-17 Nmr. *Phys. Chem. Miner.* 19:307-21

Stebbins JF, Zhao PD, Lee SK, Cheng X. 1999. Reactive Al-O-Al sites in a natural zeolite: Triple-quantum oxygen-17 nuclear magnetic resonance. *Am. Mineral.* 84:1680-4

Stejskal EO, Memory JD. 1994. *High Resolution NMR in the Solid State*. New York: Oxford University Press, Inc.

Stejskal EO, Schaefer J, Waugh JS. 1977. Magic-Angle Spinning and Polarization Transfer in Proton-Enhanced Nmr. *J. Magn. Reson.* 28:105-12

Thomas JM, Klinowski J, Ramdas S, Hunter BK, Tennakoon DTB. 1983. The Evaluation of Non-Equivalent Tetrahedral Sites from Si-29 Nmr Chemical-Shifts in Zeolites and Related Aluminosilicates. *Chem. Phys. Lett.* 102:158-62

Vankoningsveld H. 1990. High-Temperature (350-K) Orthorhombic Framework Structure of Zeolite H-Zsm-5. *Acta Crystallogr. B* 46:731-5

vanKoningsveld H, Jansen JC. 1996. Single crystal structure analysis of zeolite H-ZSM-5 loaded with naphthalene. *Microporous Mater.* 6:159-67

Vankoningsveld H, Jansen JC, Vanbekkum H. 1990. The Monoclinic Framework Structure of Zeolite H-Zsm-5 - Comparison with the Orthorhombic Framework of as-Synthesized Zsm-5. *Zeolites* 10:235-42

vanKoningsveld H, Jansen JC, vanBekkum H. 1996. The location of p-dichlorobenzene in a single crystal of zeolite H-ZSM-5 at high sorbate loading. *Acta Crystallogr. B* 52:140-4

VanKoningsveld H, Koegler JH. 1997. Preparation and structure of crystals of zeolite H-ZSM-5 loaded with p-nitroaniline. *Microporous Mater.* 9:71-81

Vankoningsveld H, Tuinstra F, Vanbekkum H, Jansen JC. 1989. The Location of Para-Xylene in a Single-Crystal of Zeolite H-Zsm-5 with a New, Sorbate-Induced, Orthorhombic Framework Symmetry. *Acta Crystallogr. B* 45:423-31

Vega AJ. 1992. CP/MAS of quadrupolar S = 3/2 nuclei. *Solid State Nucl. Magn. Reson.* 1:17-32

Wielers AFH, Vaarkamp M, Post MFM. 1991. Relation between Properties and Performance of Zeolites in Paraffin Cracking. *J Catal.* 127:51-66

Wu EL, Lawton SL, Olson DH, Rohrman AC, Kokotailo GT. 1979. Zsm-5-Type Materials - Factors Affecting Crystal Symmetry. *J. Phys. Chem.*83:2777-81

Wu JH, Xiao CD, Yee AF, Goetz JM, Schaefer J. 2000. Local chain dynamics in poly(fluorocarbonate)s. *Macromolecules* 33:6849-52

Xue X, Kanzaki M. 2001. Ab initio calculation of the 17O and 1H NMR parameters for various OH groups. Implications to the speciation and dynamics of dissolved water in silicate glasses. *J. Phys. Chem. B* 105:3422-34

Zecchina A, Spoto G, Bordiga S. 2005. Probing the acid sites in confined spaces of microporous materials by vibrational spectroscopy. *Phys. Chem. Chem. Phys.* 7:1627-42

Zeyer M, Montagne L, Jaeger C. 2003. Measuring oxygen-phosphorus distances and the orientation of electric field gradient tensors using O-17{P-13} REDOR in phosphate glasses. *Solid State Nucl. Magn. Reson.* 23:136-44